IACMI/0004-2020/3.7

3.7 Reduction of CO_2 Emissions Through Lightweight Body Panels

PROJECT FINAL REPORT

Approved for Public Release. Distribution is Unlimited.

Hendrik Mainka
Thomas Laduch
Marton Kardos
Dayakar Penumadu
Uday Vaidya
Michael Bogdanor
Shane Skop
Ahmed Arabi Hassen

Date Published
January 31, 2020

THE COMPOSITES INSTITUTE

U.S. DEPARTMENT OF ENERGY

DOCUMENT AVAILABILITY

Reports produced after January 1, 1996, are generally available free via US Department of Energy (DOE) SciTech Connect.

Website http://www.osti.gov/scitech/

Reports produced before January 1, 1996, may be purchased by members of the public from the following source:

National Technical Information Service
5285 Port Royal Road
Springfield, VA 22161
Telephone 703-605-6000 (1-800-553-6847)
TDD 703-487-4639
Fax 703-605-6900
E-mail info@ntis.gov
Website http://www.ntis.gov/help/ordermethods.aspx

Reports are available to DOE employees, DOE contractors, Energy Technology Data Exchange representatives, and International Nuclear Information System representatives from the following source:

Office of Scientific and Technical Information
PO Box 62
Oak Ridge, TN 37831
Telephone 865-576-8401
Fax 865-576-5728
E-mail reports@osti.gov
Website http://www.osti.gov/contact.html

3.7 Reduction of CO2 Emissions Through Lightweight Body Panels

Hendrik Mainka

Thomas Laduch

Marton Kardos

Dayakar Penumadu

Uday Vaidya

Michael Bogdanor

Shane Skop

Ahmed Arabi Hassen

Project Period:
02/2017 – 11-2019

Date Published:
February 2019

Prepared by:
Institute for Advanced Composites Manufacturing Innovation
Knoxville, TN 37932
Managed by Collaborative Composite Solutions, Inc.
For the
U.S. DEPARTMENT OF ENERGY
Under contract DE- EE0006926

CONTENTS Page

LIST OF ACRONYMS

ALSA ..... Ashland Laser Surface Analyzer
AM ..... Additive Manufacturing
AMO ..... Advanced Manufacturing Office
AOP ..... Annual Operation Plan
ASTM ..... American Society for Testing and Materials
BAAM ..... Big Area Additive Manufacturing
BM ..... Benchmark Material
BMC ..... Bulk Molding Compound
CAD ..... Computer-Aided Design
CED ..... Cumulative Energy Demand
CF ..... Carbon Fiber
CFTF ..... Carbon Fiber Technology Facility
CMSC ..... Composites Manufacturing & Simulation Center
CNC ..... Computer Numerical Control
CO_2 ..... Carbon Dioxide
CSP ..... Continental Structural Plastics
CT ..... Computer Tomography
DIC ..... Digital Image Correlation
DMA ..... Dynamic Mechanical Analysis
DOE ..... Department Of Energy
DOI ..... Distinctness Of Image
DSC ..... Differential Scanning Calorimetry
ECRC ..... European Composites Recycling Services Company
EE ..... Embodied Energy
eGRID ..... Emissions & Generation Resource Integrated Database
EOL ..... End-Of-life
EPA ..... Environmental Protection Agency
EuCIA ..... European Composites Industry Association
EuPC ..... European Plastics Converters
FEA ..... Finite Element Analysis
GFRP ..... Glass Fiber Reinforced Plastics
GJ ..... Gigajoule
GPM ..... Gallons Per Minute
GTI ..... Grand Tourer Injection
GWP ..... Global Warming Potential
HP ..... Horse Power
IACMI ..... Institute for Advanced Composites Manufacturing Innovation
ILCD ..... Steel hot rolled coil
IR ..... Infrared
LCA ..... Life-Cycle-Assessment
LCCF ..... Low-Cost Carbon Fiber
MDF ..... Manufacturing Demonstration Facility
MgO ..... Magnesium Oxide
MJ ..... Megajoule
MLM ..... Maximum Loss Moduli Temperature
MSU ..... Michigan State University
MTD ..... Maximum Tan Delta
NREL ..... National Renewable Energy Laboratory
OC ..... Owens Corning

ORNL.....Oak Ridge National Laboratory
PAN ..... Polyacrylonitrile
PE..... Polyethylene
PI ..... Primary Investigator
PPS.....Polyphenylene Sulfide
PPSU..... Polyphenylsulfone
R&D..... Research and Development
RFC.....Reliability First Corporation
ROI ..... Region Of Interest
SERC ..... South East Regional Corporation
SMC.....Sheet Molding Compound
SURF ..... Scale-Up Research Facility
TDIC ..... Thermal Digital Image Correlation
TDS.....Technical Data Sheet
TRACI .....Tool for Reduction and Assessment of Chemicals and Other Environmental Impacts
UT ..... University Of Tennessee
UTK ..... University Of Tennessee, Knoxville Campus
UV.....Ultraviolet
VARTM.....Vacuum Assisted Resin Transfer Molding
VE.....Vinyl Ester
VW.....Volkswagen Group of America
XCT .....X-Ray Computer Tomography

LIST OF FIGURES

LIST OF TABLES

ACKNOWLEDGEMENTS

This project was sponsored by the U.S. Department of Energy, Office of Energy Efficiency and Renewable Energy, Advanced Manufacturing Office, under contract DE-EE0006926 with the Institute for Advanced Composites Manufacturing Innovation (IACMI).

The University of Tennessee, Knoxville was integral to the success of this project. Specifically, the work of the Civil and Environmental Engineering Department, Dr. Dayakar Penumadu and Dr. Stephen Young in managing the project and the many tasks UT was involved in. Thermal characterization was performed by Zachary Cook, Hannah Maeser and Damon Vance. Mechanical Testing was done by Zach Arwood, Vivek Chawla, Joshua Crabtree, Darren Foster and Andrew Patchen. X-Ray tomography was done by James Eun and Niko Maldonado.

The authors would like to express their sincere gratitude to the Mechanical, Aerospace, and Biomedical Engineering Department of University of Tennessee for their vital contributions to the project. Dr. Uday Vaidya and his group at the Fibers and Composites Manufacturing Facility: Nitilaksha Hiremath and Vidyarani Sangnal Matt Durandhara Murthy were involved in characterization of the material samples at various stages, and Komal Kooduvalli, Ryan Dicarlo and Payton Meyers for their involvement in the data collection, modeling, and analysis of the LCA section. Further data for the LCA was provided by Cheryl Smith, Dave Hartman, Anthony Console (Owens Corning), Joe Fox, George Koosis (Ashland & INEOS Composites), Shane Skop (Scale-up Research Facility, IACMI), Scott Pregler (Shape Process Automation), Mike Siwajek, Ohiole Aki, Tina Reifert (CSP), Ted Lesk (Complete Prototype Services), Stephen Young (UTK), Marko Gernuks, Marton Kardos (Volkswagen, Germany) and Hendrik Mainka, Thomas Laduch (Volkswagen, Chattanooga).
From Michigan State University the authors would like to highlight the contribution of Shane Skop for his support in many parts of the project; Dan Houston for his help with molding, surface quality evaluation and logistics; Jim Plaunt with molding and surface quality evaluation; and Brian Klotz and Dillon Elsworth with molding and logistics.
The contribution to the design and simulation work from Purdue University is very much appreciated, especially from Michael Bogdanor for the leading the design team and his work with the liftgate CAD design and structural analysis. Siddharth Pantoji for molding simulations and SMC characterization, Himal Agrawal for molding simulations, John Yang for topology optimization, Nathan Sharp for material characterization and R. Byron Pipes for the design, modeling, and directing the simulation Team.
This project could not have been successful without the support of the industry partners. The authors

would like to thank Continental Structural Plastics for their contribution to the project, Tina Reifert and Mike Siwajek in particular.

Furthermore, the authors express their gratitude to IDI Composites: Kevin M. Cahill (Director of Technology) and Darell Jern (Material Development Specialist) for their support in material development, SMC manufacturing and molding support.

INEOS (Ashland) played a crucial role in the project as well and the authors extend their gratitude to Joe Fox (Project Manager – retired) for his support in project management; Ed Zenk (Process engineer) for bringing in his vast expertise while molding the prototypes; Dan Dowdall (Business Development manager); Tom Skelskey (Lab Manager) and Lora Mason (Lab Technician) for their help with compounding the specialty SMC materials. George Koosis (Business Development manager), Jesse Wenning (Process Engineer), Zhouhui Sun (Product Manager) and Laura Gigas (Product Manager).

The authors' gratitude goes out to Owens Corning as well: Anthony Console (Global Key Account Manager), Dr. Amol Vaidya (Senior Global Innovation Leader) and Dr. Guang Sheng (Senior Engineer S&T) for their help with modeling, and Matthew Berning (Product Leader) for material selection.

From Volkswagen Group of America, special thanks to Michael Rademacher, Yassine Ghossi, Thomas Drees, and Wolfgang Maluche for their support to the project and their contribution to its success.

EXECUTIVE SUMMARY

DEVELOPMENT OF A CLASS A LIGHTWEIGHT SMC LIFTGATE
FOR THE VOLKSWAGEN ATLAS

Lightweight construction is an integral part of Volkswagen's overall strategy of reducing CO_2 emissions. Due to its low cost, steel is the most commonly used material for automotive exterior body panels today. Unfortunately, steel has a high density, resulting in a relatively low specific strength. Glass fiber based sheet molding compounds (SMC) provide high properties in combination with lower density. The high specific strength of SMC offers an enormous lightweight potential.

To unlock the full potential of SMC materials in combination with cutting edge manufacturing processes, Volkswagen Group of America worked together with IACMI (Institute for Advanced Composites Manufacturing Innovation) and the academic partners: University of Tennessee Knoxville, Purdue University and Michigan State University; as well as the industry partners: Ashland, IDI, Owens Corning and Continental Structural Plastics. Leveraging the expertise of all project partners, reaching over the entire supply chain the project demonstrated the potential of these materials.

This report will highlight the major steps in the development process on the way to technology readiness for SMC using the example of the Volkswagen Atlas Liftgate. Over the 36-month period of the project, the work focused on three R&D areas: material development, design and simulation, and development of the manufacturing process. Material selection included alternative fibers and resin systems, and accounted for material availability, properties, and cost-efficiency. The work undertaken in the field of design and simulation has pushed the envelope of short fiber reinforced thermoset molding compound process simulation. Design iterations were virtually tested, while the final design was used to validate the simulation software against physical parts. Manufacturing development used cutting-edge technology, while experts along the supply chain were working together to ensure the best possible results. In the final stage of the project, liftgates were molded, trimmed, bonded, painted and assembled before exhaustive testing.

The result is an e-coat (electrophoretic dip coating) capable Class-A SMC liftgate, which is ready for high-volume production, and can be used as a technology demonstrator. The prototypes manufactured in the scope of this work have exhibited a mass reduction for the Volkswagen Atlas liftgate of up to 35% compared to the series production steel version, without a degradation of the functionalities.

1.1 BACKGROUND

Volkswagen Group of America and IACMI hubs in Tennessee, Michigan and Indiana - Oak Ridge National Laboratory, The University of Tennessee, Michigan State University and Purdue University (collectively referred to as the IACMI in this report) jointly worked on a project to significantly reduce the processing cost, cycle time and the waste during the mass production of automotive composites parts.

This program combined the resources of an automotive Original Equipment Manufacturer (Volkswagen Group of America) and leading composites research and development institutions (IACMI and its core partners) to develop and demonstrate materials and high-volume manufacturing technologies for light weight automotive fiber reinforced components.

The project addressed all the priority criteria for research, development and demonstration efforts to be undertaken through IACMI.

The overall project goal was the development of a composite lift gate for volumes greater than 100,000 vehicles per year with manufacturing cycle times less than 300s. The high volume composite manufacturing includes a significant cost and weight reduction compared to the steel solution used today for the Volkswagen Atlas Liftgate.

IACMI was working in every process step together with the industry partner to realize these goals.

1.2 TECHNICAL RESULTS

For a new innovative composite lift gate, a process chain containing material development, construction and design, tool manufacturing (conventional and additive) and composite production was developed. In the field of material development, new fibers (e.g. basalt fibers) and new resin systems for SMC were established and characterized.

A complete part design and simulation of the most important load cases for the liftgate were performed. Full-size components were manufactured (at rate with given cycle time) and tested to validate materials, manufacturing process parameters, and end use requirements.

The high volume composite manufacturing processes using sheet-molding compound (SMC), were successfully demonstrated for achieving low manufacturing cycle times and the required surface finish.

1.2.1 Theoretical Framework

Design development and manufacturing demonstration of the Volkswagen Atlas liftgate selected for this project was subject to the following requirements dictated by the need to industrialize the processes for automotive mass production:

- Property target: same part properties comparable to a metal lift gate
- Weight saving target: similar weight to an Aluminum version of the lift gate
- Part cost target: production costs less than Aluminum version of the lift gate
- Saving tooling costs in comparison to conventional metal parts production
- Applicable for more than 100,000 parts per year
- Class-A surface quality

How these goals were successfully reached is described in the following sections.

1.2.2 Results

The project work was performed in the following areas:

- Material Development and Testing
- Design, Modeling and Simulation
- Tooling and Prototyping
- Life-Cycle-Assessment (LCA)
- Additive Tooling

1.2.2.1 Material Development and Testing

1.2.2.1.1 Tensile and Compressive Behavior SMC Only and SMC with glass fibers

Four tensile samples from both materials (see below) were evaluated for important microstructural parameters including fiber bundle orientation using X-ray computer tomography (XCT) and identifying local failure zones within the gage section of tensile samples using digital image correlation (DIC) as initial steps to develop structure-of material-property relationship for the SMC material.

- Neat SMC: Ashland's Arotran 740, 35% glass fibers.
- Over-molded SMC: continuous glass-fiber reinforcement (Vectorply's 0/90 biaxial prepreg, 9 plies of 12" x 12" on bottom) over-molded with an 11.75" x 11.75" SMC charge on top.

1.2.2.1.2 **Tensile Behavior of SMC Only and SMC with glass fibers**

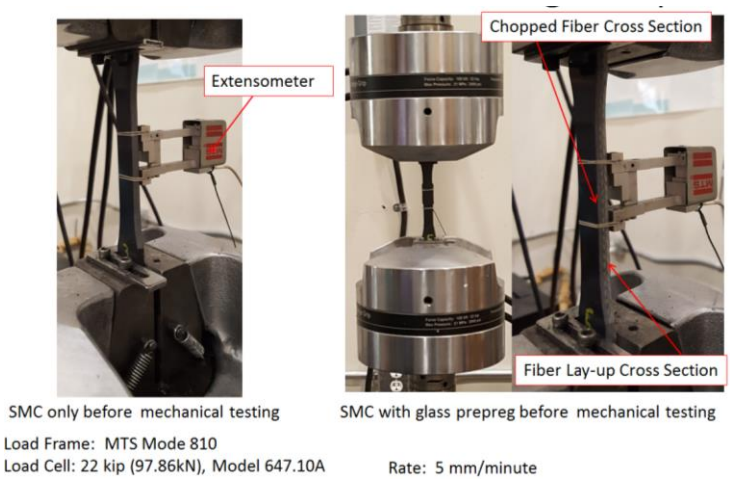

Figure 1. Tensile Testing of SMC Based Flat Panels for Mechanical Testing (ASTM D638).

Figure 1 shows the details of mechanical testing system that utilizes dog bone shaped samples based on ASTM D638. The results in Table 1 show significant increase in modulus and failure stress between SMC with glass fiber reinforcement compared to neat SMC as expected. As shown in Table 1, the average Modulus from Tensile Test for SMC only was 7,597 MPa with a minimum value of 5,852 MPa. Over molding resulted in an average tensile modulus of 15,935 MPa with a minimum value of 15,316 MPa. The tensile strength had an average value of 96 MPa with a minimum value of 80 MPa for SMC only; an average strength of 254 MPa for SMC with glass fibers. Figure 2 shows example failure behavior for SMC only and SMC with glass fiber after mechanical testing. The SMC only shows the specimen failure in a brittle behavior compared to SMC with glass fiber showing evidence of the delamination before mechanical failure. These delaminations are due to the difference in stress-strain behavior between the SMC and the prepreg side of the samples.

Table 1. Tensile Modulus and Strength for Glass SMC and Over Molding with Continuous Fibers.

SMC based Material	Width (mm)	Thickness (mm)	Tensile Modulus (MPa)	Tensile Failure Stress (MPa)	Tensile Failure Strain (%)
Mean SMC Only	12.98 (0.04)	4.58(0.09)	7,597(1,509)	96	3.55(0.18)
SMC with cont. glass fibers	13.00 (0.08)	5.35(0.02)	15,935(447)	254(12)	5.17(0.36)

Note: Standard deviation values in parentheses (four specimens were tested).

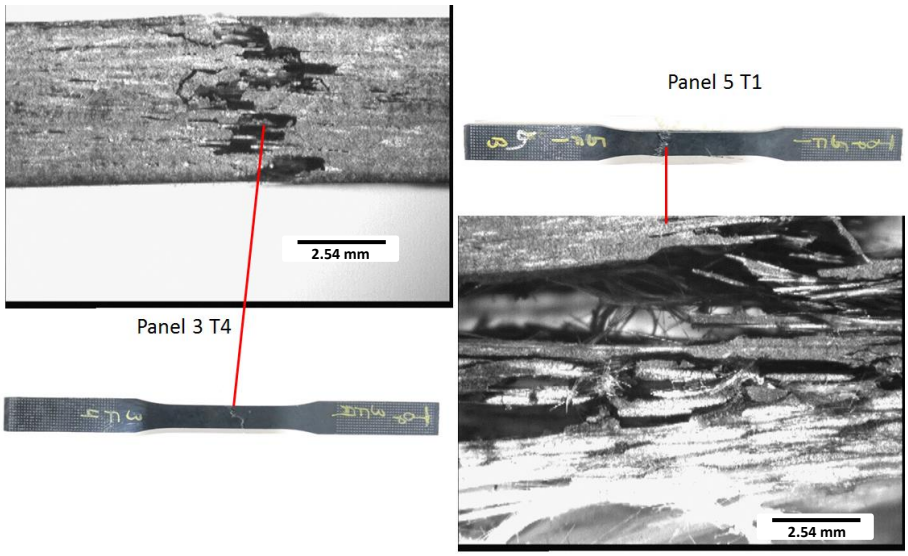

Figure 2. Optical microscopy image of cross section of SMC only (left) and SMC with glass fiber (right) after mechanical failure.

1.2.2.1.3 Tensile Behavior coupled with Digital Image Correlation (DIC) and Micro X-ray Tomography

The stress-strain behavior of tensile SMC only samples was evaluated using extensometer coupled with DIC to compare modulus values between the two techniques. Additionally, DIC technique was incorporated to identify evolution of local stress concentration region(s) within the gage region of the tensile samples when subjected to tensile load. Furthermore, the aforementioned microstructure of tensile samples obtained from XCT scans prior to mechanical testing afforded the ability to correlate local microstructure effects on failure zones (resulting from non-uniform stress concentration regions) as indicated from DIC results. As shown in Figure 3, the average tensile modulus for this particular sample was 5,101 MPa using extensometer compared to 5,237 MPa using DIC technique, indicating very good agreement (within a 3% range) between these two techniques.

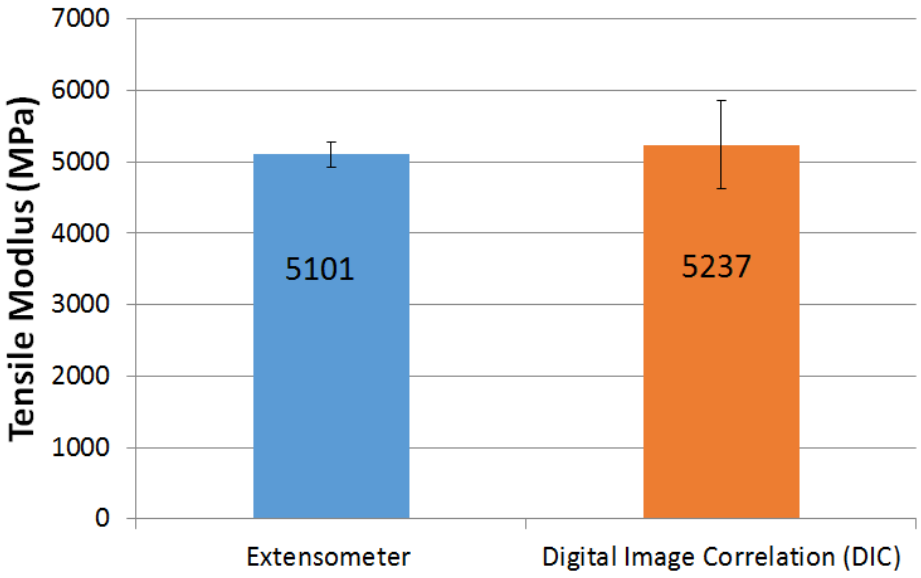

Figure 3. Tensile Modulus comparison for tensile samples using extensometer and digital image correlation (DIC).

The stress-strain behavior of tensile samples was evaluated using extensometer coupled with DIC to compare modulus values between the two techniques. Additionally, DIC technique was incorporated to identify evolution of local stress concentration region(s) within the gage region of the tensile samples when subjected to tensile load. Furthermore, the aforementioned microstructure of tensile samples obtained from XCT scans prior to mechanical testing afforded the ability to correlate local microstructure of failure zones within the samples to failure regions (stress concentration regions) indicated from DIC results.

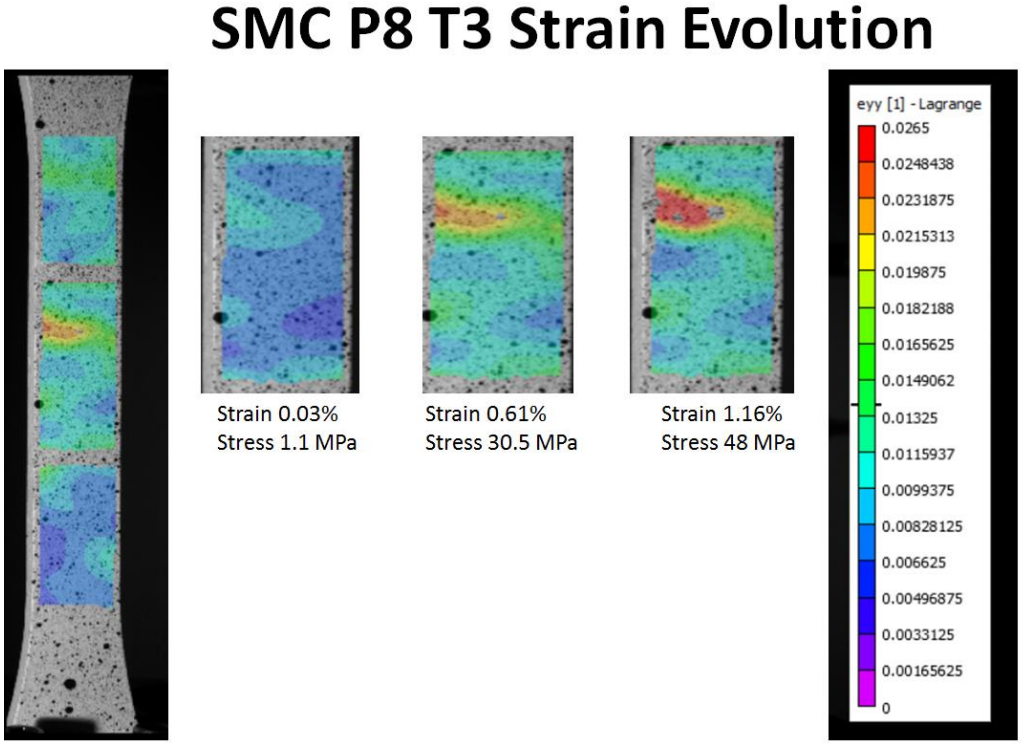
SMC P8 T3 Strain Evolution
Strain 0.03%
Stress 1.1 MPa
Strain 0.61%
Stress 30.5 MPa
Strain 1.16%
Stress 48 MPa
eyy [1] - Lagrange
0.0265
0.0248438
0.0231875
0.0215313
0.019875
0.0182188
0.0165625
0.0149062
0.01325
0.0115937
0.0099375
0.00828125
0.006625
0.00496875
0.0033125
0.00165625
0

(a)

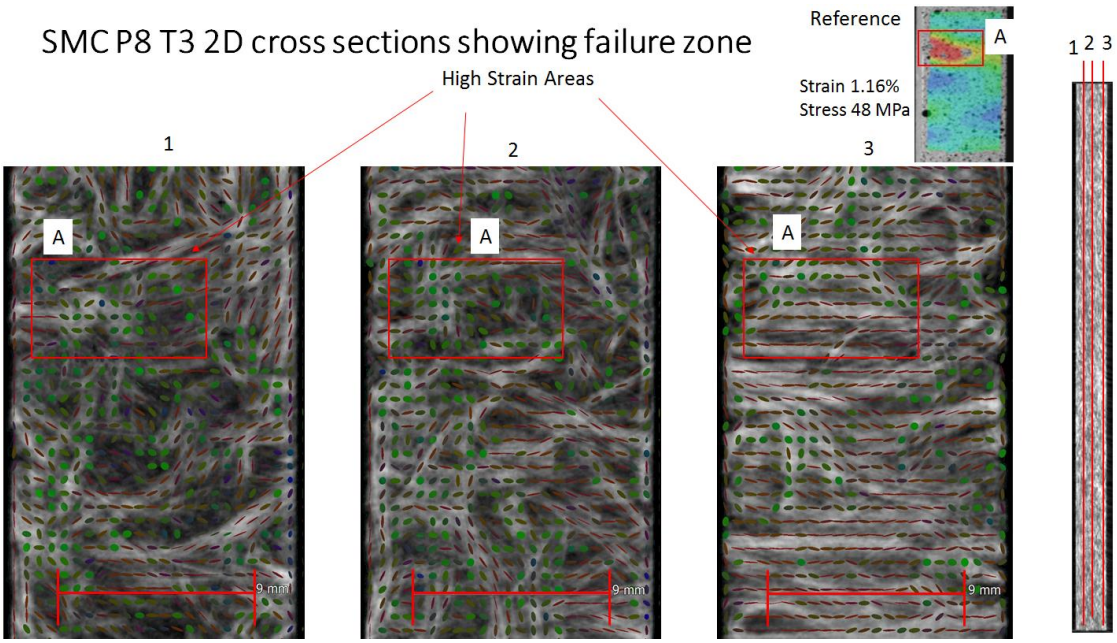
SMC P8 T3 2D cross sections showing failure zone
High Strain Areas
Reference
Strain 1.16%
Stress 48 MPa
A
1 2 3
1
2
3
A
A
A
9 mm
9 mm
9 mm

(b)

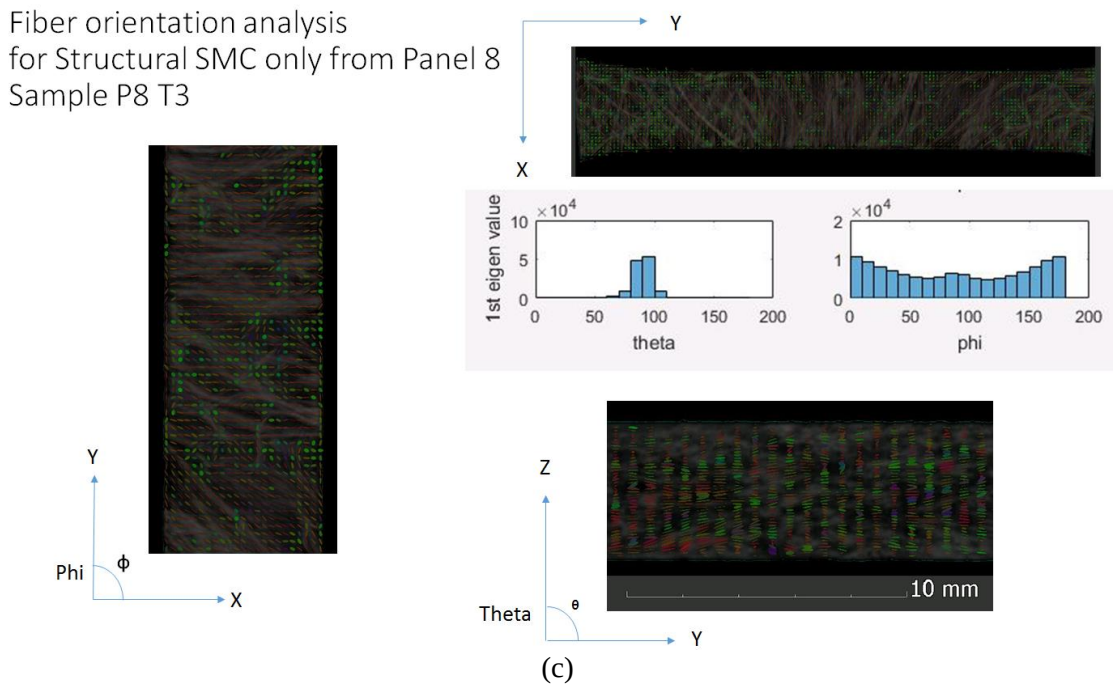

Figure 4. (a) Digital image correlation (DIC) showing deformation behavior during mechanical testing where the red regions indicate localized failure zones (b) Corresponding local failure zones regions in gage section of 2D reconstructed cross section of tensile sample before mechanical testing. (c) 2D reconstructed cross section of tensile showing fiber bundle orientation before mechanical testing.

Figure 4 summarizes the mechanical tensile behavior and fiber bundle orientation results for tensile samples from SMC panel. Figure 4 (a) and (b) shows localized fiber bundle orientation in horizontal direction correlating with stress concentration regions in red region in Figure 4 (a). This horizontal fiber orientation suggests that local failure occurred in these regions due to inadequate fiber bundle strength in vertical direction to sustain tensile load. Figure 4 (c) shows the fiber bundle orientation tensors for the tensile samples for two plane views, namely phi and theta. The tensile samples in this study showed unambiguous fiber bundle orientation in the theta plane view converging to approximately 90 degrees as shown in theta plots (Figure 4 (c)) and phi plane view showing a wider distribution of fiber bundle orientation in phi plots. These fiber bundle orientation tensor values suggests that the fiber bundles are oriented along the tensile (vertical direction) compared to horizontal direction in the gage section.

1.2.2.1.4 **Flexural Behavior**

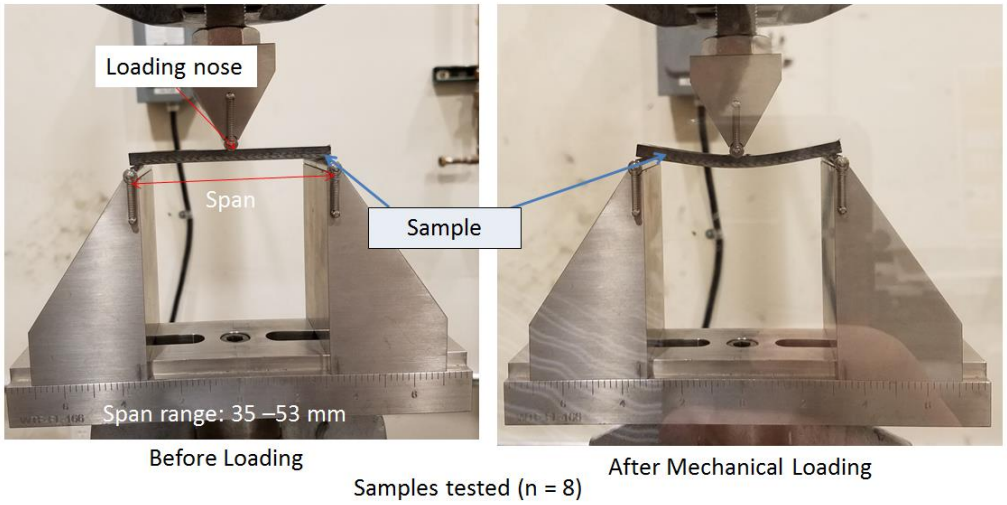

Load Frame: MTS Mode 810
Load Cell: 22 kip (97.86kN), Model 647.10A

(a)

(b)

Figure 5. (a) Flexural Testing of SMC Based Flat Panels for Mechanical Testing (ASTM D790). (b) Cross sections of SMC only and SMC with glass fibers before and after flexural loading.

Table 2. Mean Flexural Modulus and Failure Stress summary of the SMC only and SMC with glass fibers.

SMC based Material	Width (mm)	Thickness (mm)	Span (mm)	Flexural Modulus (MPa)	Flexural Failure Stress (MPa)	Flexural Failure Strain (%)
Mean SMC Only	18.96 (0.06)	4.58(0.22)	73.24(3.54)	6,959(1,510)	146 (42)	2.39(0.18)
SMC with glass fibers	18.98 (0.07)	5.42(0.04)	86.66(0.64)	14,101(683)	367(13)	3.13(0.19)

Note: Standard deviation values in parentheses.

Figure 5 shows the details of mechanical testing system that utilizes a coupon shaped sample based on ASTM D790. Table 2 summarizes the results, similar to tensile properties, showing significant increase in modulus and failure stress between SMC over molded with continuous glass fiber compared to neat SMC. As shown in Table 2, the average Modulus from Flexural Test for SMC was 6,959 MPa compared to 14,101 MPa after over molding with glass tape. The flexural failure stress had an average value of 146 MPa for SMC compared to 367 MPa with glass fibers. Figure 6 shows microstructural deformation modes for the two material systems, neat SMC shows a local flexural failure behavior compared to SMC with continuous glass fiber prepreg showing a significant amount of ductility with multiple delaminations before reaching final failure.

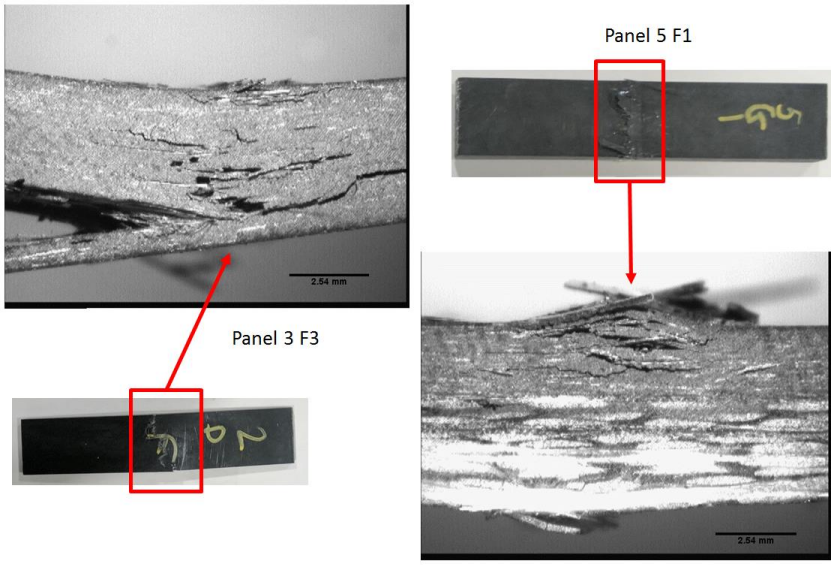

Figure 6. Optical microscopy image of cross section of SMC only and SMC with glass fiber flexural coupon samples after mechanical failure.

1.2.2.1.5 Influence of fiber volume fraction and fiber length on the evolution of pore content and the paintability of sheet molded compounds

The porosity defects from components molded using sheet molding compounds is a well-recognized issue. It is the major source of paint defects in exterior applications, hindering the widespread use of these materials despite their inherent advantages over metals and thermoplastics. This chapter discusses the influence of fiber volume fraction and fiber length on the permeability and pore content of class-A compounds. Compounds with varying glass fiber fraction and fiber length were compounded and compression molded analyze the influence of the aforementioned factors on the permeability of the fibrous network, the evolution of initial φ_{pi} to final pore content φ_{pf} and on the painted surface quality with regards to waviness and substrate-relevant paint defects. (M1: 5 wt% 0.5 inch; M2: 15 wt% 0.5 inch; M3: 5 wt% 2.0 inch; M4: 15 wt% 2.0 inch; M5: 10 wt% 1.0 inch; Benchmark Material: 29 wt%, 1.0 inch). Permeability indicates the resistance of the fiber network to being impregnated by a fluid with known viscosity. A fiber network with lower permeability is expected to allow for better pore transport, and thus less final porosity.

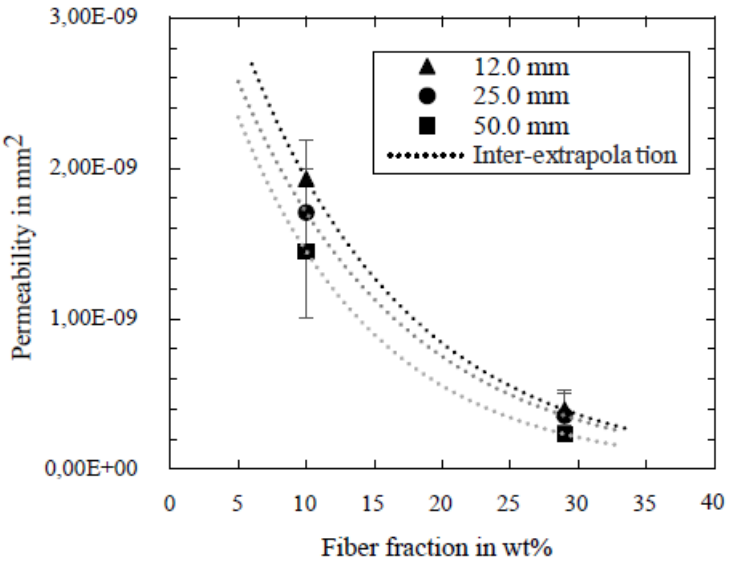

Figure 7. Permeability of fibrous network measured data with exponential trend lines.

As shown in Figure 7, while the fiber content has a very pronounced effect on the permeability values, increasing the fiber length four-fold merely leads to a 1/3 to 2/3 increase in the permeability values for the 5 wt% and 15 wt% trials, respectively. Based on these results one can expect better pore transport and thus, lower final pore content in compounds with shorter fibers and especially with lower weight fraction (W_f).

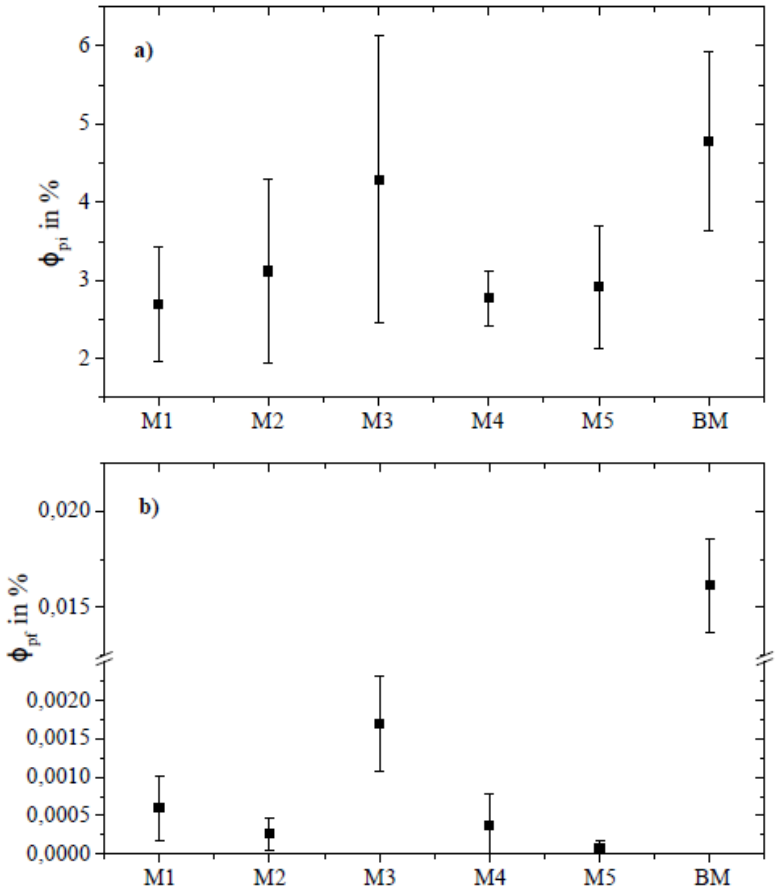

Figure 8. (a) Initial pore content φ_{pi} of compounded materials and (b) final pore content φ_{pf} of compression molded samples as measured via CT analysis. Note the break in the y-axis, as the final pore content of the commercial benchmark material (BM) compound was more than an order of magnitude higher than that of the compounds.

As Figure 8 (a) shows, the φ_{pi} of all investigated materials were in the same range, from 2.5 to 4 v%, seemingly inconclusive with regards to the effect of the investigated fiber parameters. The effect of fiber weight fraction in the investigated range - between 5 wt% and 15 wt% - seems to be negligible on the φ_{pi}. The benchmark material was also analyzed via the same method, although compounded separately at the industrial production facility of the material supplier, to serve as an indicator of the pore content for a state-of-the-practice commercial SMC material. The final porosity, however, is heavily dependent on the fiber parameters. Results indicate that lower fiber fractions lead to decreased pore contents and thus, improved paintability.

1.2.2.1.6 **Basalt Fiber Based SMC**

The basalt fiber materials from Mafic were considered for this study using two types of fiber products with varying linear density, the 300 tex (13 µm) and 500 tex (17 µm) fibers which typically give

optimum performance in tensile strength, modulus, and strain to failure. In addition to that Mafic supplies 4800 tex (17 µm) basalt fibers specifically for use in the SMC material development due to lower cost. For the targeted SMC application, UTK investigated 4800 tex material whose properties were based on single fiber tests. Tow properties were measured with tensioned tows manufactured according to recommended practices followed by carbon fiber manufacturers for consistency.

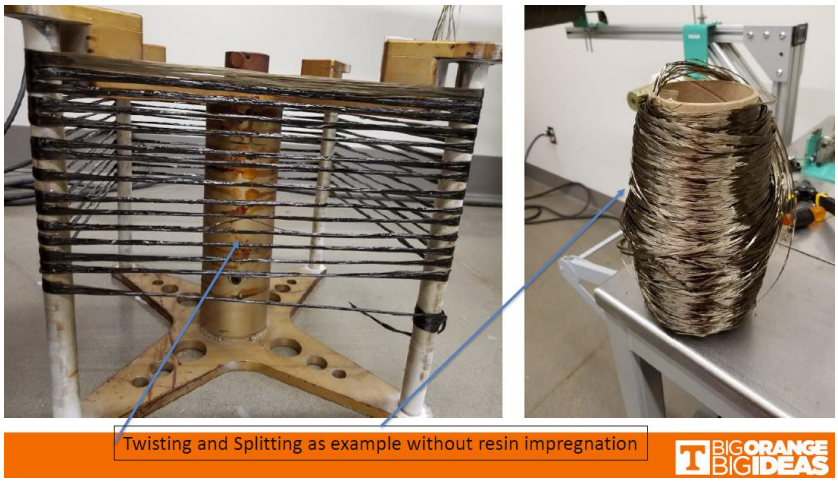

Figure 9. Epoxy Infused Basalt Fiber (4800 tex) Tows for Mechanical Testing (ASTM-D4018).

Table 3. Mean Tensile Modulus and Failure Stress summary of the infused basalt fiber tows.

Calculated Linear Density (g/cm)	Measured Fiber Density (g/cm^3)	Tensile Modulus (MPa)	Tensile Failure Stress (MPa)	Tensile Failure Strain (%)
0.0493	2.629	92,290 (5,440)	2,571 (192)	3.90 (0.56)

Note: Standard deviation values in parentheses.

The infused basalt fiber tows (Figure 9) considered for SMC development showed an average tensile strength of 2.5 GPa and a tensile modulus of 92 GPa with an axial failure strain of 3.9%. These properties are quite good and exceed the modulus of glass fibers with good ductility (Table 3). Thus, these fibers are found to be suitable and adequate for SMC development using basalt fibers.

1.2.2.1.7 Characterization of the physical and mechanical properties of the Basalt fiber SMC test panels

SMC Panels (Figure 10) made using 4800 tex Basalt Fiber with a sizing suitable for epoxy resin and Hexion optimized epoxy system were evaluated for mechanical characterization. Fiber weight fraction of SMC plates was 65 wt%.

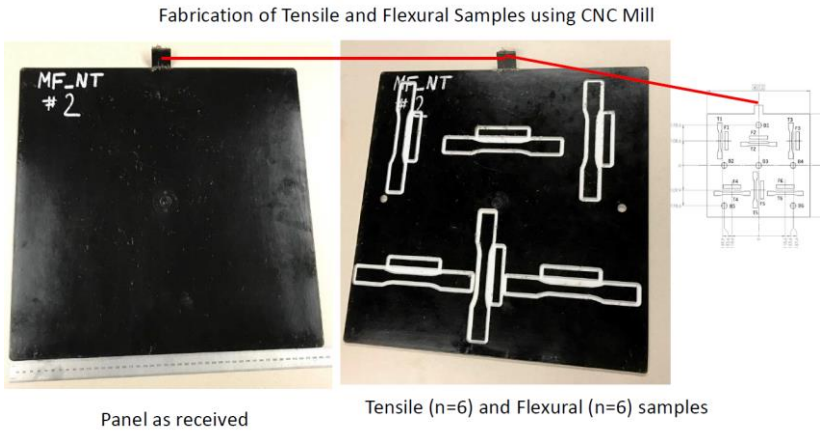

Figure 10. Epoxy Infused Basalt Fiber SMC Panel and Location of Tension and Flexure Samples Obtained Using SMC.

Tensile dog bone samples (Figure 11) were extracted using suitable cutting tools using a CNC machine and tensile behavior evaluated using ASTM D638 standard.

Characterization of the physical and mechanical properties of the Basalt fiber SMC test panels

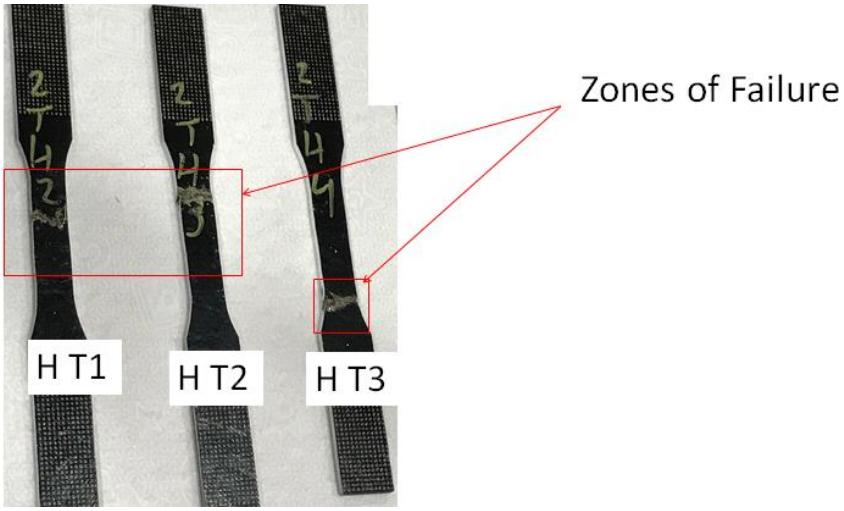

Figure 11. Tensile samples after mechanical failure.

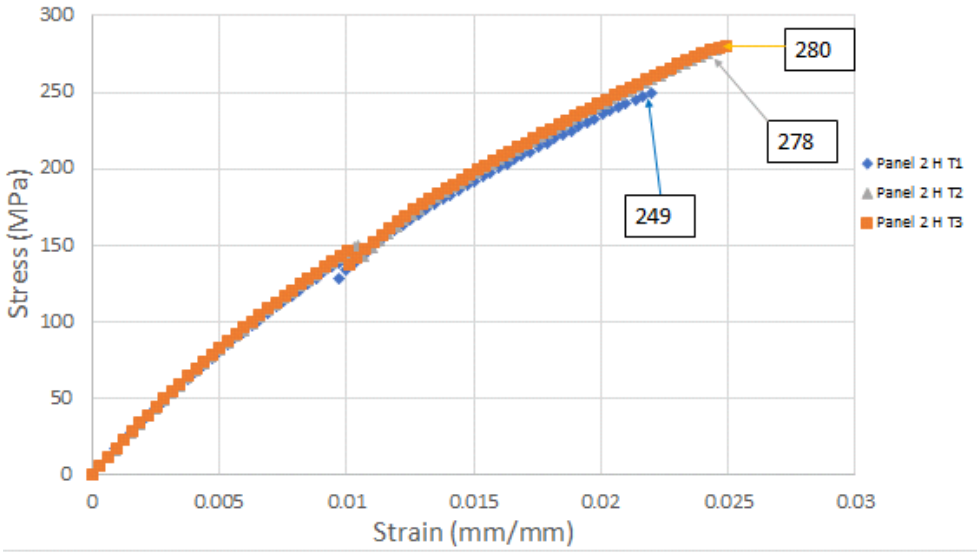

Figure 12. Stress-strain behavior of tensile samples.

Table 4. Tensile Test Results from Flat Panel Using Basalt SMC Charge.

Panel	Sample ID	Thickness (mm)	Width (mm)	Failure Stress (MPa)	Modulus (Gpa)	Engineering Failure Strain (%)
2	H T1	3.07	12.37	249	16	2.20
2	H T2	3.13	12.40	278	16	2.45
2	H T3	3.07	12.34	280	17	2.49
	Average	3.09	12.37	269	16	2.38
	Std Dev	0.03	0.03	17.3	0.53	0.16
	Max	3.13	12.40	280	17	2.49
	Min	3.07	12.34	249	16	2.20

Figure 12. and Table 4 summarize the results where the average Modulus from Tensile Test was 16 GPa with a minimum value of 16 GPa. The tensile strength had an average value of 269 MPa with a minimum value of 249 MPa.

1.2.2.1.8 **Low Cost Carbon Fiber Based Material System**

Two types of low cost carbon fibers were considered for possible SMC application. One of them was based on large tow textile PAN and the other was Zoltek's PX35. Both materials were made into fabric format and infused with epoxy resin using VARTM technique to compare mechanical properties

summarized as below.

Table 5: Mechanical Properties of Carbon Fiber Candidates for SMC in Continuous Format.

Vacuum Infused		
Property (Cross-ply)	**LCCF (41% V_f) Epoxy**	**Zoltek (48% V_f) Epoxy**
Tensile strength (MPa)	550 (79.77 ksi)	700 (101.52 ksi)
Tensile modulus (GPa)	60 (8.7 Msi)	58 (8.41 Msi)
Flexural strength (MPa)	600 (87.02 ksi)	750 (108.77 ksi)
Flexural Modulus (GPa)	50 (7.25 Msi)	48 (6.96 Msi)
ILSS (MPa)	TBD	48 (6.96 ksi)

As can be seen from Table 5, the low cost carbon fiber (LCCF) from the Carbon Fiber Technology Facility (CFTF) performed well for stiffness-based applications providing results similar to or better tensile and flexural modulus compared to Zoltek carbon fiber. Thus LCCF is a promising candidate material for carbon based SMC material development and for chopped fiber based Injection molded and BMC based materials for automotive applications.

1.2.2.2 Design, Modelling and Simulation

The design, modeling, and simulation effort for the SMC liftgate was led by the Composites Manufacturing & Simulation Center (CMSC) at Purdue University, with regular input from the project team and significant support in design guidance and final CAD model review and release from Continental Structural Plastics (CSP). The workflow to redesign the liftgate based on its manufacturing-informed performance using SMC is outlined in Figure 13. The starting point for the liftgate design was the current steel liftgate construction for the vehicle. Redesign of the assembly for SMC included the consolidation of multiple parts to reduce assembly operations, incorporation of ribs and local part thickening to improve structural performance, and limited exterior surface redefinition to meet molding condition requirements. The final SMC design was required to retain the studio surface for the exterior panel and maintain all internal interface points for the equipment supported by the liftgate including the interior thermoplastic trim panels. Design and modeling of the SMC liftgate was performed in CATIA from Dassault Systemes. Simulation of the liftgate incorporated the manufacturing-informed performance of the structure in design optimization using multiple software

packages including Moldex3D from CoreTech System Co. for molding simulation, Digimat from e-Xstream Engineering to map local material properties of the composite to the structural model, and Abaqus from Dassault Systemes for finite element analysis of the structural performance of the model. The final design from Purdue's CMSC was provided to the tooling supplier for the project at Century Tool and Die after final review and detailed design from CSP. This design was successfully molded and assembled in the later phases of the project with overwhelmingly positive results. The remainder of this section provides more detail into each of the steps in Figure 13 that led to the successful lift gate design.

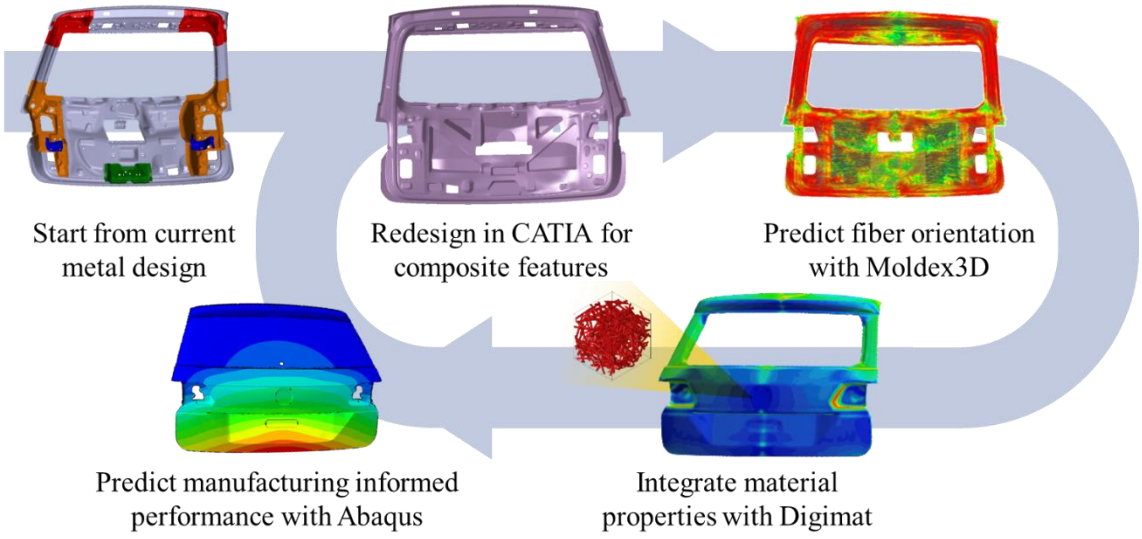

Figure 13. Process flowchart for manufacturing-informed performance design.

1.2.2.2.1 Steel Baseline Model and Design Requirements

The current design of the liftgate consists of twelve separate stamped steel parts that are assembled through a combination of welded and adhesively bonded joints. The parts of the current steel design are shown in Figure 14. In addition to the tooling and production costs associated with manufacturing each of the individual parts, the assembly operations required to join the parts together represents a significant portion of the overall cost of the liftgate. The combined mass of these twelve steel parts is roughly 23 kg and the dimensions of the assembly are shown in Figure 15. The liftgate assembly is designed to pass several load cases defined by Volkswagen to satisfy the look, feel, and finish requirements for the component. It is not part of the energy management system for the vehicle during crash and impact events, and therefore dynamic analysis is not required for the part design.

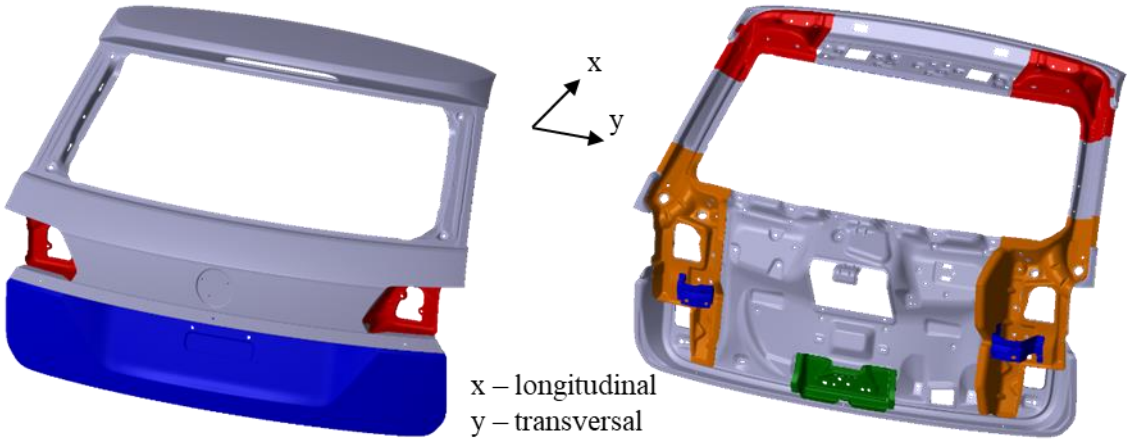

Figure 14. Existing Steel Design with twelve separate stamped parts.

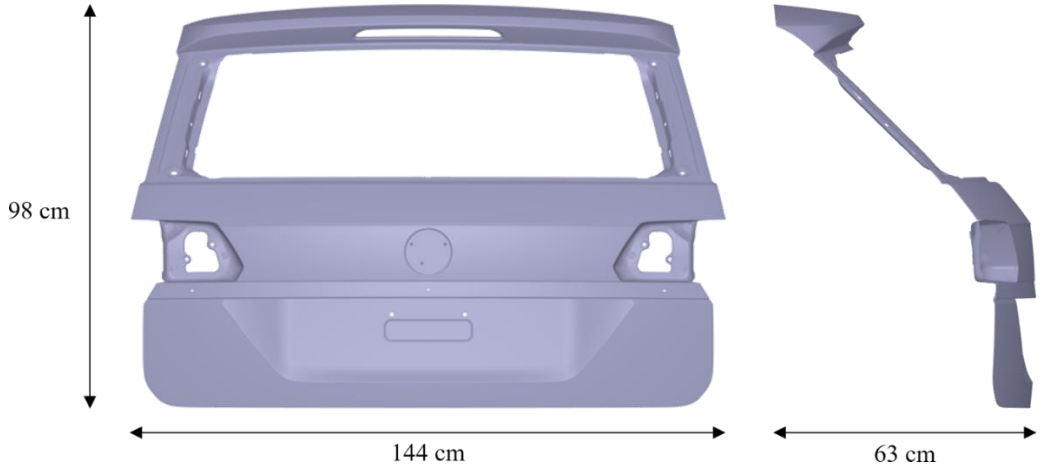

Figure 15. Dimensions of the assembled liftgate in the axes of the vehicle coordinate system.

The redesigned liftgate is intended to be a “drop-in” replacement for the current steel version. The performance of the SMC liftgate was required to be comparable to that of the current steel version to fit the overall design requirements for the vehicle. While maintaining the current level of performance, the SMC redesign was intended to reduce the number of individual parts from twelve down to three, with a mass comparable to a conceptual aluminum version, which was roughly 70% of the mass of the steel version, which equaled 16.1 kg. The mass reduction and part consolidation were accomplished through utilizing the geometry flexibility afforded by the compression molding process.

One of the most critical design considerations for the assembly was that the outer panel was required

to maintain a Class-A surface finish. In addition to the surface quality, several surfaces from the current steel design were required to remain unchanged in the SMC redesign. These unchanged surfaces included the exterior studio surface for the outer panel including the edges of part, the interface surface for the rear window glass, the weather-sealing surface on the inner panel, and the attachment points for the taillights, emblem, electronics, wire harnesses, lock mechanism, hinges, stop buffers, gas strut mounts, and thermoplastic interior trim panel. These surfaces on the inner panel are shown in Figure 16. The red loop surface near the extents of the liftgate is the surface where the weather sealing for the assembly is attached to create a watertight seal for the structure. Inside of this region, a thermoplastic trim panel covered the inner structural panel from view. The inner structural panel for the liftgate was permitted to deviate from the steel surface in these regions if the attachment surfaces and the holes remained in the same locations. The exposed surface of the inner panel outside of the weather seal was intended to remain largely unchanged to maintain the same look as the steel version, but slight modifications were allowed in order to increase bond width between the inner and outer panels and improve moldability.

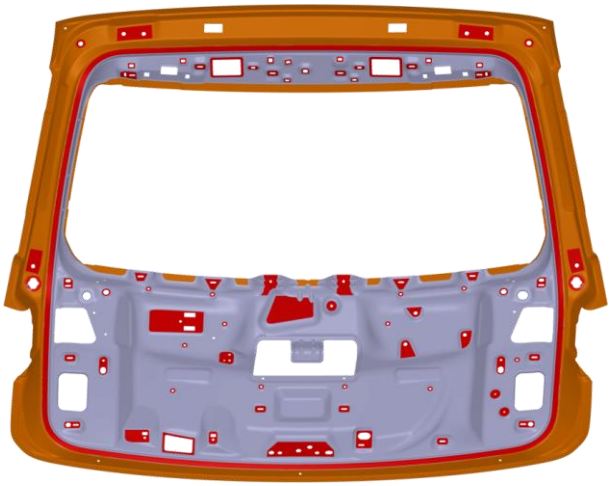

Figure 16. Surfaces of the steel inner panel to remain in the SMC redesign. Red indicates interface surfaces that are immovable; orange indicates surfaces that should remain unchanged, but can be modified out of design necessity.

The structural analysis of the liftgate for this design effort was performed against six critical load cases that were selected by Volkswagen from the full design specification for the component. The down-selected loading cases provide a broad representation of the important performance criteria for the assembly while reducing the complexity of the analysis. The load cases shown in Figure 17 included torsion of the stop buffer, torsion of the edge, bending of the stop buffer, bending of the lower edge, bending of the roof frame, and eccentric flexural rigidity of the liftgate. Each of these load cases

assessed the stiffness of different critical regions of the liftgate for ensuring the proper feel during operation for end users. Out of these load cases, bending of the stop buffer and bending of the lower edge were the most challenging load cases to pass for any construction method of the liftgate.

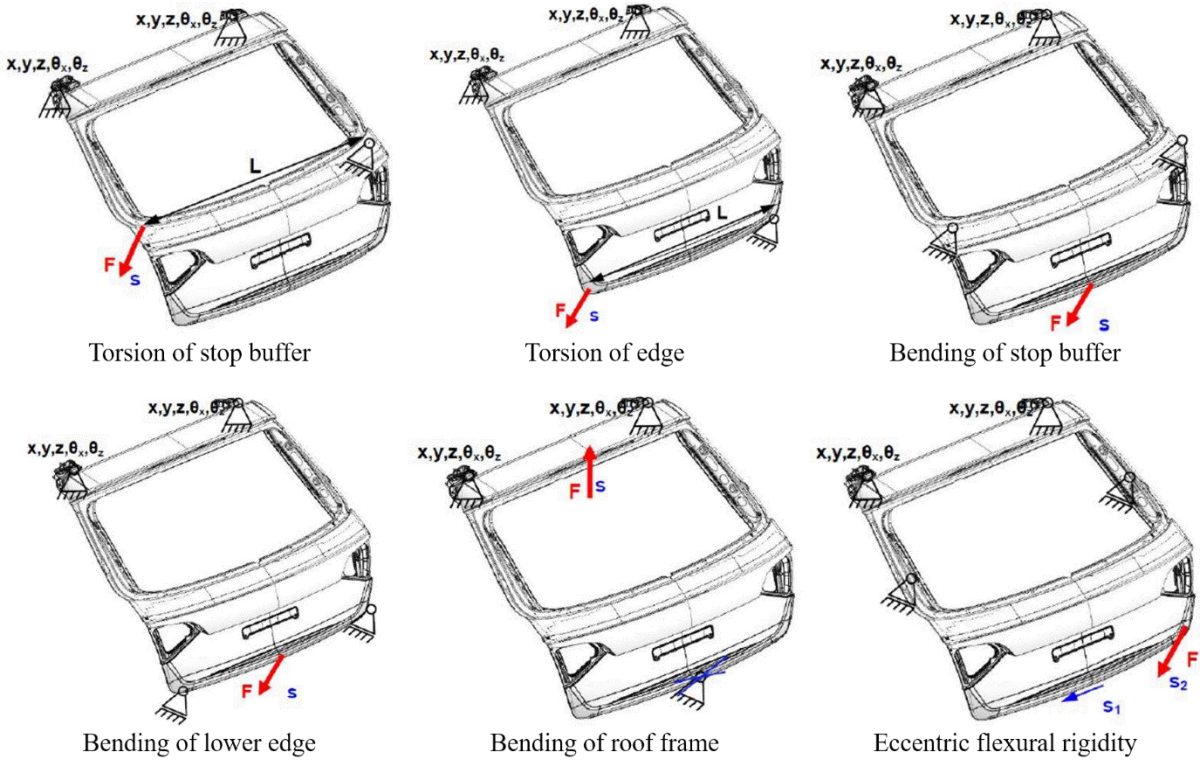

Figure 17. Load cases provided by Volkswagen for structural analysis of the liftgate assembly.

The first set of analyses in the design effort was performed on the current steel version of the liftgate. This was done to verify that the structural analysis approach to be used in evaluating the performance of the redesigned liftgate is aligned with the design intent of the load cases. The geometry of the twelve separate steel parts were taken from CATIA model of the current steel design and meshed in CATIA using the "Octree Tetrahedron Mesher" with a nominal element size of 15mm using 3D quadratic tetrahedron elements. The adhesive connecting the various steel components was explicitly modeled in the finite element analysis to capture the connectivity between the subcomponents and was meshed using the same approach. Weld locations were taken from the CATIA model and used to create tie constraints between the joined surfaces in the model. The steel was modeled as linear elastic with a Young's Modulus of 200 GPa and Poisson ratio of 0.3, whereas the adhesive was modeled with Young's Modulus of 5000 MPa and Poisson ratio of 0.3. The loading and boundary conditions were applied to the model as described in the loading specifications and the linear elastic analysis was

performed in Abaqus. The results of the static analysis for the steel liftgate show that the current version passes all the defined load cases from Figure 17. The deformed shapes of the steel liftgate assembly are shown in Figure 18 for each of the load cases. The actual values of deformation removed due to their proprietary nature. Based on this analysis and coordination with the Volkswagen team, there is a reasonable degree of confidence that the loading cases are being modeled correctly in the analysis and the basic approach will be suitable for the analysis of the SMC redesign.

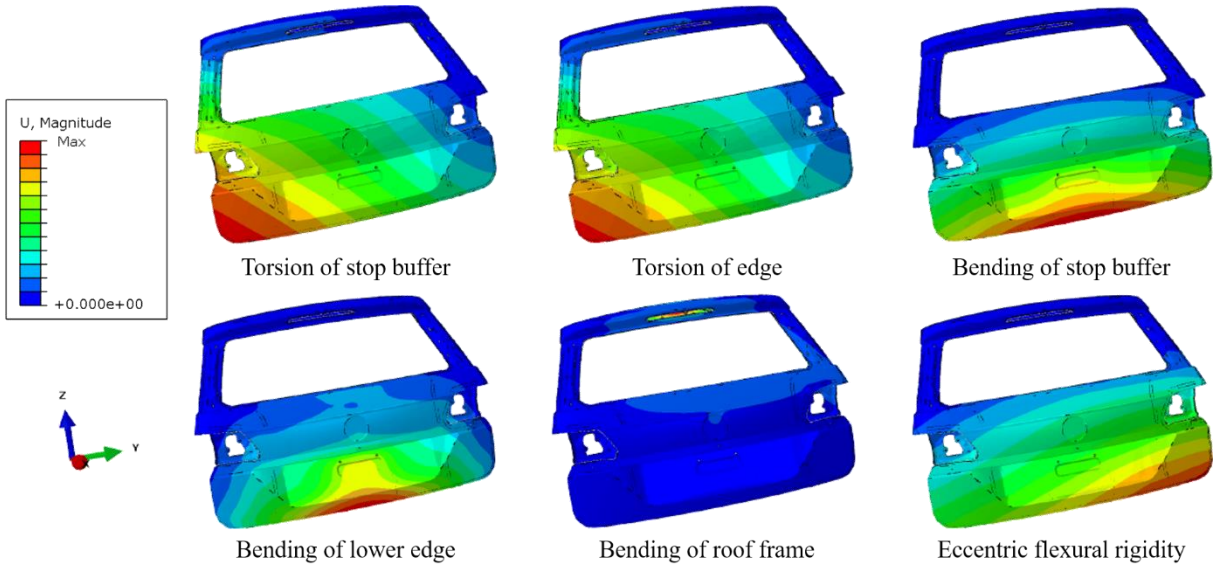

Figure 18. Contour plot of the magnitude of deformation for the steel baseline liftgate model for all six load cases.

1.2.2.2.2 **Liftgate Redesign for SMC Production**

The general design approach for the SMC version of the liftgate centered on combining the four separate parts of the exterior panel, including the insets for the taillights, into a single molding cavity. Similarly, the main inner panel was designed to integrate the functionality of the seven remaining reinforcing parts utilizing the additional design flexibility afforded by the flowability of the SMC. Several geometric features were incorporated into the SMC redesign to improve the structural performance of the panels and improve their moldability. Unlike stamped panels, which are limited to the shapes that the 2D sheet can conform to, the molded SMC material can produce 3D topologies without such restriction. For the outer panel, the tail light insets, for instance, required separate stampings as a single sheet of steel could not be deformed into the deep pockets of the geometry. For the inner panel, the ribs and stiffeners required for structural stiffness are not possible with stamping.

Two grades of commercially available SMC material were selected for this project and provided by IDI Composites. These materials were deemed the best choice to proceed with, based on a material selection process, accounting for mechanical properties, availability and the application-specific business case. Since the basis of comparison was the original steel design, the application of low cost carbon fiber did not fit the business case. Although basalt fiber properties and prices were both fulfilling requirements in the material selection process, the epoxy resin of the material would not be able to withstand the high temperature e-coating process.

S31-31T-29 is a class-A vinyl ester-based SMC with 29% glass fiber content by weight. STC2450 is likewise based on a vinyl ester resin but is intended for structural applications and has 50% glass fiber content by weight. The density of the STC2450 is 1.6 g/cc and the S31-31T-29 is 1.9 g/cc due to the various additives that are included in the formulation to provide the Class-A finish.

One of the primary concerns in the design of SMC parts for manufacturability is the interaction of the part geometry with the part-specific molding direction. Molding direction denotes the angle at which the main plane of the part is set concerning the mold opening direction. This includes the orientation of the shear edges at the edge of part and the draft angles on interior features like ribs and vertical walls. It is also a key concern on the design of the outer panel where the Class-A surface is required. The relative orientation of the Class-A surface to the molding direction has a significant impact on the pressure that is experienced locally in the part. As a general reference, a Class-A surface requires that the angle between the surface tangents and the molding direction, i.e. the draft angle, should be greater than 15°. Figure 19 shows the draft angle analysis of the initial surface of the joined outer panels with the molding direction aligned to the longitudinal axis from the vehicle coordinate system, as shown in Figure 14. Based on this analysis, there are several regions that do not have the required draft angle for a class-A surface. The insets for the taillights show a draft angle that is less than 15°, but greater than 5°. Since these surfaces will not be exposed when the tail light is in place, the Class-A requirement is not necessary, and the 5° angle is enough for moldability. Another consideration for this region is that the steep surfaces for the lights are at opposing angles to one another, which means that the lower region of the liftgate is required to be molded with the molding direction aligned with the longitudinal axis of the vehicle.

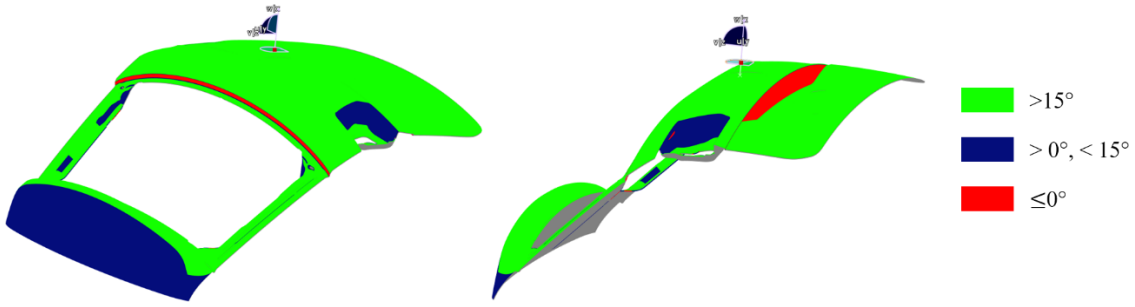

Figure 19. Draft angles from original studio surface of the liftgate.

There are three more regions in the outer surface of the liftgate that are not compatible with the molding direction required by the tail light region and the need for a 15° draft angle: the region above the license plate, the region below the window, and the top of the spoiler. The surface quality requirement on the region above the license plate is relaxed from the Class-A standard due to being obscured from view by its location and additional design elements. The surface is also able to be rotated slightly to get away from the initial 0° draft angle. The small region below the window, while still requiring a 15° draft angle for a Class-A surface, was able to be modified from its initial angle to achieve the required angle. The top surface of the spoiler, however, cannot be modified from the initial geometry.

As the lower section of the outer panel requires that the molding direction be along the vehicle longitudinal axis and the upper section cannot use this molding direction, the outer panel must be split into two separate parts. Out of the candidate locations for splitting the geometry, the most straightforward approach was to separate the outer panel where the pillars at the sides of the window connect to the lower section of the panel. For the prototyping effort in this project, the two separate parts can be configured in the tool to be molded in a single cavity, separated using the waterjet when the other holes and openings are cut in the part, and then assembled together using a tabbed connection for additional stiffness before being joined to the inner part. This configuration is shown in Figure 20. To balance the draft angle on the top and bottom surfaces of the spoiler, the top section of the outer panel was rotated 25° as shown in Figure 20. This also reduces the overall depth of the molding cavity and the resulting size of the molding tools.

Limited additional changes were made to the outer panel beyond combining the panels and dividing the resulting surface for draft angle. Ribs and rapid thickness changes in the SMC panel can have a detrimental effect on the Class-A finish through rib read-through that presents during the initial

molding where residual stress and non-uniform curing. As such, these features were limited to the inner panel. One variation for the outer panel that was applied was the incorporation of a return flange around the exterior edge of the panel to provide a clean edge appearance. This feature is shown in Figure 21. The nominal thickness of the outer panel was selected to be 2.75 mm based on best practices for the class-A finish.

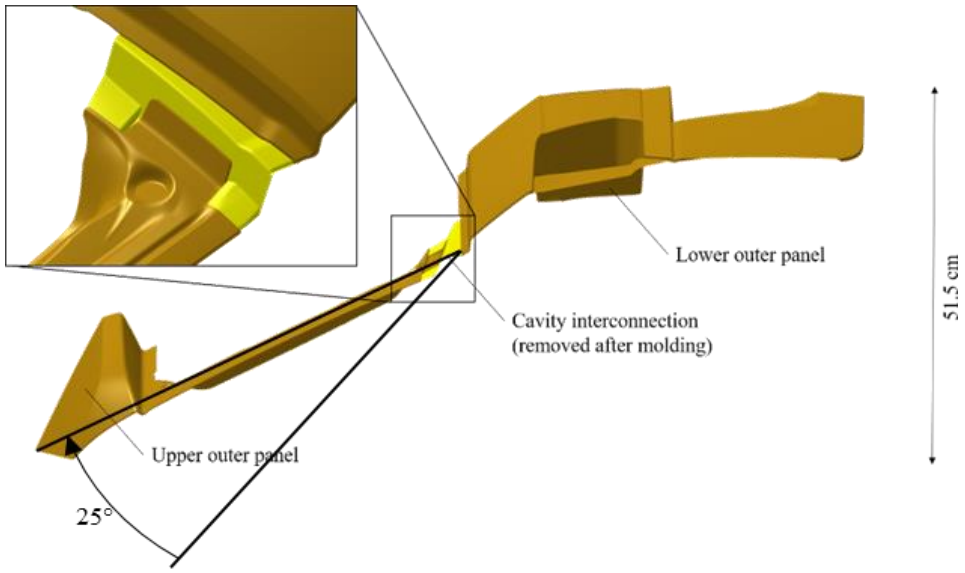

Figure 20. Modification to outer liftgate molding strategy to accommodate molding angles and combine molding cavities.

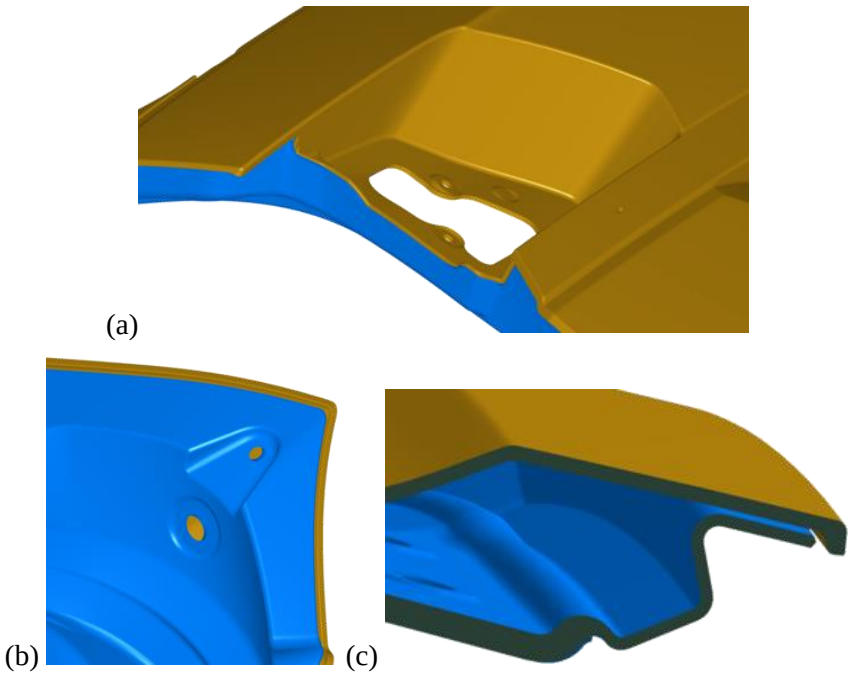

Figure 21. Locations for return flanges to be added to outer.

As a preliminary exercise to guide the redesign of the inner panel, a non-parametric topology optimization was performed on the liftgate assembly to identify regions where additional reinforcement would be required. To perform this analysis, the main inner and outer panel surfaces were used to bound the volume of the liftgate, and the entire inner region of the volume was meshed. The topology optimization was performed with Tosca, using the Abaqus finite element solver, to reduce the volume of the active mesh while maximizing the performance of the liftgate against the six load cases provided. As this is a conceptual design step, the resulting geometry in Figure 22 is not meant to provide a directly manufacturable result, but rather guide the engineers and designers in the detailed design effort for where to place reinforcing elements. From this analysis, significant stiffening is required in the pillar sections (windshield frame). Furthermore, additional reinforcing elements are required across the lower section of the liftgate to provide stiffness across the lower edge, and significant redesign is required across main portion of the liftgate for bending and torsional stiffness. For the pillar region, the best option for providing stiffness is a repeating rib structure. For the lower section, the capability of the SMC to flow into deep pocket shapes allows the inner panel surface to be entirely redesigned to provide additional contact with the existing outer panel and increase the section modulus of the assembly through elements that are perpendicular to the outer panel structure and the effective axes of bending for the load cases.

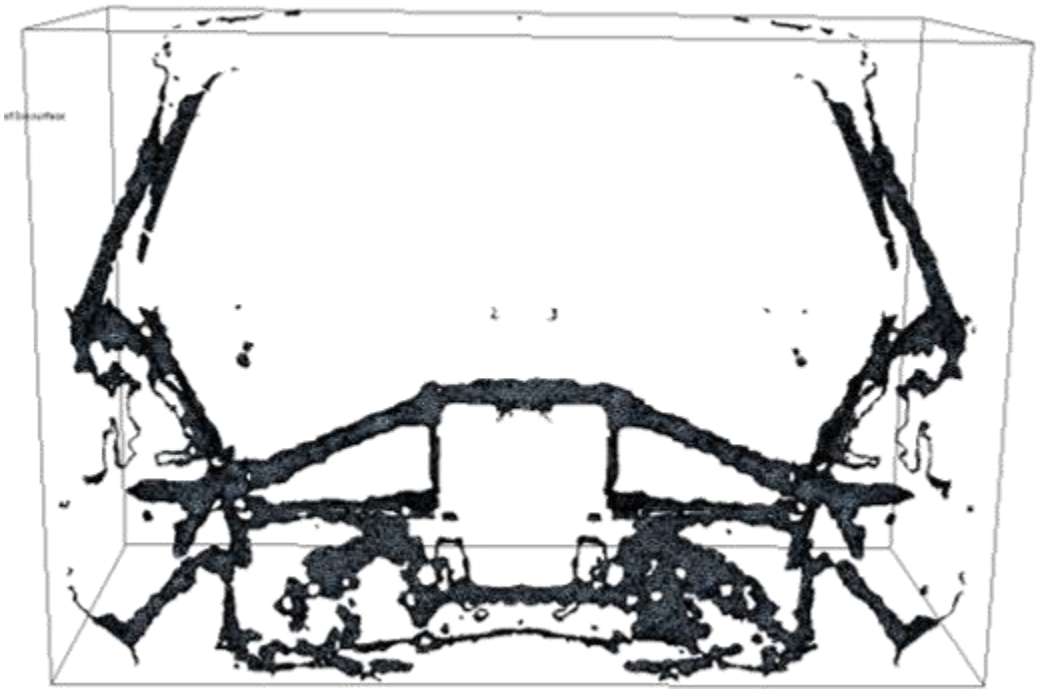

Figure 22. Results of the preliminary Tosca topology optimization.

The molding direction for the inner panel is somewhat more flexible than for the outer panel. Accordingly, the molding direction for the inner panel shown in Figure 23 was selected to minimize the volume of the tools required to mold the inner panel. This molding direction impacts the geometry of any ribs and stiffeners that are added to the inner panel such that the draft angle on these features yields a moldable result. Design of the inner panel considered both the manufacturability of the part and the manufacturing-informed performance of the resulting structure. From a manufacturability standpoint, several design guidelines were followed to ensure that the part was able to easily be removed from the tool. Additionally, the part is designed to avoid tall, thin sections of metal on the tool that are susceptible to deformation and inadequate heating during the molding process.

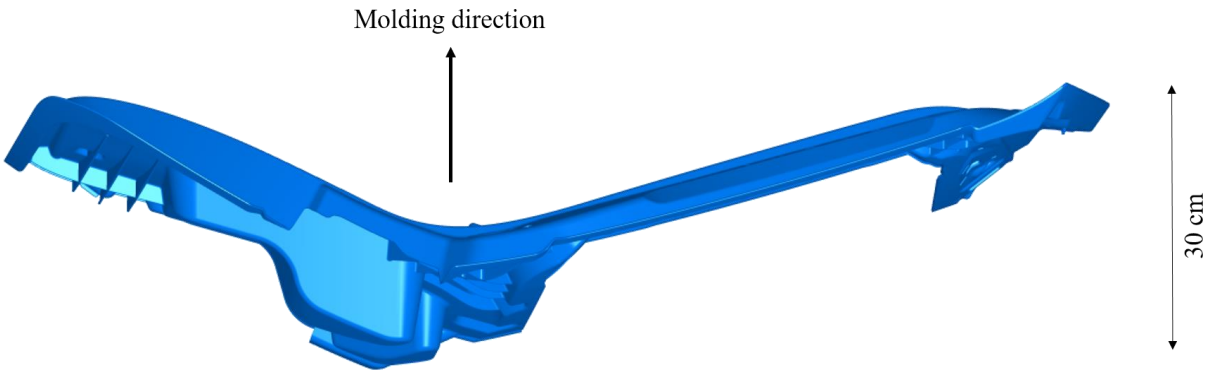

Figure 23. Molding direction for inner panel to minimize tool volume.

The resulting draft angles for the surfaces of the inner panel with respect to the molding direction are shown in Figure 24. The nominal thickness of the inner panel was 2.25 mm based on current best practice, with local regions thickened by up to 40% to provide additional stiffness or local support for the presence of attachments, such as the lock, hinges, stop buffers, and gas struts. The pillar sections are designed with ribs that are nominally 2 mm thick with a 1.5° draft angle on either side for moldability. The spacing between the ribs was decided to balance the stiffness provided by the geometry while maintaining enough material in the tool to ensure adequate heating and stability. The walls of the deeper draw stiffeners in the main region of the panel were designed with a greater degree of draft to improve demolding. Special care was given in the fillet radius for the standing ribs and the base of the stiffeners to permit the glass fibers to flow into these regions during the molding process. This is necessary to avoid fiber-matrix separation during flow.

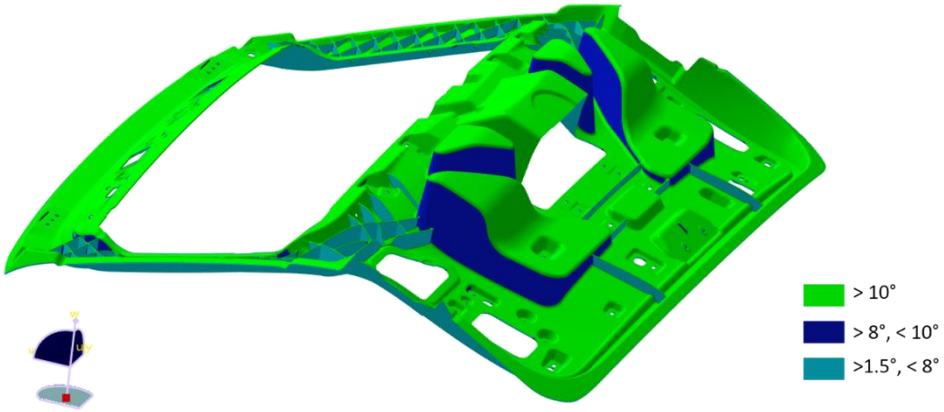

Figure 24. Draft angles for the redesigned SMC liftgate with respect to the molding direction.

The inner and outer panels of the liftgate are joined around the edges and under the emblem and the license plate using an epoxy adhesive. Slight modifications we made in the surface of the inner panel to increase the width of the bonding flanges to a target of 25 mm. The region under the window and around the tail light insets were also modified to increase the contact between the two panels along the edges. Mastic drops were added to locations where the deep pockets in the inner panel were designed to contact with the outer panel. The epoxy adhesive was not used in these regions the adhesive bonds would read through to the outer panel during the painting process. The mastic drops do not typically exhibit this same effect.

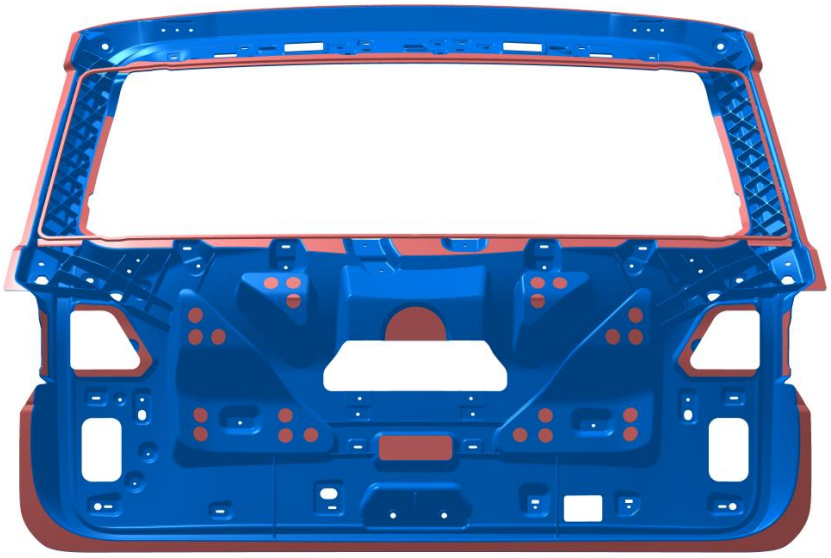

Figure 25. Location of epoxy adhesive and mastic (red markings) on the inner panel .

1.2.2.2.3 **Molding Simulation and Fiber Orientation Prediction**

Significant effort was made in the SMC redesign process to prevent adverse manufacturability conditions in the final design. Design for manufacturing-informed performance was likewise a core component of the project. This includes incorporating the effects of the manufacturing process for the SMC compression molding and the resulting fiber orientation state in the structural analysis of the liftgate. Flow simulation in Moldex3D was utilized in this design effort to predict the orientation state of the fibers in both the inner and outer panels for the liftgate. Fiber orientation is critical for determining the local anisotropic material properties of the SMC that are present in various regions of the liftgate.

Moldex3D simulates the flow of the SMC by modeling the molding cavity with an Eulerian mesh, where the molded material is able to move with respect to the fixed mesh as the initial charge geometry flows to fill the mold as the two halves of the mold close. The flow of the material under these conditions is defined using computational fluid dynamics, where the flow behavior is governed by the viscosity of the material, which is temperature and degree of cure dependent for the thermoset SMC. Additional details on the use of flow simulation on this project can be found in the conference paper presented at the ASC 2017 conference on this project[1].

A series of experiments were performed using the digital scanning calorimeter (DSC) and rheometer at the Purdue Composites Manufacturing and Simulation Center labs for the paste used in both SMC grades to characterize the viscosity of the of the SMC and incorporate this information into the molding simulation. The paste includes the resin and any additives included in the SMC formulation, but does not include glass fibers. The DSC experiments are used to characterize the cure kinetics of the material, i.e. the development of stiffness in the material as the polymer chains cross-link under the application of heat. Likewise, the rheometer is used to measure the viscosity of an SMC sample as it is gradually heated and cured. Figure 26 shows the evolution of viscosity in the Class-A SMC paste as the sample is heated at a rate of 5 °C/min. The viscosity is superimposed with the estimated degree of cure in the sample from an autocatalytic cure kinetics model fit to the DSC experiments. As the paste heats up, there is an initial drop in viscosity by an order of magnitude before the material starts to cure and the cross-linking polymer chains solidify and develop the modulus of the cured material.

[1] M. J. Bogdanor, H. Mainka, T. Laduch, N. Sharp, R. B. Pipes, M. Rademacher, “Reduction of CO2 Emissions through Lightweight Body Panels Design and Optimization of a SMC Liftgate for the Volkswagen Atlas," Proceedings of the 32nd ASC Technical Conference, West Lafayette, IN, Oct 23-25, 2017.

This drop in the viscosity is the ideal point to close the mold and flow that material as the force required to close the press is directly correlated to the viscosity of the material. The viscosity is incorporated into the Moldex3D analysis using the Castro Macosko model[2] built-in to the software. The software then incorporates the effect of the suspended fibers, which have essentially infinite viscosity, in the effective viscosity of the SMC.

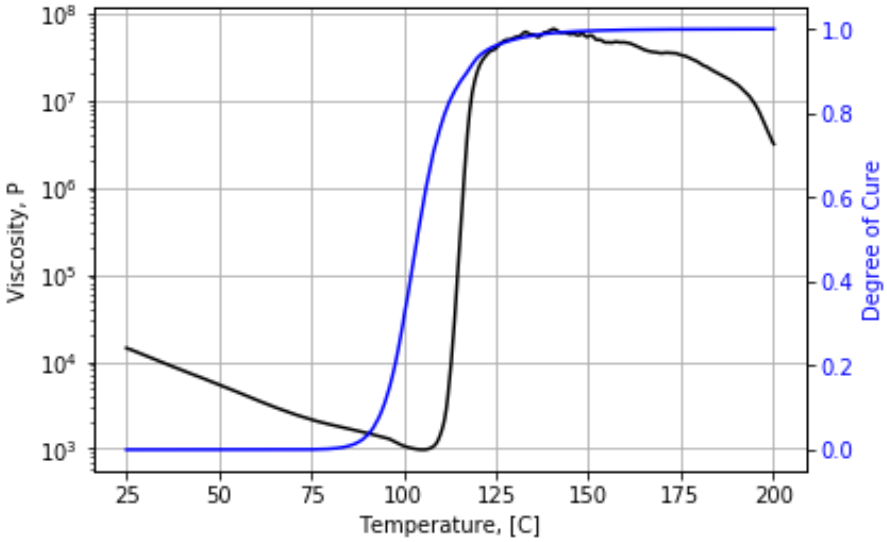

Figure 26. Viscosity and degree of cure vs. temperature for the S31-31T-29 paste at a ramp rate of 5 °C/min.

The key result from the molding simulation is the predicted final orientation state of the fibers. The orientation of the fibers begins as a uniform planar random distribution in the initial charge, where the orientation vector of any sampled fiber in the SMC is essentially uniformly random but lies in the plane due to the manufacturing process of the SMC. There is some effect of the conveyor direction on the orientation state, where the distribution is not truly uniform, but this effect is typically not very large. As the charge flows through the cavity, the orientation state of the fibers will evolve due to the squeezing behavior between the two halves of the tool and the variety of flow conditions based on the tool geometry and interactions with the boundaries of the cavities.

Moldex3D and similar flow simulation tools have typically arisen out of the demand from the injection molding industry for flow simulation. Compression molding simulation support in commercial tools is growing but is not the typical use case that these software packages, and their default settings, are designed for. It is helpful to consider a few key differences between the flow processes in injection

[2] http://support.moldex3d.com

and compression molding while setting up such analyses. One of the most critical differences is that the injection molding typically considers a thermoplastic material with a hot material flowing through a relatively cooler tool. Conversely, compression molding in this case uses a thermoset polymer where a room temperature material is placed onto a hot tool and then flows. As a result, injection molding flow have a “no-slip” condition at the tool surface where the material freezes and the velocity profile over the channel will be parabolic. Compression molding, however, creates a boundary layer of high temperature resin that has a lowered viscosity before curing which induces a slip boundary layer and plug flow of the material. Also, the flow distances in compression molding are typically much shorter than in injection molding as the material starts in the middle of the tool, rather than being introduced from the tool boundary. This leads to much fewer highly aligned regions in the final part but local regions, especially in large and complex geometries can still exhibit such high alignment.

The predicted fiber orientation from the flow simulation is shown in Figure 27 for the outer panel and Figure 28 for the inner panel. These figures show the component of the orientation tensor in the global Z direction as indicated by the coordinate system in the figure. A value of 1 would indicate that all fibers are aligned in the Z direction near that point and 0 indicates that no fibers are aligned in the Z direction. The thin-walled nature of the panels yields fiber orientations that predominantly tangential to the surface, i.e. fibers do not significantly orient in the direction of the surface normal. In both simulations, the initial charge covered roughly 70% of the final surface with overlapping charges along the header, pillars, and lower section of the cavity. The resulting fiber orientations for the inner and outer panels both show significant alignment in the Y-axis shown where the material flowed away from the centrally placed charges.

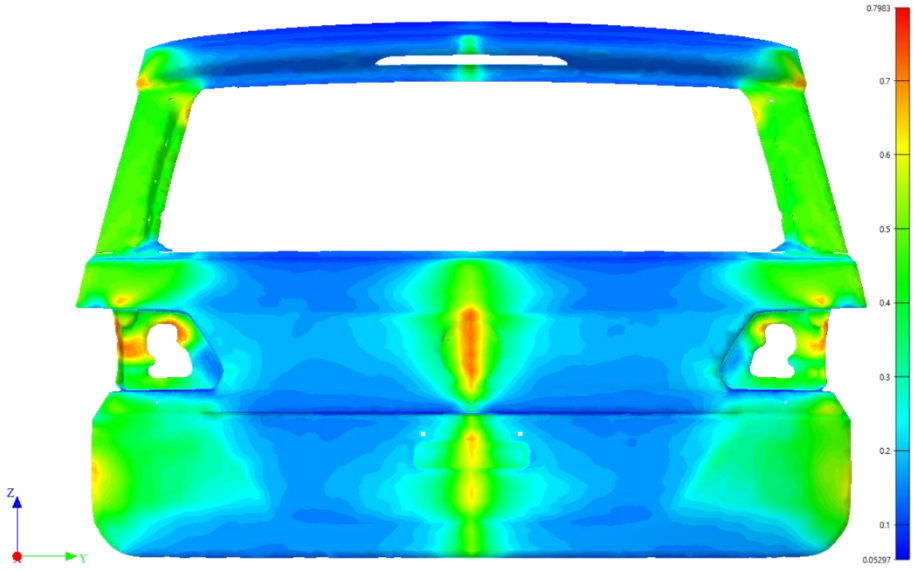

Figure 27. Fiber orientation component in the global Z direction for the outer panel from Moldex3D

flow simulation.

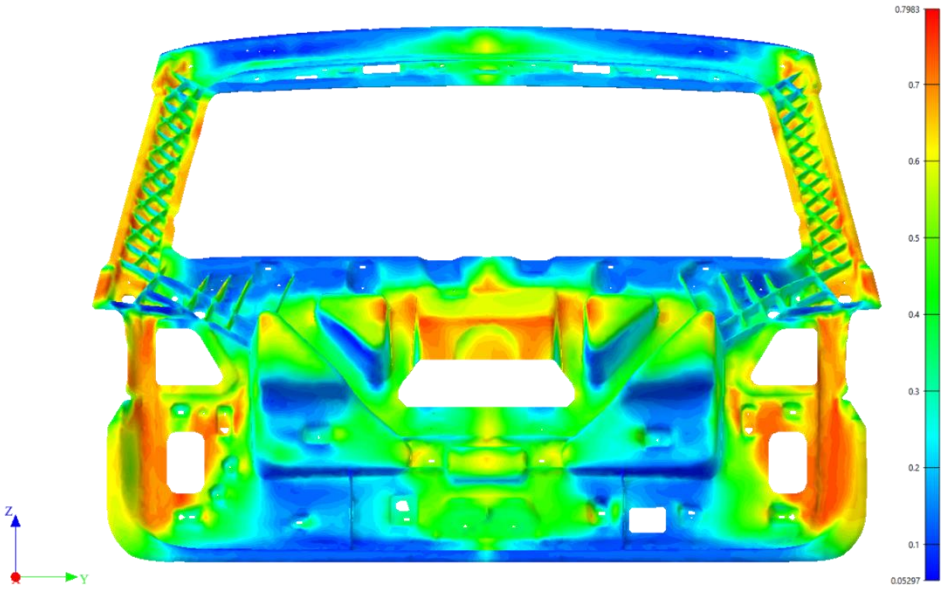

Figure 28. Fiber orientation component in the global Z direction for the inner panel from Moldex3D flow simulation.

The flow patterns for the inner panel exhibited more variation than in the outer panel accounting to the complexity of the inner panel geometry. For instance, the pillar sections for the inner panel are showing more alignment of fibers in the Z direction for the main surface than in the outer panel, while the fiber alignment in the ribs is less aligned. Also, there is more z alignment of the fibers predicted along the sides of the lower section.

1.2.2.2.4 **Material Modeling and Characterization**

In addition to the chemo-rheological characterization that was performed to inform the molding simulation, the mechanical properties of the two SMC materials were characterized for the structural analysis of the liftgate. Typically, the modulus and strength of an SMC material are reported in data sheets as isotropic quantities, as in Figure 29 and Figure 30, showing the data sheet values for the two SMC grades used in this project. This information is useful for the preliminary design of the components and was utilized in the early stages of the design effort to provide design direction for the effects of adding ribs, stiffeners, and thickening in various regions of the liftgate. As the design progressed closer to the final design, incorporating the manufacturing-informed local material properties dependent on the fiber orientation increased in importance. In order to account for the fiber orientation dependent material properties in the material models, a series of sample plaques were

manufactured at IDI Composites for both SMC grades that exhibit varying flow characteristics and resulting fiber orientations. The Digimat material model for the micromechanical properties of the composite was calibrated to these experiments and utilized in the structural analyses.

SERIES: S31 CLASS A SMC
PRODUCT DESCRIPTION: TOUGH CLASS A SMC

Properties	S31-31T-29	S31-41T-36	S31-51T-40
Glass Content	29%	36%	40%
Flexural Strength Test Method: ASTM D790	231 MPa	193 MPa	170 MPa
Flexural Modulus Test Method: ASTM D790	11,031 MPa	8,400 MPa	8,000 MPa
Tensile Strength Test Method: ASTM D638	105 MPa	105 MPa	82 MPa
Tensile Modulus Test Method: ASTM D638	11,037 MPa	9,300 MPa	7,500 MPa
ALSA Value Test Method: Ashland Method	46.1	59	65
Orange Peel Test Method: Ashland Method	9.6	9.0	8.5
Distinction of Image Test Method: Ashland Method	100	89	80
Specific Gravity Test Method: ASTM D792	1.9	1.5	1.2

Figure 29. Material data sheet from IDI Composites for the S31-31T-29 Class-A material.

PRODUCT SERIES: STC 2400 SERIES SMC
PRODUCT DESCRIPTION: HIGH STRENGTH VINYL ESTER HYBRID COMPOSITES

Properties Units	STC-2450	
	Imperial	SI
Impact Strength-Izod Notched Test Method: ASTM D-256	38 ft.lb./in.	1,330 J/m
Flexural Strength Test Method: ASTM D-790	48,000 psi	193 MPa
Flexural Modulus Test Method: ASTM D-790	1,800 ksi	14 GPa
Tensile Strength Test Method: ASTM D-638	30,000 psi	138 MPa
Tensile Modulus Test Method: ASTM D-638	2,700 ksi	12 GPa
Water Absorption (24 Hrs @ 23C) Test Method: ASTM D-570	0.1 to 0.3%	0.1 to 0.3%
Specific Gravity (+/- .03) Test Method: ASTM D-792	1.5 to 1.8	1.5 to 1.8
Shrinkage Test Method: ASTM D-955	0.0 to 0.2%	0.0 to 0.2%
Barcol Hardness Test Method: ASTM D-2583	30 to 60	30 to 60

Figure 30. Material data sheet from IDI composites for the STC2450 structural material.

Four types of SMC plaques were manufactured for both SMC materials and cut into ASTM D638 coupons for tensile testing, differing in the initial charge pattern used to create the plaques. Charge pattern denotes the arrangement of SMC charge(s) inside the mold, as placed into the cavity for compression molding. These charge patterns are shown in Figure 31 superimposed on the panels after the individual coupons were waterjet cut. These charge patterns are intended to induce different flow

phenomena: a planar uniform random distribution, fibers aligned longitudinally or transverse to the loading direction, and to induce a knit line, respectively.

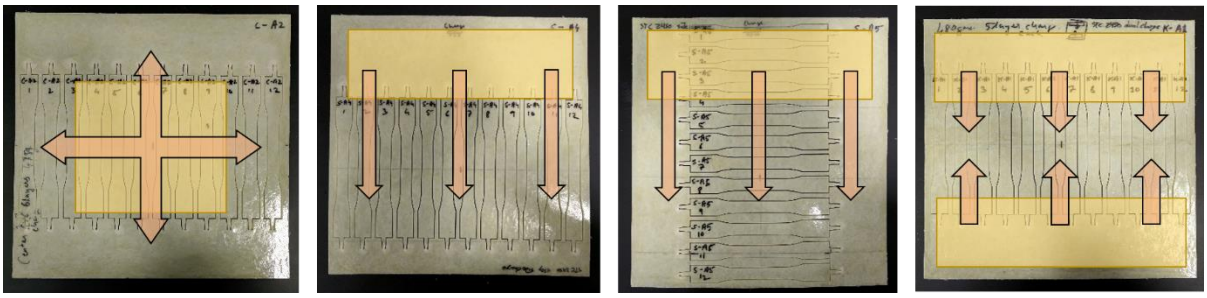

Figure 31. Initial charge placement and coupon locations for mechanical testing.

The summary of the measured strength and stiffness for the STC2450 and S31-31T-29 materials for each of the initial charge conditions is shown in Table 6. The measured stiffness of the STC2450 from the center charge specimens of 12.4 GPa is very close to the 12 GPa design value reported in the data sheet in Figure 30. The measured stiffness of the S31-31T-29 from the center charged plaque was 9.4 GPa, compared to the data sheet value of 11 GPa. The variation in stiffness can be attributed somewhat to material variability from plaque to plaque. In this project, only a limited number of plaques were used in the characterization effort to demonstrate the general process of calibrating the material model to orientation-dependent data. In the actual design process, a larger set of characterization experiments would be conducted to understand plaque-to-plaque variability. It is worth noting that the fiber content for the materials STC2450 and S31-31T-29 are denoted in weight fractions. That is 50 wt% and 29 wt%, which equate to a volume fraction of 31 vol% and 22 vol%, respectively. Additionally, the additives included in the S31-31T-29 are typically stiffer than the vinyl ester resin, which increases the stiffness of the composites accordingly and contributes to the relative similarity in stiffness between the two materials.

Table 6. Measured strength and stiffness values for STC2450 from ASTM D638.

		Charge Type			
		Center	**Double**	**Longitudinal**	**Transverse**
Stiffness [GPa]	Mean	12.4	9.5	12.7	11.1
	St. Dev.	1.24	0.89	1.28	0.83
	CoV	10.1%	9.3%	10.1%	7.5%

	Max	15.4	11.1	16.3	12.2
	Min	11.2	8.4	11.5	9.8
Strength [MPa]	Mean	151.7	16.9	118.0	109.0
	St. Dev.	19.3	3.9	16.7	21.9
	CoV	12.7%	22.9%	14.1%	20.1%
	Max	195.0	26.4	150.6	156.8
	Min	131.9	10.4	87.3	75.8

Table 7. Measured strength and stiffness values for S31-31T-29 from ASTM D638.

		Charge Type			
		Center	**Double**	**Longitudinal**	**Transverse**
Stiffness [GPa]	Mean	9.4	9.3	13.6	10.5
	St. Dev.	0.64	0.93	0.72	1.30
	CoV	6.8%	10.0%	5.3%	12.4%
	Max	10.7	10.5	14.9	13.0
	Min	8.3	7.3	12.0	8.6
Strength [MPa]	Mean	81.1	21.1	136.7	43.5
	St. Dev.	8.4	2.5	9.1	8.8
	CoV	10.4%	11.7%	6.7%	20.3%
	Max	98.9	25.3	150.4	60.2
	Min	69.1	16.4	122.0	33.1

The material data obtained from these experiments was used to further calibrate the flow simulation model and the mechanical material model in Digimat. In the flow simulation solver, a set of fiber interaction coefficients are used to describe the fiber orientation evolution as flow occurs. These coefficients balance the fiber's tendency to align with the flow direction with the propensity of the collection of fibers to diffuse in orientation angle with respect to one another. The Digimat mechanical models are based on the properties of the constituent fiber and matrix, the volume fraction of fibers, and the aspect ratio of the fibers. The volume fraction (31 vol% or vol 22%) and the mechanical properties of the E-Glass fibers (E=72 GPa, ν=0.22) are known. The constituent properties of the matrix are influenced by the incorporation of additives and the chemistry of the vinyl ester and the aspect ratio of the fibers is not an explicitly measurable quantity, as the fiber do not remain straight

during the forming process. As such, the fiber interaction coefficients, matrix mechanical properties, and effective aspect ratio were calibrated for the two material models to match the spatially varying stiffness properties measured across the plaques with the center and side charges.

The calibration process for these model parameters begins with a flow simulation of the plaques with the center and side charges to predict the fiber orientation in the panels. The fiber orientation is then mapped onto a structural model consisting of the twelve coupons cut from each panel as shown in Figure 32. Then the structural analysis model is run with a Digimat material model and the stiffness of each coupon is extracted and compared with the experimental result. For each material, the fiber interaction coefficients, matrix modulus and Poisson ratio, and aspect ratio are optimized to minimize the sum of the squared errors between the simulation and the experiment. There is some natural variability in the experiments that goes beyond the spatial variation effects from the flow process that would require additional experimentation to fully describe, but the trend of the simulation results in Figure 33 is in line with the experimental result. The results for the S31-31T-29 material show similar behavior and fitting to the STC2450 in Figure 33. This calibration process does provide a reasonable model for the orientation dependent material properties and the resulting material models are used in the manufacturing-informed performance simulations for the liftgate.

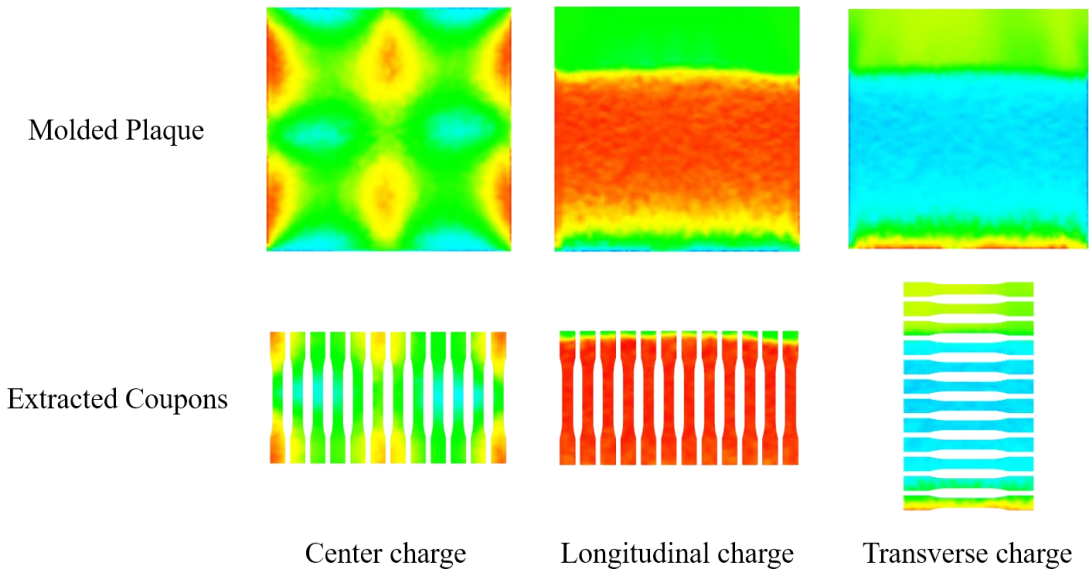

Figure 32. Virtual coupons extracted from simulated plaque molding.

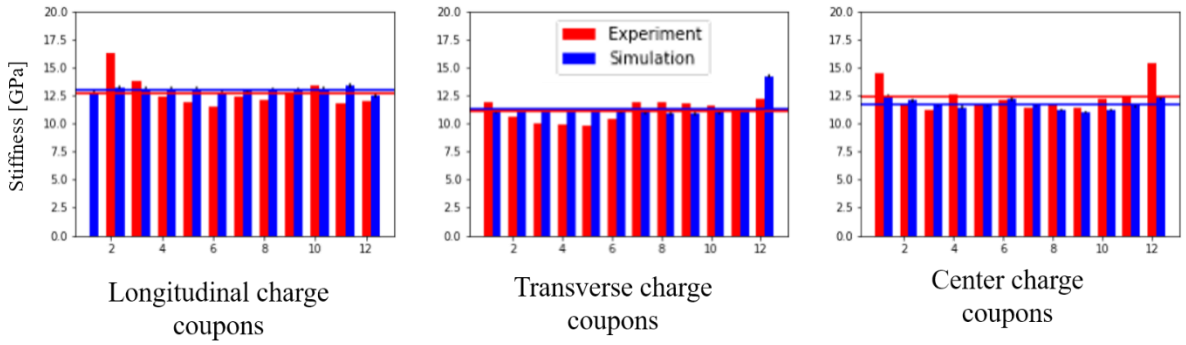

Figure 33. Stiffness simulation result for the STC2450 material.

1.2.2.2.5 **Structural Analysis and Optimization**

The structural analysis of the liftgate was performed in Dassault Systemes' Abaqus finite element package. The finite element meshes were created in CATIA from the geometry of the inner and outer panels, adhesive, and window glass. Each of these regions was meshed used the Octree Tetrahedron Mesher to create quadratic 3D elements. Solid elements were used in the analysis to capture the complex geometry of the panels and provide the most direct information from the CAD model. Two types of FEA results were used in the design process as shown in Figure 34. The first level of fidelity uses Python scripting to take the finite element mesh exported from CATIA and tie the adhesive nodes to the respective surfaces of the panels and the glass, create multi-point constraints connecting reference points to the critical surfaces of the model, apply the boundary and loading conditions, create the load cases, and apply isotropic material properties to each of the model regions. This analysis is run using the Abaqus solver on an 8-core workstation in three minutes. A separate python script was used to post-process the results and generate a summary of the performance of the design against the load cases along with the assembly mass. This analysis drove the rapid iteration of the liftgate geometry redesign informing the directional design of the inner panel.

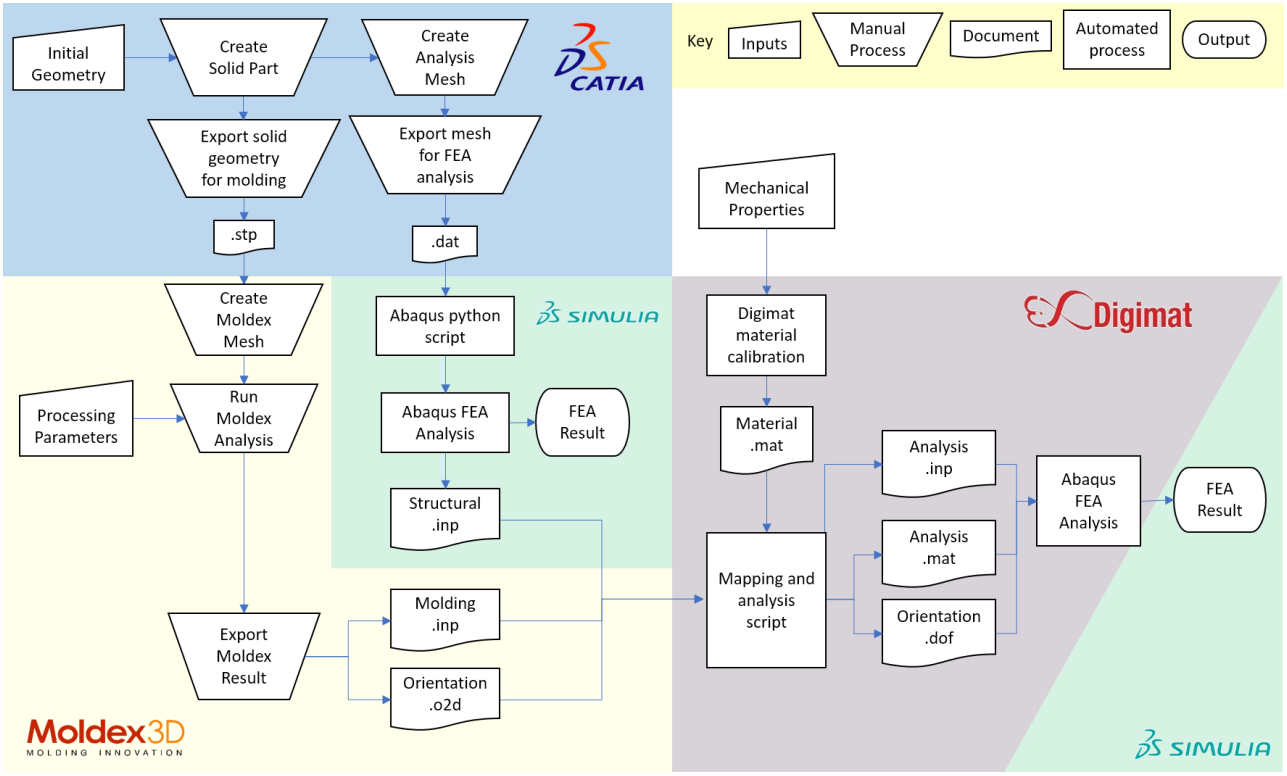

Figure 34. Information workflow for the integrated manufacturing-informed performance simulation.

The manufacturing-informed performance workflow utilized the same structural model of the liftgate but incorporates the fiber orientation information from the Moldex3D analysis with the calibrated micromechanical model from Digimat. The mapping of fiber orientation from the molding mesh to the structural mesh was performed using the Digimat-RP module. The Abaqus analysis with the coupled Digimat material model required significantly more computational resources than the isotropic material model due to the increased cost of the material point dependency of mechanical properties. This is on top of the time required to run the flow simulations in Moldex3D, which takes 10+ hours. Additionally, while the structural analysis generation and fiber orientation mapping are automated through scripting, the Moldex3D model generation, analysis, and post-processing require manual intervention, adding significant time to the process.

As a result, a typical workflow utilizing the manufacturing-informed performance simulation relies heavily on the basic analysis for design iteration and optimization with periodic checking against the manufacturing-informed performance analysis. The mapping process in Digimat-RP can handle the transfer of data from molding meshes to structural meshes that do not identically match, so a single molding simulation can be used for multiple geometry iterations. When significant changes to the geometry occur, or when time permits, further flow simulations can be run with the latest CAD data

to synchronize the fiber orientation information. In this way, the design process can proceed rapidly while still being informed by the manufacturing process.

1.2.2.2.6 Design, Modeling, and Simulation Conclusion

The result of the manufacturing-informed design process was a liftgate design that met the load case requirements, with a combined mass of the SMC panels of 12.8 kg. Compared to the current steel design mass of 21.8 kg, this represents a 40% mass savings. The design incorporated the best practices in SMC design with part design guidance from the manufacturing and design experts at Continental Structural Plastics (CSP) as well as the project partners in the Vehicles Technology Area and located at the IACMI Scale-Up Research Facility (SURF). The conceptual design from Purdue was then provided to CSP, where their expert designers reviewed and revised the final design to prepare the geometry to be delivered to the tooling manufacturers at Century Tool and Die. The comparison between the geometries are shown in Figure 35 for the inner panel and Figure 36 for the outer panels. There is some slight variation in the performance between the conceptual model and the final model delivered for final tooling from differing CAD strategies, but the design intent remains.

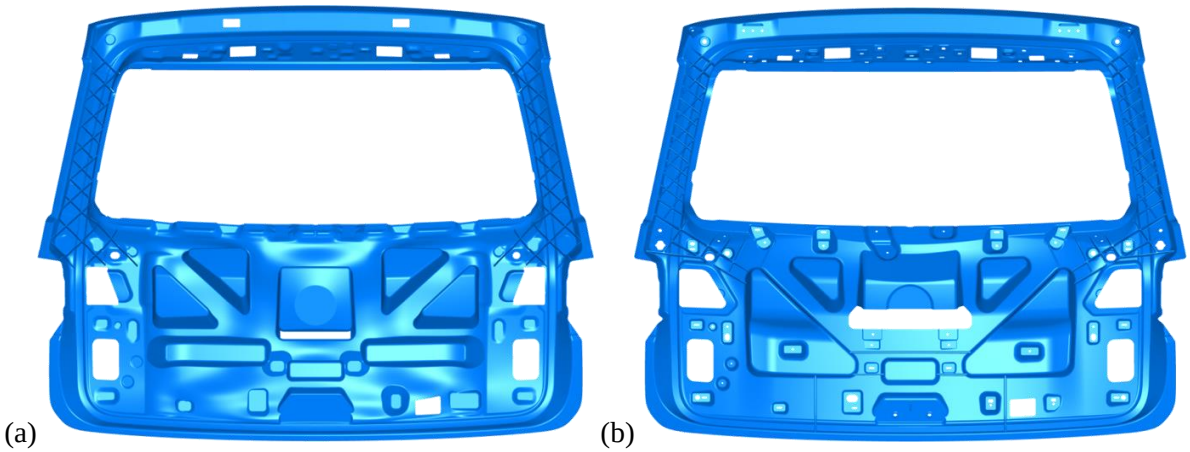

Figure 35. SMC inner panel from (a) Purdue design and (b) CSP final detailed design for tooling. Modifications were necessary to improve manufacturability.

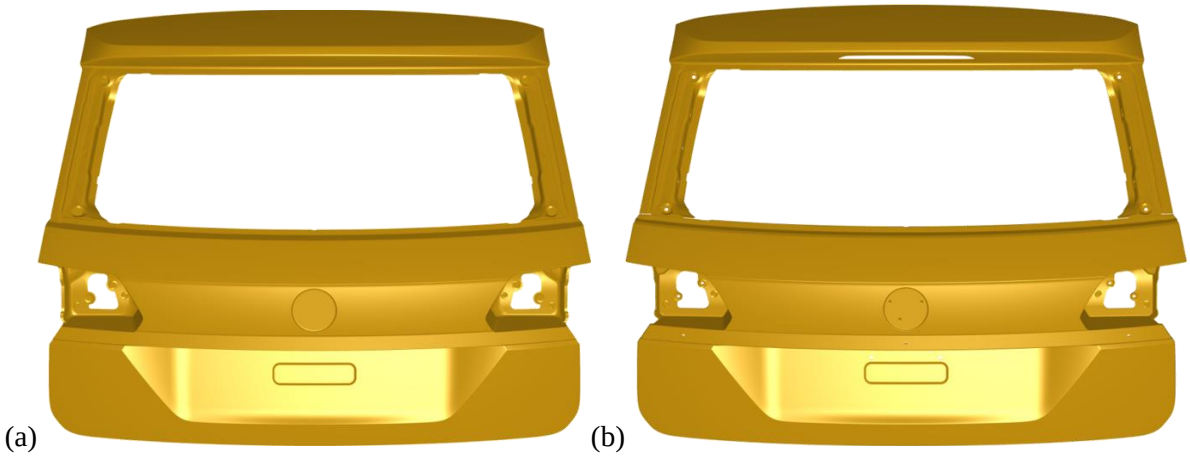

Figure 36. SMC outer panel from (a) Purdue design and (b) CSP final detailed design for tooling.

This final design process included fine-tuning the placement of the ribs to avoid the required holes in the panel, some redefinition of the inner panel surface, integration of fillets onto the ribs, and significant detail work on the outer panel to combine surfaces and incorporate the return flange on the edge. The final geometry from CSP was analyzed using the manufacturing-informed performance simulation workflow. The contour plots for the displaced shape of the liftgate under the design loads are shown in Figure 37. The model was predicted to fulfill load cases 1, 2, 5, and 6, and perform slightly under the specifications for load cases 3 and 4. This was accepted in order to kick off the tooling manufacturing within the project timeline and with the understanding that there are still multiple options left to designers in the final design of the liftgate to improve the structural performance including local thickening or additional ribs at the bottom of the inner panel, incorporation of unidirectional reinforcing patches, or localized steel reinforcing. Each of these design modifications would involve removing material from the tool and minor increase to the assembly complexity. This redesign effort would occur after the results of the physical testing of the liftgates performed outside the scope of this project.

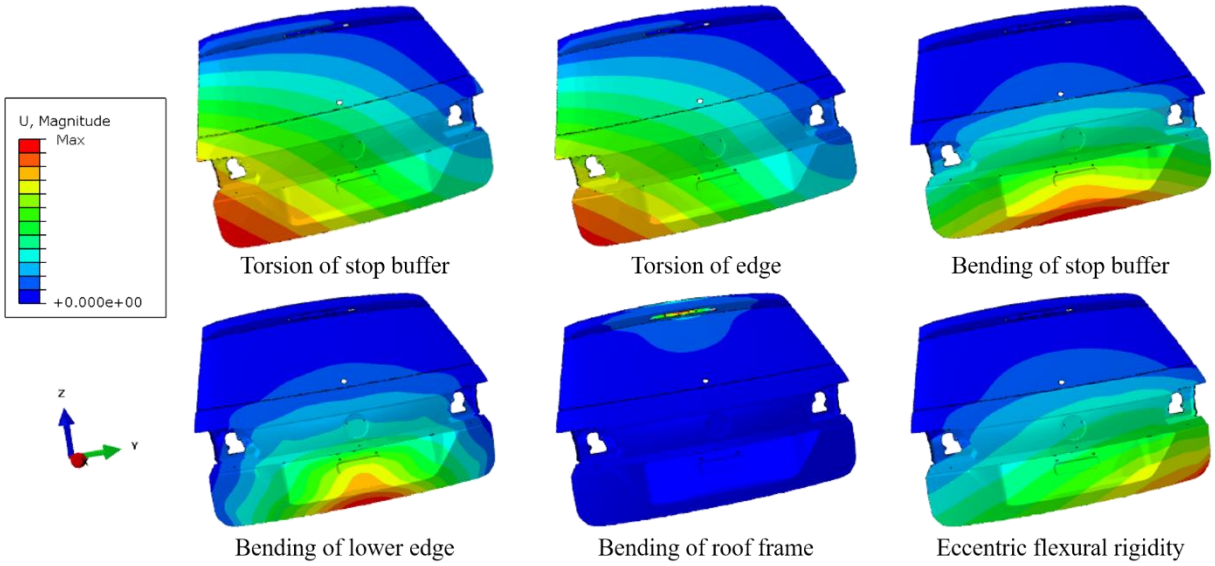

Figure 37. Contour plot of the magnitude of deformation for the SMC liftgate model for all six load cases.

The design, modeling, and simulation in this project produced the promising redesign from a steel liftgate construction to a drop-in SMC replacement with reduced weight, cost, and. Integration of manufacturability and performance in composites design from the outset reduces rework and redesign and was critical to the success of this task. The SMC expertise from CSP, IDI, and SURF demonstrated the combination of institutional knowledge and design guidelines with the integrated simulation workflow approach employed at the Purdue CMSC to design for manufacturing-informed performance.

1.2.2.3 Tooling and Prototyping

1.2.2.3.1 Tooling Design

Once part designs were finalized by the project team, they were sent to four tooling suppliers for competitive bids. Based on initial bids and previous experience with tooling companies, two suppliers were short-listed for further review, Paragon DE and Century Tool and Gage. Figure 38 and Figure 39 provide the tooling designs provided by both suppliers. Since, the scope of the project was centered on providing an optimal Class "A" surface finish, the outer panel tool designs were placed under greater scrutiny during review, with Class "A" being the deciding factor for both tools. As such the decision to go with Century tool as the mold manufacturer was based on several key aspects of their design for the outer mold. These were: the improved draft angle of the upper spoiler (See Figure 40), the addition of load wells between upper and lower portion of the part to equalize pressure and an internal vacuum system. Century Tool was also identified as an industry leader in providing Class "A" tooling for compression molded MSC by tier 1 project partners.

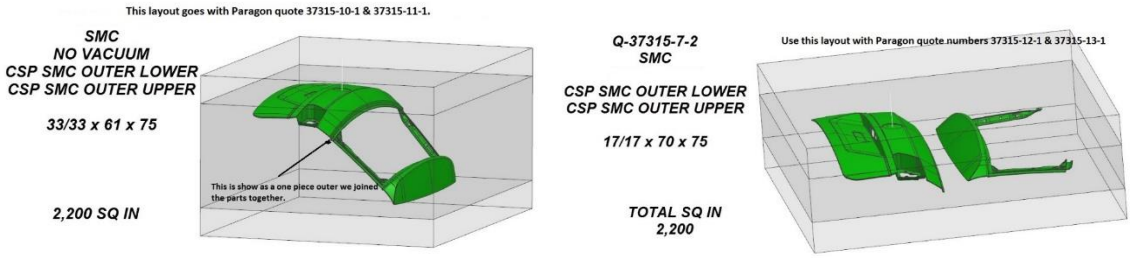

Figure 38 Paragon DE Options for tool design

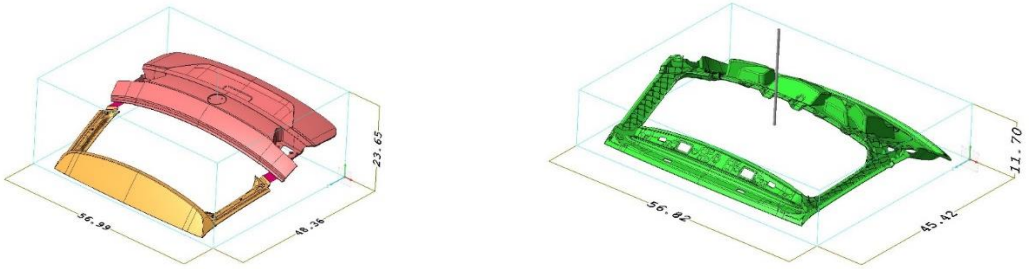

Figure 39. Century Tool proposed designs for inner and outer tools

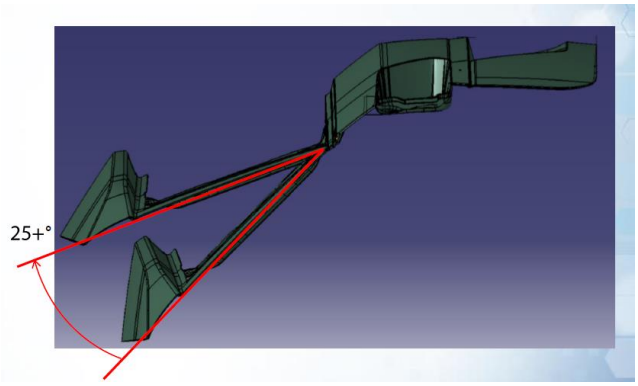

Figure 40. Optimized part tooling geometry with appropriate die position for Outer Panel, showing improved spoiler draft angle.

The final tooling design for the outer tool can be seen in Figure 41 below, alongside the internal steam circuits. The final mold is P20 steel consistent with production quality molds widely used in industry, finished with a 1200grit polished, chromed surface for optimal class-A appearance. The tool utilizes hydraulic core-side ejectors with SUMMO air poppets on both core and cavity sides of the tool. Dual vacuum ports on upper and lower tool halves allow for proper vacuum levels (22-25 inHG) to be reached quickly upon firing.

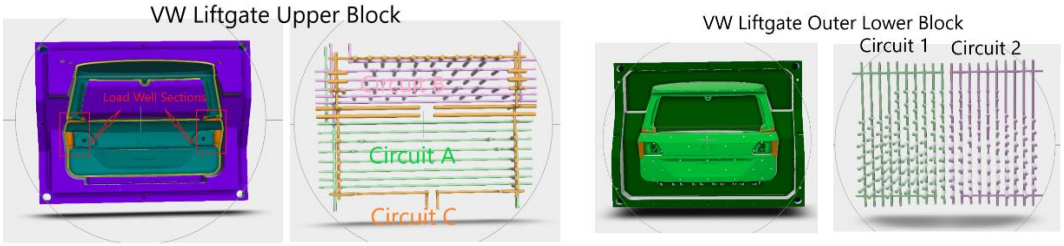

Figure 41. Finalized outer tooling design and steam line geometry

The final tooling design for the inner tool can be seen in Figure 42 below, alongside the internal steam circuits. The design maintains a die pull angle aligned with the rib sections of the part to aid in de-molding. The final mold is un-chromed Aluminum due to cost considerations, Aluminum represented an approximate 36% cost savings over P20 steel. Hydraulic ejection was only built into the cavity side of the mold, which proved problematic due to large areas of ribs in the core section. This resulted in some project delays as manual knock-out pins needed to be added to the core side as a result of the initial molding trial at MSU-SuRF.

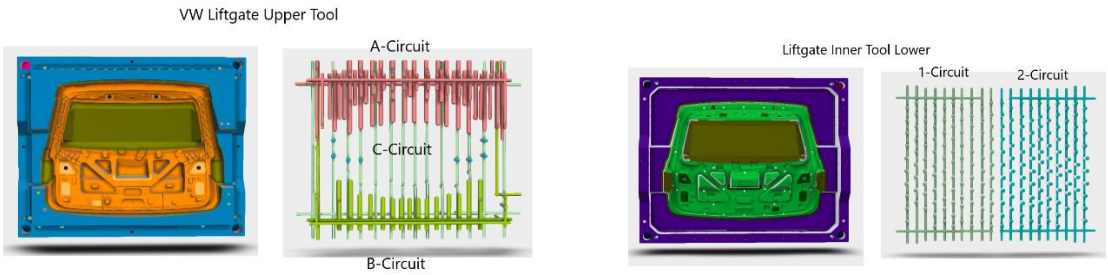

Figure 42. Finalized inner tooling design and steam line geometry

1.2.2.3.2 **Prototype Manufacture and Process Chain**

The process chain is as follows material manufacturing occurred at IDI Composites International utilizing previously evaluated and approved SMC materials (S31-31T-29 and STC 2450). SMC was then shipped to the MSU-Scale-up Research Facility (SuRF) for molding on the Schuler 4000t Compression press in previously discussed molds supplied by Century Tool and Gage. Molded liftgate inner and outer parts were then packaged and shipped to Shape Process Automation for trimming via automated 90k Waterjet. The trimmed components were delivered to Excel PatternWorks for hand bonding, bonded assemblies were then sent to CSP-Huntington for conductive priming. Final topcoat was applied at VW-Chattanooga.

1.2.2.3.2.1 Molding

Molding trials occurred first at Century Tool and Gage for initial try-outs and tooling sign-offs. The inner tool was signed off after the initial trial on Feb 14, 2019, with the outer tool being approved for chroming on Feb 15. A second trial on the outer tool was conducted after chroming, to ensure proper tool function prior to shipping to MSU-SuRF. The molding of the prototype liftgates occurred over a four-week period, with an initial unsuccessful attempt on the inner tool, which highlighted a design flaw in the tool requiring additional work. The outer parts were molded while the inner tool was being re-worked, with the inner molding recommencing after said re-work was complete.

1.2.2.3.2.1.1 Outer Molding

Molding of lift-gate outer panels occurred over five consecutive days near the end of April 2019, with S31-31T-29 SMC manufactured at IDI on April 5, 2019. A total of 68 outer skins were molded to dial in charge pattern, press parameters and to obtain the 20 qualified parts required to satisfy project

milestones. The initial charge pattern was developed at Century Tool and Gage for the tool qualification try-outs/sign-offs with a weight of 17.65 lbs. to achieve desired nominal part thickness of 2.75mm and consisted of three main pieces, which are summarized in Figure 43 below. The initial charge pattern produced satisfactory parts to qualify the mold utilizing standard SMC press parameters (850 tons, 290/300F, 120s). The initial tool qualification parts highlighted several areas of defects that needed to be addressed in order to produce 20 good quality parts[3] for the project, with main areas of concern being significant flow-lines on the upper spoiler and lower license plate area and porosity along the spoiler ridge.

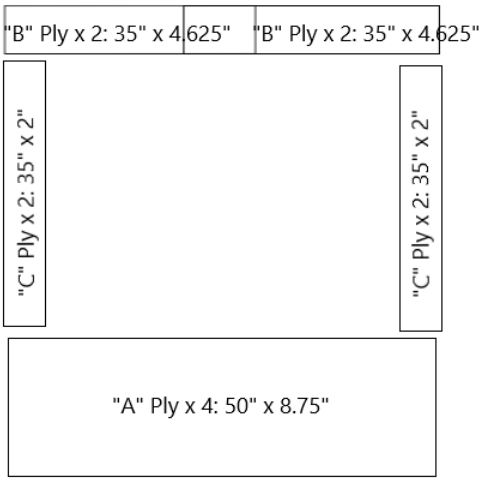

Figure 43. Initial SMC charge pattern developed by Century Tool

Due to timing constraints, a carefully designed design of experiments was not implemented, but defect improvements were obtained through systematic changes to press parameters and charge patterns to achieve a satisfactory part. The final press cycle can be seen in Figure 44 below, highlighting the main difference between standard SMC press parameters by the addition of a “bump tonnage” period (i.e. 25% pressure increase from its nominal value for 10 seconds) at the beginning of the cycle. This higher initial pressure made significant improvements to the porosity/non-fill issues in the upper spoiler that were noted in the initial parts molded at Century Tool, as well as making some improvements to overall surface appearance.

[3] Parts were assessed by experts concerning completeness of filling and surface quality.

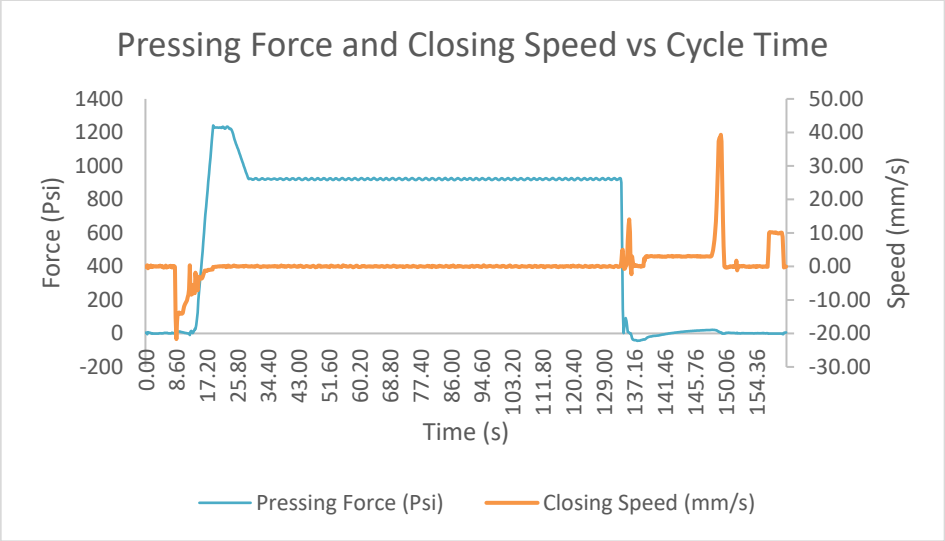

Figure 44. Graph of optimized press cycle for Outer lift-gate parts

Modifications to the initial charge pattern were required to reduce flow-lines in two key areas (lower license plate area and along the upper spoiler), as well as to reduce rippling along the spoiler area due to tool draft angle. Spoiler area issues were minimized by increasing the flow in said area, by decreasing the width of the "B" plies to 3 ½" and adding to 2 extra plies. It is believed that increasing the ply height in that area allowed greater pressure on the material during the closing sequence, prior to the full close of the tool. This higher initial pressure during closing is required to reduce rippling caused by this section seeing lower pressure due to the draft angle during the closed press cycle. Additional mold-flow analysis might be able to determine the optimal material height to achieve the best surface in this section. Issues in the lower license plate area were mitigated by breaking up the 4 ply "A" stack into separate "A" and "D" ply stacks, with "A" placed above the license plate "waterfall" and "D" placed below the license plate "waterfall", and the addition of an "E" ply overlapping the two. This eliminated the flow-lines that resulted in material flowing down the license plate "waterfall" leading to a significantly better overall surface appearance. The finalized charge pattern can be seen below in Figure 45, note that some charge dimensions were modified in order to achieve uniform part thickness and not as a result of part defects.

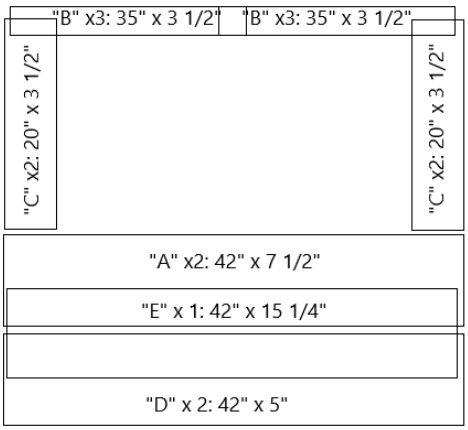

Figure 45. Finalized Outer SMC charge pattern

Overall, a total of 29 lift-gate outers were molded utilizing the optimized charge and press parameters developed during the trials, these parts were evaluated press side and approved via a qualitative visual inspection by the project team. A quantitative raw SMC surface specification was not provided to empirically classify good and bad parts, hence a qualitative visual inspection was utilized. Approved parts were shipped to SPA for trimming.

Figure 46. Outer lift-gate as molded.

1.2.2.3.2.1.2 Inner Molding

Molding of inner lift-gate panels occurred over a two-day period from May 2 to 3 2019, after additional tool alterations were completed to incorporate manual knock-out pins in the core-side rib sections. Parts were molded utilizing STC 2450 SMC manufactured at IDI Composites International at the beginning

of March 2019, due to time constraints associated with the unforeseen tool alterations, the decision was made by the project team to move forward with material that was past its typical manufacturers shelf life. This led to some blistering issues during the molding trials that were mitigated with a 20s increase in cycle time. The inner charge pattern developed by Century Tool and Gage for the initial tool try-out/sign-off did not require modification for qualification parts, charge pattern can be seen below in Figure 47. Parts weights were targeted at 13.5 lbs. at a nominal thickness of 2.25mm, press parameters can be seen in Figure 48 below. Note, that a "bump tonnage" period was not included in the inner panel molding cycle, as this part did not have to fulfill class-A requirements.

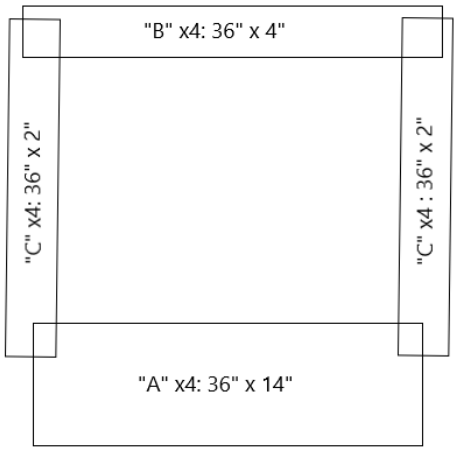

Figure 47. Finalized inner lift-gate SMC charge pattern

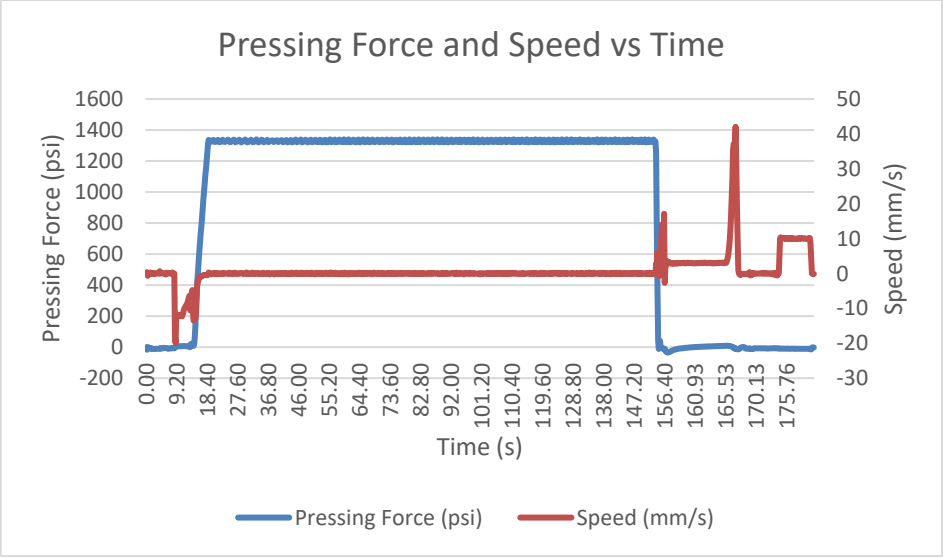

Figure 48. Finalized inner lift-gate molding parameters

Overall, a total of 60 lift-gate inners were molded with ten parts being scrapped due to molding defects, with thirty of the best parts being chosen to ship to SPA along with the outers for trimming.

Figure 49. Inner lift-gate as molded.

1.2.2.3.2.2 Trimming (SPA)

Molded composite lift-gates were shipped from MSU-SuRF to Shape Process Automation in Auburn Hills, MI. The parts were trimmed utilizing a 90k waterjet system at shape using a dual robot system to trim both inner and outer at the same time to mimic a potential production scale-able trimming option. Entire trimming cycle was completed in five and a half minutes.

Figure 50. Trimming set-up at SPA for inner and outer panels.

Figure 51. Inner lift-gate panel after trimming.

Figure 52. Outer lift-gate after trimming.

1.2.2.3.2.3 Bonding (Excel PatternWorks)

Trimmed composite parts were shipped to Excel PatternWorks in Dearborn, MI to be hand bonded utilizing the Pliogrip 5500 epoxy adhesive provided by INEOS (formerly Ashland) and Uniseal 162.7 Mastic for vibration reduction. Hardware was provided by Complete Prototype Solutions for hinge and latch plates composed of 2.0mm and 1.5mm e-coated 1008/1010 mild steel, respectively. All bond flanges and hardware locations were scuff sanded with 80-grit sandpaper, in accordance with industry best practices. Bond gap thicknesses were set at 1mm utilizing glass beads along the bond flange to maintain proper gap requirements. Assemblies were cured according to INEOS specifications consisting of a 30 min bake in a pre-set oven at 300 °F, with pressure applied via clamps and sand bags. Figure 53 and Figure 54 show the adhesive layout and the locations of the 162.7 mastic.

Figure 53. Adhesive location as applied at Excel PatternWorks.

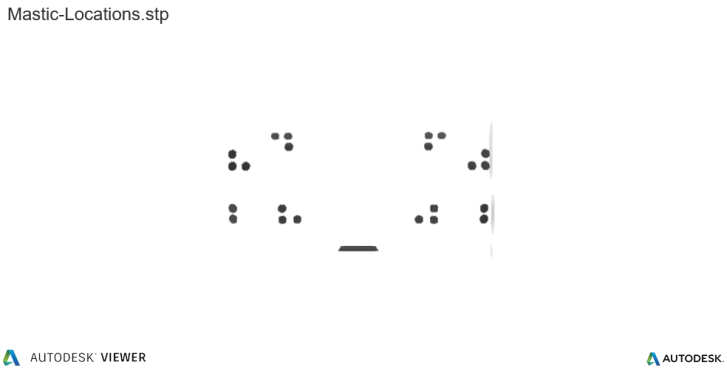

Figure 54. Mastic locations as applied at Excel PatternWorks.

Figure 55. Denotes scuff sanded bond flange and placement of hinge plate reinforcement.

Figure 56. Highlights hand application of glass beads, mastic locations and applied adhesive to bond flange.

Figure 57. Denotes an assembly ready for bake cycle with clamps and sandbags to achieve adhesive contact.

1.2.2.3.1 **Thermal Characterization of Molded Liftgate**

Figure 58 and Figure 59 shows example results for inner liftgate analyzed for its spatial uniformity and local fiber bundle orientation using thermal digital image correlation[4] (TDIC) technique developed at the University of Tennessee by Professor Penumadu. TDIC is a contactless technique using a thermal camera and two high-resolution optical cameras to spatially track strains in three dimensions of a liftgate during cooling phase after compression molding. Figure 58 shows the liftgate with speckle

[4] Penumadu, D. K., M., Invention disclosure: Technique: fiber and bundle orientations and mechanical properties of fiber reinforced composites using thermal digital image correlation (TDIC). *University of Tennesseee Research Foundation* **2018**, UTRF 18162-03.

pattern applied to track spatially resolved mechanical behavior for a given thermal loading. Results here are demonstrated for a molded part in the laboratory and IR lamps were used to provide target thermal loading increment. The technique is developed for implementation on a molded part as it is demolded and allowed to cool after compression molding step of SMC material in the final part configuration. Figure 59 (a) shows the cooling of the liftgate after being subjected to heating by infrared (IR) heat lamps. The three points denoted as point 1, point 8 and, point 12, in the region of interest (ROI) clearly shows differences in local temperatures cooling curves which are a result of local fiber volume fraction, resin and pore content, and fiber orientation, as well as part local part geometry. For example at point 1, approximately 50.5 $^{\circ}$C a change of temperature, ΔT, compared to T of 37 $^{\circ}$C for point 8, and 24.5 $^{\circ}$C for point 12. The non-uniformity of temperature across the (ROI) of the liftgate could is partly due to the IR heat lamps were small in comparison to the field of view of the liftgate. However, the temperature showed similar trends for all location points indicating the temperature profile can be reliability measured during cooling. Figure 59 (b), Figure 59 (c), and (d) shows the corresponding strains in response to T. The spatial strain shown is for strain along x-direction (Figure 59 (b)); y-direction (Figure 59 (c)) and z-direction (Figure 59 (d)) were normalized against the overall T observed during the cooling phase. The regions where higher strains are observed corresponds to matrix rich regions and higher thermal expansion of neat resin. Conversely, the regions showing the lower expansion near zero suggests fibers are parallel to the strain axis.

Figure 58. Images showing portion of liftgate (a) prior to and (b) after applying speckle pattern.

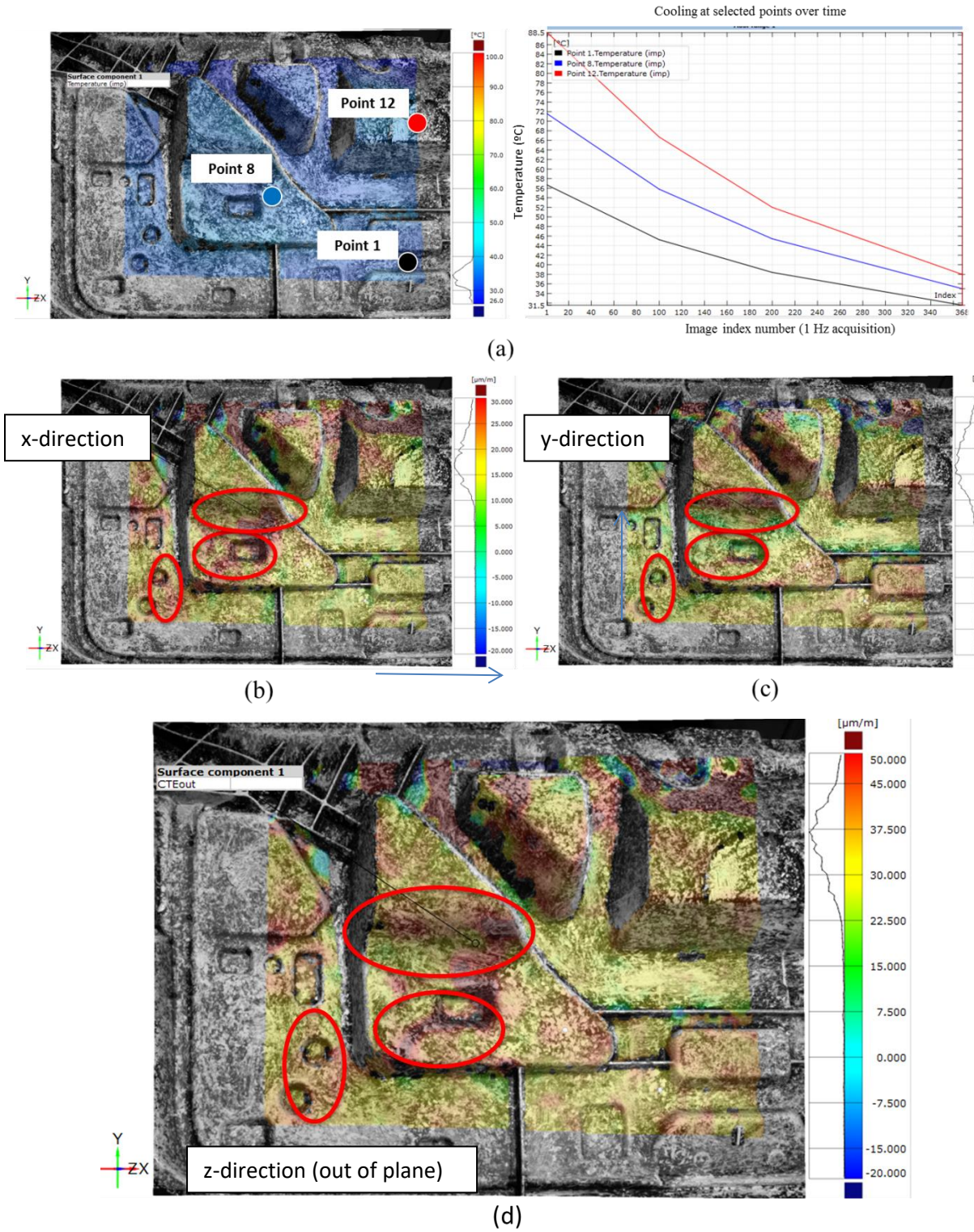

Figure 59. Example region of interest liftgate showing cooling temperature profile after heating with IR heat lamps and corresponding strains in the (b) x- (c) y- and out of plane, z -directions.

Figure 60. Example inner lift gate showing regions of interest for dynamic mechanical analysis (DMA).

Samples extracted from inner and outer liftgates were characterized using dynamic mechanical analysis (DMA). Four Specimens (60 mm length x 15 mm width) were extracted from inner and outer liftgates each similar to regions of interest denoted for the inner liftgate shown in Figure 60. The specimens were evaluated for response until 250 °C at 3-5 °C per minute at 1 Hz. The DMA results are summarized in Figure 61 and Table 8. The temperature dependent modulus values can be obtained from this data along with variation as a function of location from the molded liftgate.

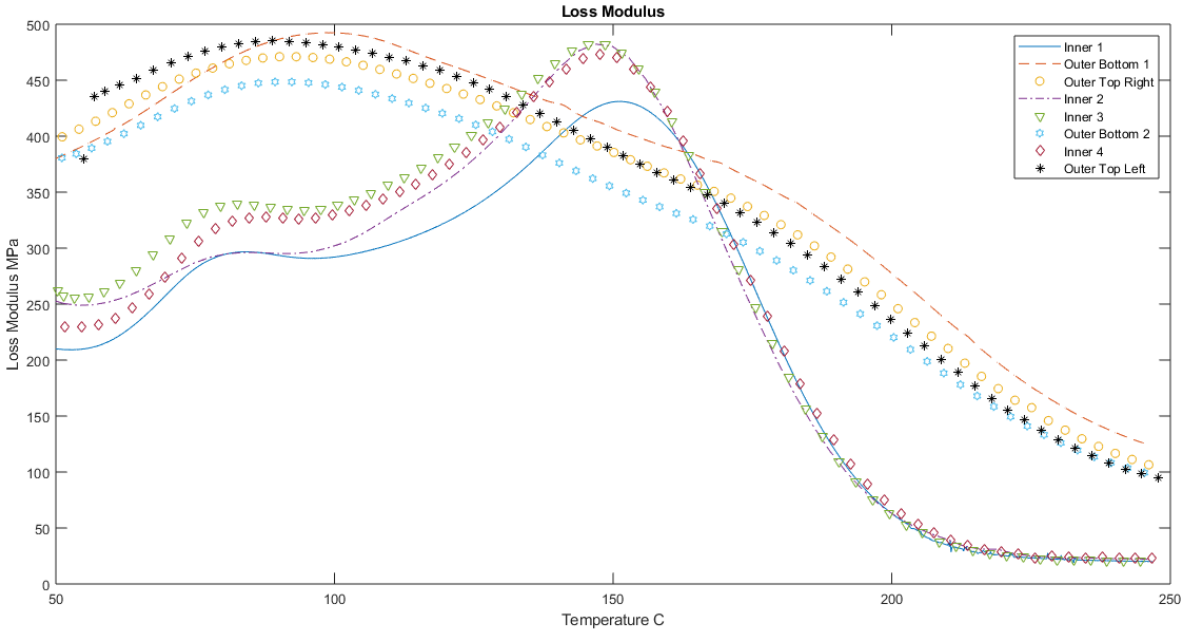
Loss Modulus
Loss Modulus MPa
Temperature C
Inner 1
Outer Bottom 1
Outer Top Right
Inner 2
Inner 3
Outer Bottom 2
Inner 4
Outer Top Left

(a)

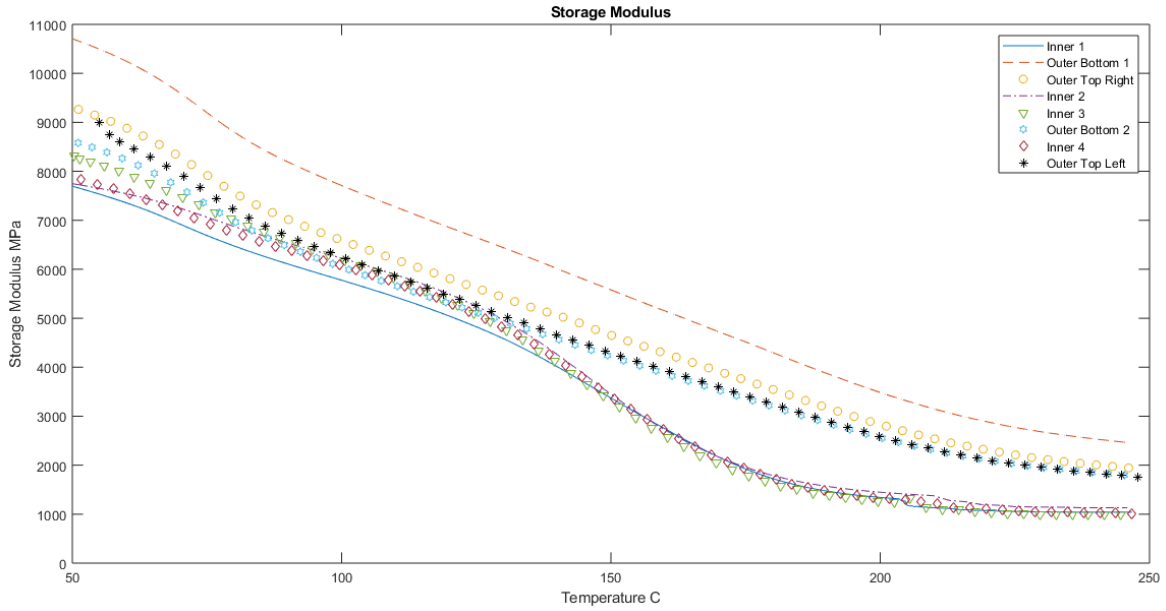
Storage Modulus
Storage Modulus MPa
Temperature C
Inner 1
Outer Bottom 1
Outer Top Right
Inner 2
Inner 3
Outer Bottom 2
Inner 4
Outer Top Left

(b)

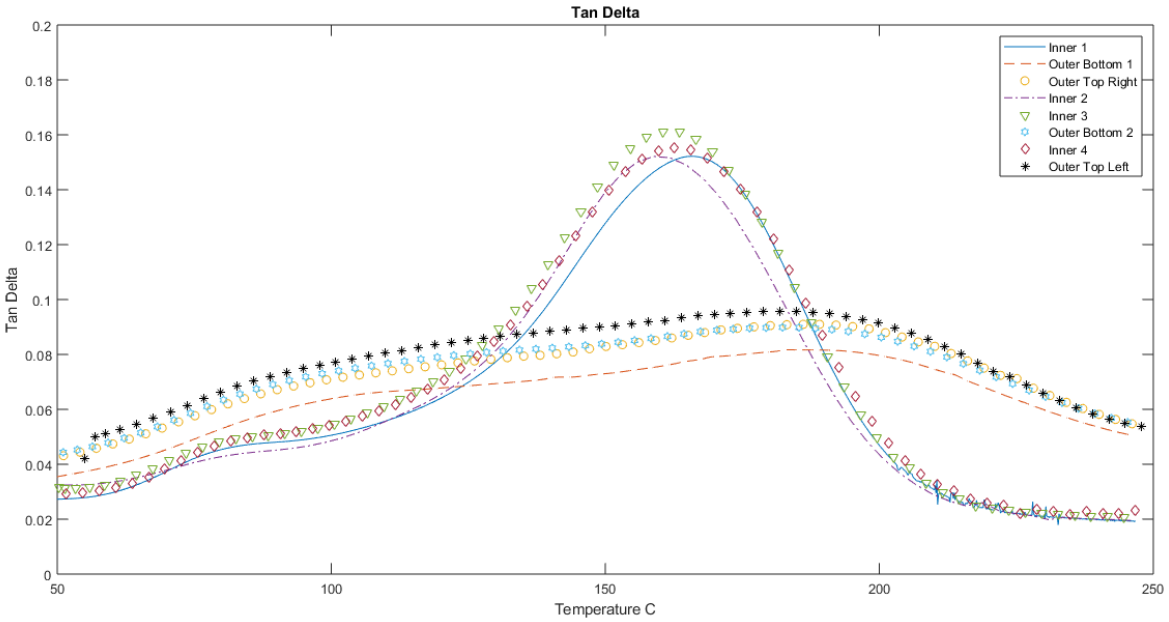

(c)

Figure 61. (a) Loss Modulus, (b) Storage Modulus, and (c) Tan delta of the SMC of liftgate.

Table 8. Summary of Loss Moduli, Maximum Loss Moduli Temperature (MLM), Tan Delta, and Maximum Tan Delta Temperature

Sample	Max Loss Moduli Mpa	Temp of MLM °C	Max Tan Delta	Temp of MTD °C
Inner 1	431	151	0.152	166
Inner 2	483	136	0.152	147
Inner 3	483	136	0.160	151
Inner 4	473	156	0.155	171
Outer Bottom 1	492	106	0.082	191
Outer Bottom 2	450	82	0.090	173
Outer Top Right	471	100	0.091	196
Outer Top Left	485	66	0.096	160

As shown in above, the inner liftgate had a consistent loss modulus behavior exhibiting a peak around 483 °C for three of the four samples. In contrast, the outer liftgate show more variability of ranging from 450 to 492 °C. The maximum tan delta (MTD) temperature ranged from 147 to 171 °C for inner liftgate and 160 to 196 °C for the outer liftgate. The storage modulus (Figure 61) was variable for both inner and outer liftgates, largely depending on local fiber volume fraction and orientation.

1.2.2.3.1.1 Priming (CSP)

Bonded assemblies were then sent to the CSP-Huntington facility for conductive priming on their production paint line. Coating the plastic composites with an electrically conductive material is necessary for the subsequent electrostatically assisted paint application process.

1.2.2.3.1.2 Top-Coat (VW Chattanooga)

Primed assemblies were shipped from CSP to VW-Chattanooga for final topcoat and component testing.The painted liftgate prototypes were presented at the IACMI Members meeting, at the SPE ACCE 2019, CAMX 2019 and during grand opening of the Volkswagen Group innovation Hub in Knoxville.

Figure 62. Presentation of project results at SPE ACCE 2019, Novi, MI

Figure 63. Grand Opening Volkswagen Group Innovation Hub Knoxville January 17, 2020

1.2.2.4 Life-Cycle-Assessment (LCA)

A cradle-to-grave life cycle assessment (LCA) was employed to investigate the embodied energy (EE) and greenhouse gas emissions associated with the production, use, and disposal/recycling of Volkswagen's Atlas SMC liftgate. The functional unit considered is one GFRP liftgate part produced through the SMC process comprising both inner and outer panels with auxiliary hinges and latch reinforcements weighing 14.87 kg. SimaPro v.9.0.0.33 LCA software (https://simapro.com) was used for analysis with input for the various materials, processes, and waste scenario processes obtained through extensive industry survey regarding series production complimented by literature values and data from published library databases (Ecoinvent 3.4 [using –allocation, cut-off by classification] [1], ELCD [2], and US-EI 2.2 [3]). North America is the focus area of this study as most of the manufacturing (except glass fiber) is assumed to occur within the northeast or southeast regions of the United States. The CED (cumulative energy demand) method [4, 5] was applied to determine the EE along with the TRACI (tool for the reduction and assessment of chemical and other environmental impacts) methodology [6, 7] proposed by the US Environmental Protection Agency (EPA) to extract greenhouse gas emission values using the Global Warming Potential (GWP) impact category. This study caters to the physical allocation by mass approach wherein the focus of the study is determined by the materials and processes encompassing the SMC liftgate.

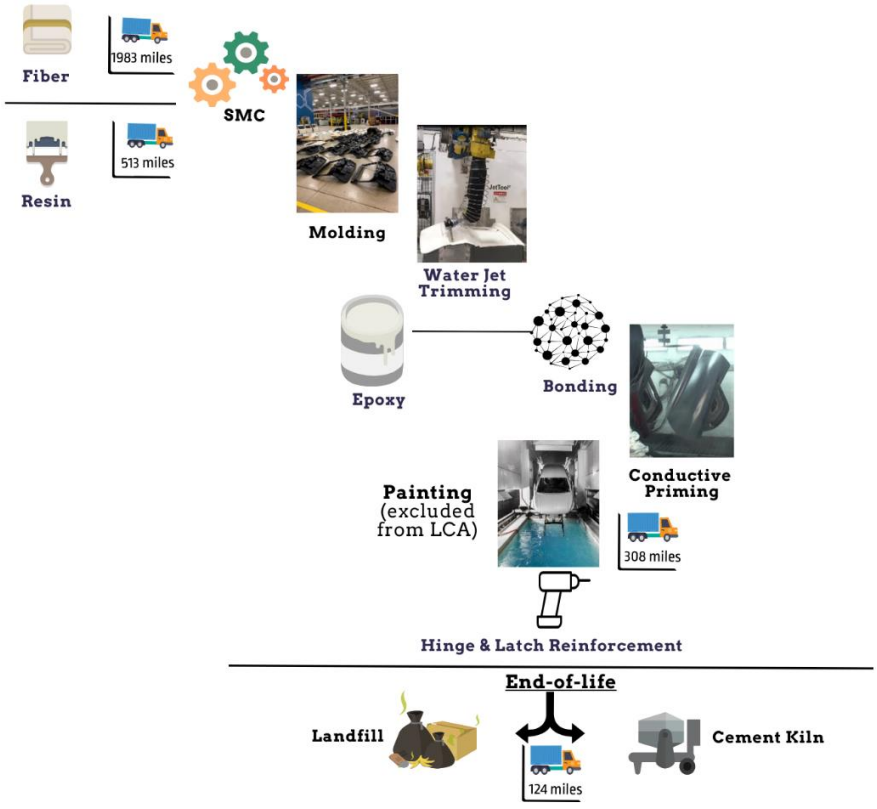

Figure 64. Cradle-to-grave schematic for the SMC liftgate component

1.2.2.4.1 **Cradle-to-gate analysis**

Owens Corning manufactures and supplies the glass fiber roving reinforcement that goes into the SMC composite that is molded and finished for the VW Atlas liftgate prototype production. The manufacturing location for this was stated to come from Tlaxcala, Mexico (transport distance: 3191 km/1983 mi). All resins and other miscellaneous solvents taken for analysis (vinyl ester, polyester, epoxy, magnesium oxide, limestone, and other solvents) are assumed to have been procured from Ashland's facility located in Philadelphia, PA (transport distance: 826 km/513 mi). Transport to (either landfill or cement kiln) EOL location is estimated to be 200 km/124 mi. Scrap percentages have been accounted for in the analysis. Therefore, weights decrease after certain initial processing steps. Transportation has been calculated separately from the main production process for clear demarcation.

Table 9. Process step with associated data source

Process Step	**Process description**	**Type**	**Dataset with database source**	**Value**	**Unit**
Inner Panel	GF:VE = 50:50 (3.06 kg:3.06 kg) 6.12 kg	Materials	● Glass fiber {RoW} | production | Cut-off, U ● Bisphenol A epoxy based vinyl ester resin {RoW}| production | Cut-off, U		
Outer Panel	GF:PE*:$CaCO_3$:MgO:Other solvents = 29:33:33:1:4 (2.3403 kg: 2.6631 kg: 2.6631 kg: 0.0807 kg: 0.3228 kg) = 8.07 kg (*PE = polyester in this study)	Materials	● Glass fiber {RoW}| production | Cut-off, U ● Polyester resin, unsaturated {RoW}| production | Cut-off, U ● Limestone, crushed, for mill {RoW}| production | Cut-off, U ● Magnesium oxide {RoW}| production | Cut-off, U ● Solvent, organic {GLO}| production | Cut-off, U		
Original weight of Inner and outer panels	Weight: 14.6257 kg		Contains the above 'Inner Panel' & 'Outer Panel' processes adjusted for original weight	878 47	MJ kg CO_2 eq
SMC	The outer contains roughly 50% $CaCO_3$ in the PE resin. The other content would be catalyst consumed in the reaction, thickener (MgO), mold release and other small amounts of modifiers that are of minimal percentage. Specialty parts will require additives for UV protection, flame protection, etc. This is not considered for the current	Process	● Electricity, medium voltage, at grid, eGrid, RFC/US US-EI U	0.8 0.04	MJ kg CO_2 eq

	part. 14.6257 kg considering both panels with original weight of GF and resins before discarding offal. 0.06 kWh input energy based on 20,000 lb/hr throughput				
Molding	Sheets received from the SMC manufacturer are compression molded in a 4000-ton Schuler press with cycle times: Inner -140 s; Outer -120 s; Weight per part: Inner -13.5 lb ± 0.5 lb; Outer -17.8 ± 0.5 lb. Input energy consumption: 15.89 kWh (7.3 kWh outer + 8.59 kWh inner) for both panels weighing 14.6257 kg → 14.4795 kg	Process	● Electricity, medium voltage, at grid, eGrid, RFC/US US-EI U Scrap of 1% (0.1462 kg) is considered to be discarded to the landfill at this step ● Waste plastic, mixture {RoW}| treatment of waste plastic, mixture, sanitary landfill | Cut-off, U	214 11	MJ kg CO_2 eq
Trimming	90,000 psi water jet trimming application. Wastewater output was calculated to be 0.62 GPM. Jet Tool is used for trimming (EP94-100D with a 100 HP motor); 25.8 kWh energy consumption input calculated for both panels based on cycle time of 3min/part (6 min total). Weight considered: 14.4795 kg → 14.19 kg	Process	● Electricity, medium voltage, at grid, eGrid, RFC/US US-EI U ● Waste water/m3 0.62 GPM wastewater; For 6 min total = 3.72 gal Scrap of 2% (0.2895 kg) is considered to be discarded to the landfill at this step ● Waste plastic, mixture {RoW}| treatment of waste plastic, mixture, sanitary landfill | Cut-off, U	139 7	MJ kg CO_2 eq
Bonding	A 2-part epoxy adhesive is used for bonding. The bond line is heated to 260 °F to speed up this process in order to achieve green strength. Cycle time to bond and cure each part is 1 min. Energy was calculated based on the Fanuc automotive paint robot with power rating of 3 kW (3-phase). Weight considered: 1 lb → 0.454 kg	Material	● Epoxy resin {RoW}| epoxy resin production | Cut-off, U	38 1.7	MJ kg CO_2 eq
		Process	● Electricity, medium voltage, at grid, eGrid, RFC/US US-EI U		
Priming & curing	Personal communication with Dürr regarding energy usage. Rough guidance value was obtained for BiW (400 kWh) and calculated based on percentages from literature [8].	Process	US EI-2.2 database was referenced ● Proxy_Materials for basecoat painting, at plant NREL/US U ● Electricity, medium	123 6	MJ kg CO_2 eq

	NREL's dataset on basecoat painting was considered proxy for this step as specific chemicals are unknown. The estimation was that 1 gal of material is required to coat 10 liftgates, therefore, 0.1 gal weight was considered for coating.		voltage, at grid, eGrid, SERC/US US-EI U		
Hinge & Latch reinforcement	Thickness –Latch Plate Reinforcement: 1.5mm +/- .1 (1008/1010 Mild Steel) Hinge Reinforcement: 2.0mm +/- .1 (1008/1010 Mild Steel) Laser machine from American Industrial Company was referenced for this step with a 3 kW power rating. Cycle time is estimated to be 10 seconds total. Weight considered: 2 hinge plates (0.1 lb each) and 1 latch plate (0.3 lb each) = 0.5 lb → 0.226 kg The steel dataset taken from World Steel considers recycling within its dataset. Therefore, a separate recycling step is not included (to avoid double counting) [9].	Process	● Laser machining, metal, with CO_2-laser, 3200W power/US- ● Steel hot dip galvanized, including recycling, blast furnace route, production mix, at plant, 1kg, typical thickness between 0.3 - 3 mm. typical width between 600 - 2100 mm. GLO S	6 0.4	MJ kg CO_2 eq
EOL landfill scenario	14.644 kg of waste is considered to be discarded to the landfill, which constitutes the plastic scrap. Steel is excluded from this calculation as the recycling value has been accounted for within the Hinge & Latch process step (for 0.226 kg).	Process	● Waste plastic, mixture {RoW}| treatment of waste plastic, mixture, sanitary landfill | Cut-off, U	0.2 1	MJ kg CO_2 eq
EOL cement kiln co-processing scenario	Out of the final 14.87 kg at the EOL stage, the steel portion (0.226 kg) is dismantled prior to shredding and sent for recycling. GFRP (14.644 kg) is co-processed in a cement kiln where resin is burned to generate energy and fiber is recovered to be used as filler for cement. Primary and secondary shredding for the composite parts alongside sorting is considered for modeling	Process	● Modified using US-EI 2.2 database Portland cement, at plant NREL/US U (Avoided product/avoided energy considered for co-processing) ● Electricity, medium voltage, at grid, eGrid, SERC/US US-EI U	7 54 13 0.6 Total 20 54.6	MJ kg CO_2 eq MJ kg CO_2 eq MJ kg CO_2 eq

Transportation	Considering all transportation distances from: 1) GF from Mexico → US (3191 km x 5.5661 kg = 1.78E4 kgkm) 2) Resins from Philadelphia → Salisbury, NC (826 km x 9.0593 kg = 7.48E3 kgkm) 3) SMC molded, trimmed part → Chattanooga, TN (496 km x 14.644 kg = 7.26E3 kgkm) 4) Assuming EOL distance to be 200 km –can be applied for both landfilling or recycling scenarios (200 km x 14.87 kg = 2.97E3 kgkm)		● Transport, freight, lorry 16-32 metric ton, EURO3 {RoW}| transport, freight, lorry 16-32 metric ton, EURO3 | Cut-off, U	1) 38 2 2) 16 1 3) 16 1 4) 6 0.4 Total 76 5	MJ kg CO_2 eq MJ kg CO_2 eq MJ kg CO_2 eq MJ kg CO_2 eq MJ kg CO_2 eq

1.2.2.4.2 **Vehicle Use Energy**

It has been studied that the vehicle use phase energy exceeds the energy consumed within the production phase [10]. The use phase for a vehicle consists of two parts (1) The EE of the fuel production and (2) Fuel consumed during the lifetime of the vehicle (Figure 65). This value is obtained from tailpipe emission data from specific vehicles calculated based on lifetime driving distances [11, 12]. This study excludes tailpipe emission values as this has not been recorded with the new GFRP part. Calculations are based on a total driving distance of 200,000 km (124,274 mi) and use phase energy is estimated per liftgate part.

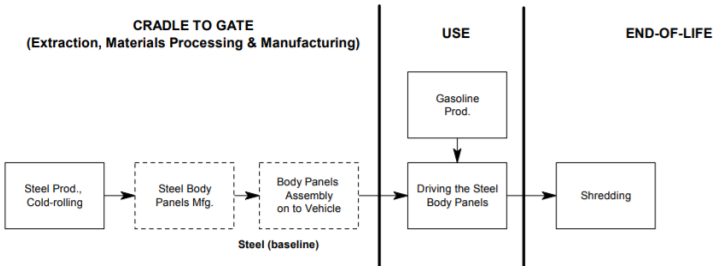

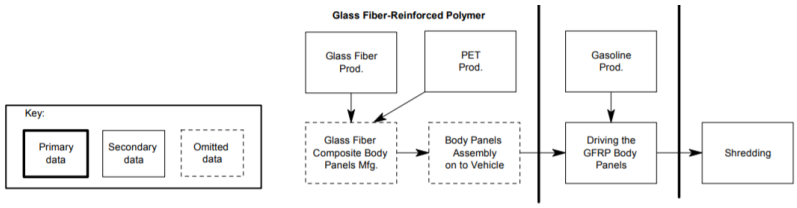

Figure 65. Cradle-to-grave system boundaries of a steel versus GFRP part [13]

Table 10. Vehicle and liftgate part use phase calculation derived from [13]

	Steel Liftgate	**GFRP Liftgate**
Mass of component (lb)	**46.52** (21.1 kg)	**31.28** (14.87 kg)
Mass of vehicle (curb weight in lb)	**4500** (2041 kg)	(4500 – 46.52) + 31.28 = 4484.76 **~ 4485** (2034 kg)
Fuel Efficiency (mpg)	(S4) 22/26 & (V6) 17/24 **22.25**	Assumption: 6.6% increase in fuel efficiency per 10% reduction in curb wt. [7]. This excludes secondary weight savings due to engine and powertrain adaptations [11] Here, 0.2178% increase in fuel efficiency → 0.048 + 22.25 = 22.298 **~ 22.3**
Lifetime fuel consumed by vehicle (gal)	(124,274÷22.25) **5585.34** 21142.81 L	(124274÷22.3) **5572.83** 21095.46 L
Lifetime fuel consumed by part (gal)	**57.74** 219 L	**38.86** 147 L

**Information obtained from online/other published sources. The rest are calculated values. Fuel consumed by final part was obtained by multiplying fuel consumed by vehicle with the ratio of the mass of the liftgate part to the mass of the entire vehicle*

Considering the primary energy of gasoline (well-to-tank & tank-to-wheel) as 39.6 MJ/l [15], the use phase energy (without tailpipe emission consideration) is as follows:

39.6 MJ/L x 21142.81 L = **837,255 MJ ~837 GJ** 39.6 MJ/L x 219 L = **8672 MJ ~8.6 GJ**

39.6 MJ/L x 21095.46 L = **835,380 MJ ~835 GJ** 39.6 MJ/L x 147 L = **5821 MJ ~5.8 GJ**

Difference based on vehicle use phase energy influenced by steel versus GFRP liftgate components: 1875 MJ or 1.8 GJ	**Difference based on part energy use based on steel versus GFRP liftgate components: 2851 MJ or 2.8 GJ**

1.2.2.4.3 **End-of-Life (EOL) Options**

Final disposal of the part has been divided into two scenarios: (1) Landfilling is taken as the baseline. Consideration has been given for waste treatment based on the plastic content. (2) The second option looks into cement kiln as a method for co-processing wherein the resin is burned off with fiber reinforcement used as a filler during the production of cement.

1.2.2.4.3.1 Landfill Scenario

The landfill is considered the baseline scenario. The EE to landfill 14.644 kg of the final liftgate part is found to be 0.165 MJ. The overall GWP related to landfilling this amount is 1.145 kg CO_2 eq.

1.2.2.4.3.2 Alternative Cement Kiln Scenario

According to EuCIA (European Composites Industry Association), EuPC (European Plastics Converters), and ECRC (European Composites Recycling Services Company), cement kiln manufacturing has been studied as one of the more sustainable options for reusing GFRP scrap [16-20]. For this case, the cement kiln data from the Ecoinvent database was considered for modeling. According to Job [21], for every kilogram of waste that is burned from the resin, 12 MJ of energy is generated. Pickering [22] mentions that not more than 10% of the fuel input from a cement kiln may be replaced with GFRP. Therefore, the assumption in this study is that GFRP will replace 10% of all of the inputs from nature that the original filler would otherwise contain within cement. This constitutes the system expansion concept [23]. Within the SimaPro software, 'Portland cement' was considered for analysis from the US-EI 2.2 database. In the traditional method, inputs from nature constitute lime, shale, clay, sand, iron ore, slate, gypsum, and other minerals. Within the GFRP waste scenario that was modeled, the shredded 14.644 kg ends up as input for the cement kiln process. Here, GF and $CaCO_3$ content from the shredded liftgate constitute 8.063 kg of the EOL liftgate from this and the remaining 6.581 kg comes from the remaining resins. Assuming 12 MJ/kg energy production by burning GFRP, the resin part constituting 6.581 kg is assumed to generate 78.972 MJ within the cement kiln. The equivalent amount of cement that may be produced by adding the 8.063 kg of GF as replacement for the original filler material is 49.56 kg. When the EE of the model entailing size reduction, energy credits, and cement kiln processing was analyzed, net energy of 19.45 MJ was seen with 54.73 kg CO_2 eq net greenhouse gas emission. Virgin cement production for the same 49.56 kg amount would otherwise require 298.66 MJ with 69.17 kg CO_2 eq, which demonstrates an overall energy reduction of 93% and greenhouse gas emissions by 21% for the same process. .

1.2.2.4.4 Final Results Summary and Related Assumptions

<u>Production (Embodied Energy)</u>

Total EE related to production of 1 SMC liftgate (cradle-to-gate) = **1399 MJ**
Total GHG emissions related to production of 1 SMC liftgate (cradle-to-gate) = **73.14 kg CO_2 eq**

Transportation

Total EE related to transportation of 1 SMC liftgate = **76 MJ**
Total GHG emissions related to transportation of 1 SMC liftgate = **9.4 kg CO_2 eq**

Use Phase

Use phase energy associated with 1 GFRP SMC liftgate part = **5821 MJ**

EOL

EE related to landfilling 1 SMC liftgate (grave) = **0.2 MJ**
GHG emissions related to landfilling 1 SMC liftgate (grave) = **1 kg CO_2 eq**

EE related to cement kiln co-processing (including avoided products) = **20 MJ**
(EE of virgin cement processing for the same amount of cement = 299 MJ)
GHG related to cement kiln co-processing (including avoided products) = **54.6 kg CO_2 eq**
(GHG emissions of virgin cement processing for the same amount of cement = 69.17 kg CO_2 eq)

It is seen that the energy peaks are prevalent within the use phase of the vehicle, with production constituting only 24% (excluding EOL & transport).

Assumptions and Estimations

1. Although the liftgate prototype was worked on at various industry partner facilities across the country such as IDI for the SMC manufacturing, IACMI's SURF facility for molding, Shape Process Automation for water jet trimming, Excel Pattern Works for bonding, CSP for priming and Volkswagen Chattanooga for painting, the final part is assumed to be performed at a facility in South Carolina and completed at the Volkswagen facility in Tennessee.

2. The eGRID RFC electricity regional fuel mix dataset is considered for processing the SMC, molding, trimming, bonding, priming, and hinge and latch reinforcement stages as the assumption is that the first part of production will occur in the northern part of the United States and considers the RFC (Reliability First Corporation) regional fuel mix data. The priming and hinges are assumed to be assembled in the southeast (Chattanooga, TN) and considers the SERC (South East Regional Corporation) dataset [11].

3. In spite of several steps involved prior to and after the conductive priming and curing stage, only these were considered for analysis here as the others are consistent across both steel and SMC parts and hence would not play a difference. The painting step was excluded as this step contains proprietary information and is also consistent for both types of liftgate [24-26].

4. A multiplier is required for 3-phase power consumption. The equation considers a multiplier of $\sqrt{3} \sim= 1.73$ for those power ratings obtained from industry estimating loading of 80% (unless

specified).

5. Steel ELCD dataset mentions that “the LCI does not include any further processing beyond the steelworks gate such as bending, shaping, cutting, welding etc. The LCI includes credits and burdens associated with end of life recycling, applying a burden to the scrap input and a credit for recycling of the product at end of its life. Therefore, end of life recycling does not need to be modelled separately. Burdens associated with shredding and baling at end of life are not included.” Therefore, primary and secondary size reduction and sorting have been accounted for separately.

1.2.2.5 Additive Tooling

In this work, we investigated the use of large-scale Additive Manufacturing (AM) technology in order to fabricate a compression mold for SMC composites. Molds and dies are essential elements in the fabrication of composite structures. In the last decade, the US molds and dies market has been in a steady decline, and most of the companies are outsourcing the manufacturing of their molds and dies to foreign entities. The reason for this is the extremely high cost for such tooling, as they have to fulfill challenging requirements, such as heated up to SMC molding temperatures (130 ºC - 150 ºC) while withstanding pressures up to 13.8 MPa (2000 psi). AM technology can be used to reduce the lead time and cost of the fabrication of molds and dies.

The Oak Ridge National Laboratory (ORNL) Manufacturing Demonstration Facility (MDF) team has displayed success in using AM technology to fabricate several molds and dies for different applications, ranging from autoclave molds and trim molds to high pressure/temperature in autoclave molds. To our knowledge, ORNL is one of the first teams worldwide to investigate and use AM technology for SMC compression molding applications. In this work, we have used the Big Area Additive Manufacturing (BAAM) system, developed at ORNL in collaboration with Cincinnati Inc., which enables rapid manufacturing of large parts (e.g. 6 m length x 2.5 m width x 1.8 m height) using feedstock in pellet form (<$10/kg), see Figure 64. We have investigated several high temperature feedstock materials such as Polyphenylene sulfide (PPS) with 50% by weight carbon fiber and Polyphenylsulfone (PPSU) with 25% carbon fiber (CF) to fabricate the AM SMC molds. Carbon fibers are necessary due to the extreme mechanical requirements on the tooling.

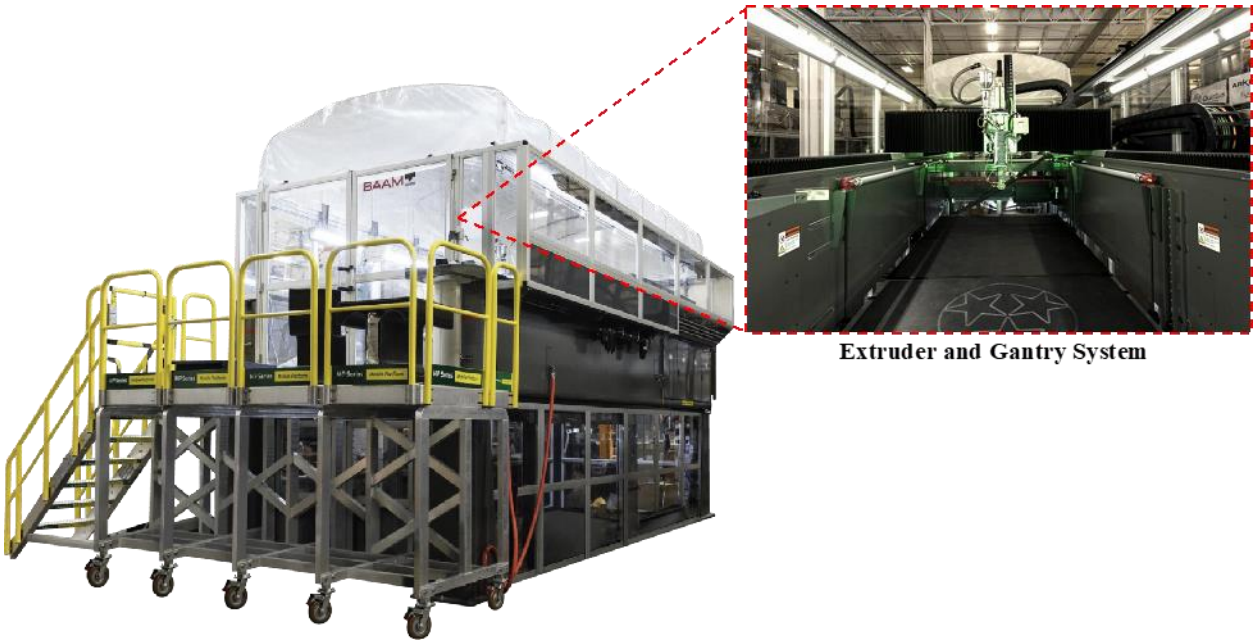

Figure 66. BAAM system located at MDF/ORNL

1.2.2.5.1 **Flat AM Mold**

As a proof of concept, we started with a flat demonstration mold with dimensions of 355.6 mm x 355.6 mm (14" x 14"). Figure 67 shows the mold design, and the print direction. We modified the overhang angles in the mold (i.e. 90º) for printing and added 45º machinable supports to support these overhang angles, see Figure 67. We added slots at the back of the female mold that act as a housing for the ejector pin system. For initial testing, the mold needed to withstand 150 psi and be heated up to 130 ºC - 150 ºC. PPS/CF50% by weight was used to print the mold.

BAAM systems are extrusion deposition systems that use large nozzles (i.e. in this case 10.16 mm or 0.4") to obtain high deposition rates. This leads to a surface with a poor resolution. The printed mold was oversized by 0.5 a bead width (i.e. 5.08 mm (0.2")) that was then machined in order to obtain a smooth molding surface. Figure 68 shows the mold during machining process. First, the mold surface was machined, and tracking balls were mounted. Theses tracking features were used to register and located the part during the machining of the mold back face. A pneumatic ejector pin system was designed and manufactured, as seen in Figure 69. Locations for four ejector pins were drilled and the ejector pins were installed in place.

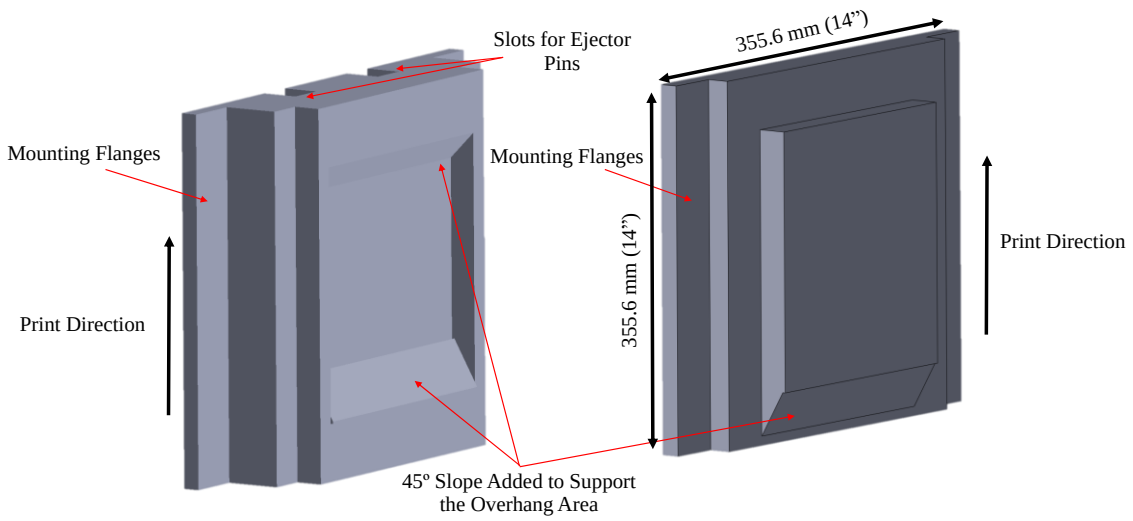

Figure 67. Flat AM mold (355.6 mm x 355.6 mm) design showing modifications adapted for printability

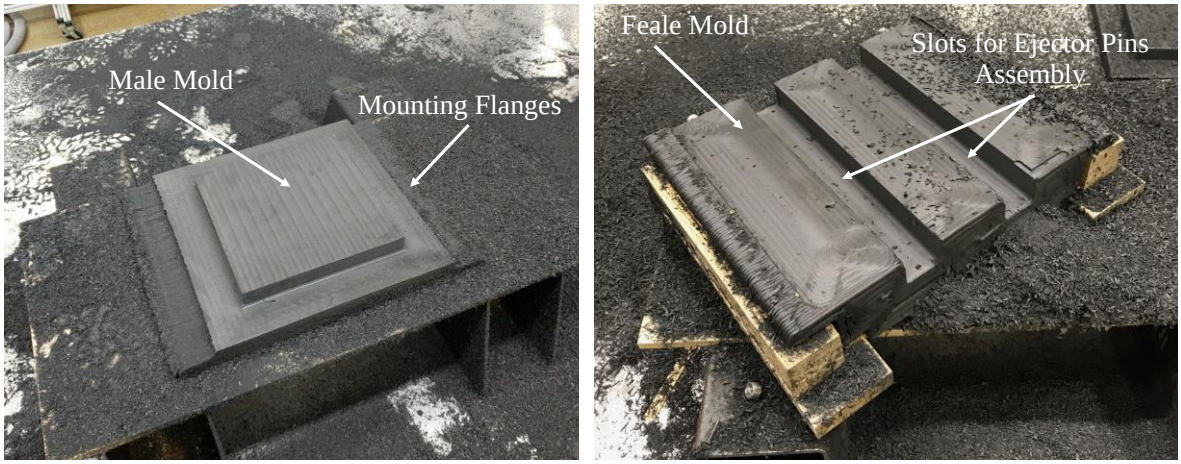

a) b)

Figure 68. Machining of the AM flat mold, (a) Machining of the male mold, (b) Machining of the backside of the female mold

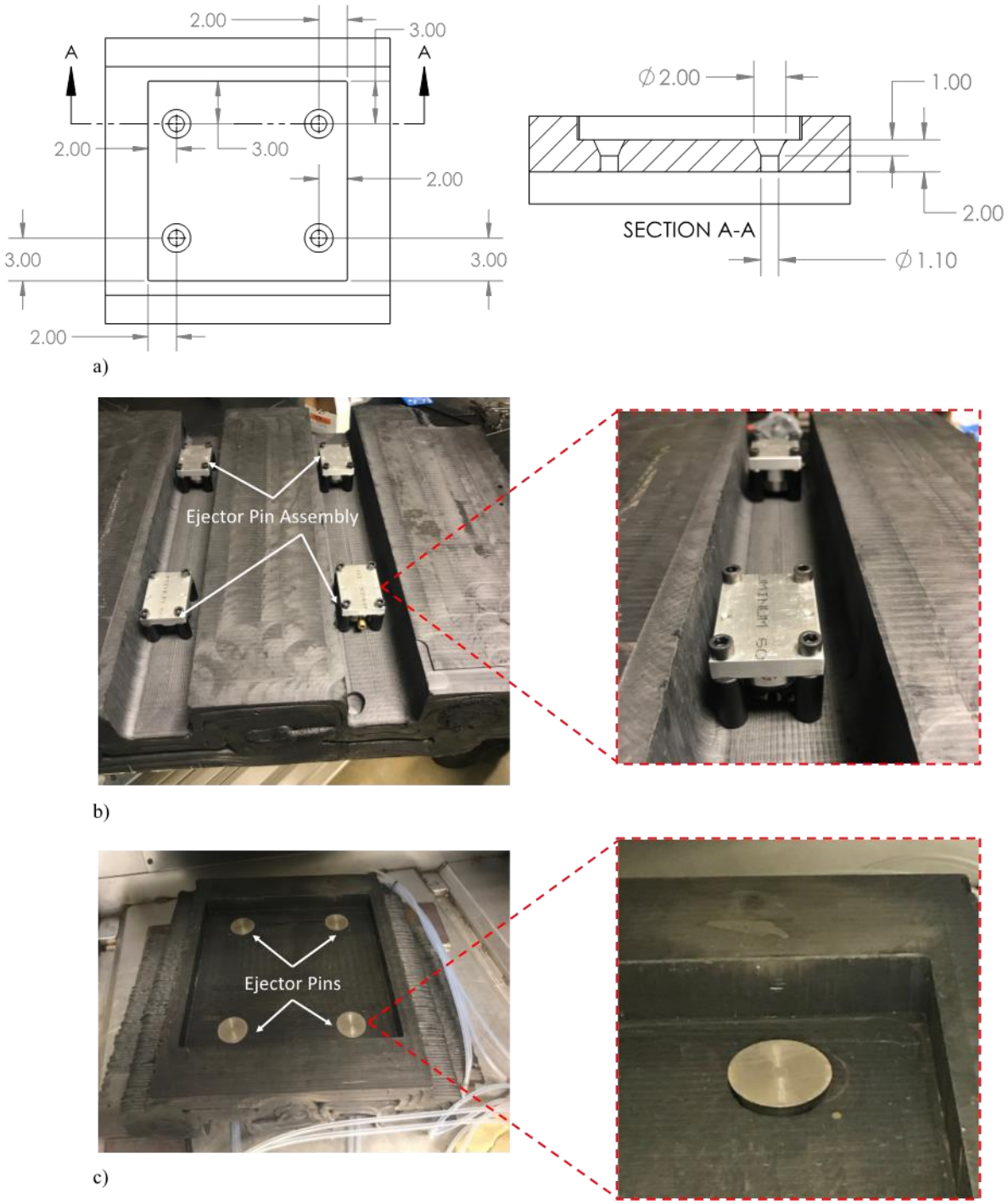

Figure 69. Ejector pin system; (a) Schematic for the ejector pins locations and size (Dimensions are in inches), (b) Backside of the female mold showing the ejector pin assembly system, and (c) Front side of the female mold showing the ejector pin system

The mold was mounted to the press and heated for 12 hours at 180 ºC. The plate temperature was kept at 190 ºC. The temperature of the molding surface was monitored as seen in Figure 70. We noticed that there is an average heat loss of 15 ºC-20 ºC when the mold is open for loading the SMC charges.

Therefore, we added insulation around the AM molds in order to reduce the temperature drop (i.e. keep the temperature of the mold at 150 ºC before starting the molding trials), see Figure 70. The SMC material (522.3 g), provided by IDI Composites, was placed directly on the PPS/CF mold surface. The mold temperature was ~150 ºC. A pressure of 10 Ton and a dwell time of 5 min was applied. Figure 71 shows a successful molded SMC composite panel using the AM mold. The SMC panel was demolded easily from the mold PPS/CF surface. Twelve parts were produced using the AM mold. The ejector pin system was used successfully, and it was noticed that the SMC material did not flow between the ejector pins clearances during the molding process.

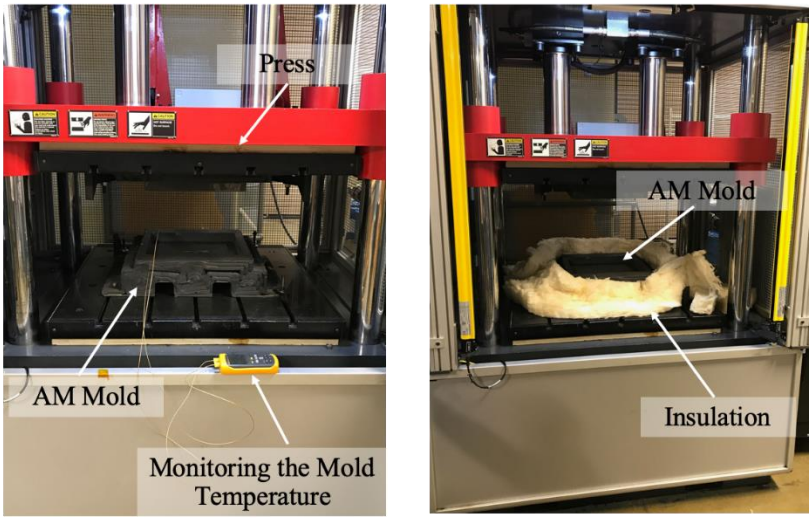

Figure 70. (a) AM mold mounted to the press where the molding surface was monitored using thermocouples, and (b) Insulation added to the mold in order to reduce the temperature drop during loading of the SMC charge

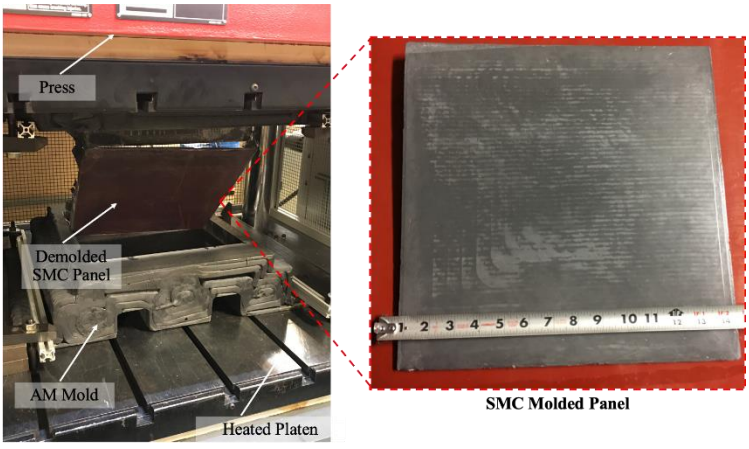

Figure 71. Compression molding process of the SMC panel using the AM flat mold

1.2.2.5.2 **Seat Back AM Mold**

This section discusses scaling up the technology to manufacture a mold for an automotive component

(seat back mold). The mold is 812.8 mm x 685.8 mm x 304.8 mm (32” x 27” x 12”) in length, width and height, respectively. The mold was modified for printability by adding machinable support structures to overhang areas, as seen in Figure 72. The mold was successfully printed out of PPSU/CF 25% using the BAAM machine at the MDF/ORNL. A 10.16 mm (0.4”) nozzle was used and each mold half was printed in 4 hours. The molds were fully machined using an approach similar to the one used for the flat 355 mm x 355 mm (14” x 14”) mold, as seen in Figure 72. The mold was loaded to the press and was heated using the press platen. The platen temperature was set to 190 ºC, but after heating for 12 hours we noticed that the molding surface only reached to 105 ºC, which is below the SMC molding temperature. This is attributed to the low thermal conductivity of the feedstock material. We then integrated insulation to the mold, see Figure 73, in order to maintain the heat inside the mold and keep it above the SMC molding temperature. After heating the mold for 12 hours with the integrated insulation, the temperature of the molding surface increased to 120 ºC -125 ºC. SMC charges were loaded into the mold and 30 Tons of pressure was applied. During the molding process we noticed that the molding surface lost 10 ºC -15 ºC of heat during the time of opening the two mold halves to place the SMC charge and the mold could not hold the required temperature for the entire trial period. Heating up the mold to compensate for the 10 ºC -15 ºC temperature drop takes a significant amount of time due to the low thermal conductivity of the feedstock. Figure 74 shows the results for the molding trial. It can be noticed that there are some locations where the SMC was consolidated and molded successfully, whereas in other locations the SMC did not consolidate due to the low temperature profile at these locations.

There were several challenges identified during testing of the scaled-up mold, which are summarized as:

- Low thermal conductivity of the AM feedstock material for BAAM: This resulted in a poor heat transfer during the heating process of the large AM mold. The mold was heated by conduction through the press’s heated platens. Moreover, the low thermal conductivity and heat capacity resulted in a rapid heat loss during the demolding process and led to a long recovery time for the molding temperature. This results in a longer cycle time and produces molded parts that are partially consolidated.
- Anisotropic nature of the AM process: This resulted in a non-uniform thermal profile a cross the molding surface. This non-uniform thermal profile resulted in, a) non-uniform consolidation of the SMC, and b) dimensional distortion during the heating process that resulted in mold cracking, see schematic in Figure 74 b).

Figure 72. Seat back AM mold; (a) Male mold showing integrated supports for overhang areas, (b) Female mold as-printed, (c) Male mold after machining, and (d) Female mold after machining

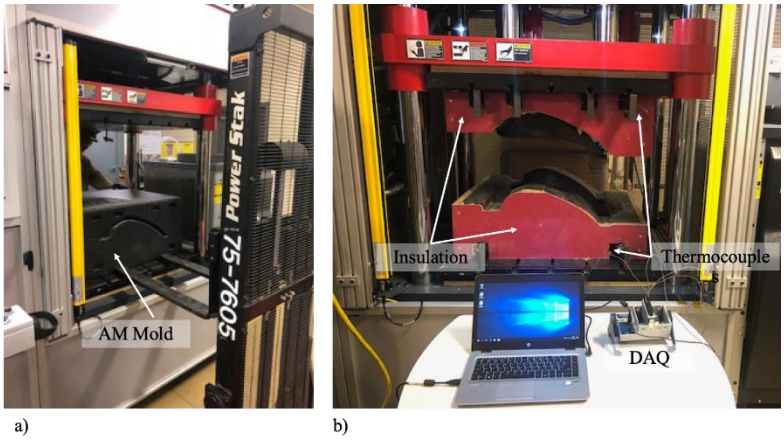

Figure 73. (a) Loading the AM seat back mold to the press using a forklift, and (b) AM mold with integrated insulation; multiple thermocouples were placed into the mold in different locations in order to monitor the molding surface temperature

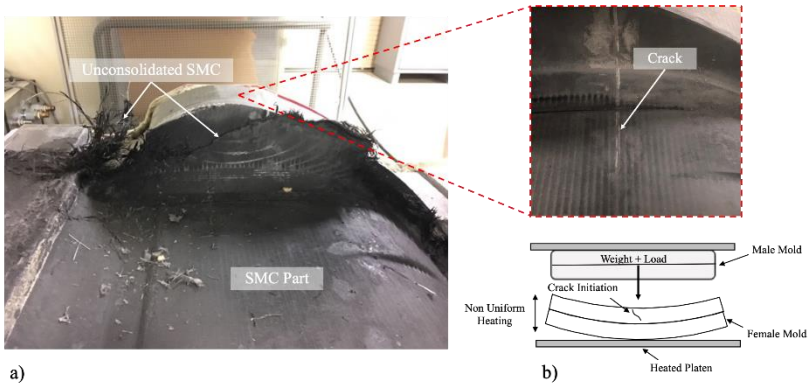

Figure 74. (a) Molded SMC part showing areas with low temperature profiles and unconsolidated composite. The anisotropic nature of the AM process led to non-uniform heat and distortion of the mold that resulted in a crack initiation (b) during the compression process.

1.2.2.5.2.1 Solutions for the Challenges of Scaling Up

Heating a large AM mold just by conduction from the heated platen comes with challenges. The challenges are that the AM feedstock material has low thermal conductivity and the methods used to heat up the mold are inefficient. In order to overcome these challenges, we have proposed and investigated two solutions:

a) Enhancing the thermal conductivity of the AM feed stock material (Not a proposed milestone in this effort)

In the scope of another project, ORNL successfully developed a new, high thermal conductivity feedstock material in collaboration with Techmer PM. This effort was supported by the Department of Energy (DOE) Advanced Manufacturing Office (AMO) with funds from an ORNL/MDF Annual Operation Plan (AOP) (Not supported by the current funding of this project). However, this material was designed and developed with an AM compression molding application in mind. The high thermal conductivity material, PPS/CF feedstock, has an increase of 299.5%, 28.23%, and 109% in the thermal conductivity for the in the x-direction (Deposition direction), y-direction (Perpendicular to the deposition direction), z-direction (Layer height direction), respectively.

b) Efficient active heating methods for large AM molds (Milestones proposed and developed under this work)

- Active heating through cartage heater:

The project team investigated the use of active heating to heat AM tools, as shown schematically and experimentally in Figure 75 (a) and (b), respectively. Unidirectional blocks of PPS/CF 50% by weight were printed, machined and drilled for holes to house thermocouples and cartridge heaters. Three different heights (i.e. 76.2 mm (3”), 152.4 mm (6”) and 304.8 (12”)) were investigated in order to study the effect of sample height on the heat transfer through the material. Thermocouples were distributed

at different locations in the blocks, in order to investigate and study the effect of the heating on the final temperature profile across the height of the printed blocks. The heating profile for the printed blocks was monitored using IR camera. Different scenarios have been investigated, as shown in Figure 75 (a). The experiment was conducted twice for each block, first without the cartridge heater and the second time with integration of the cartridge heater. The experimental results were compared to a simulation performed by the ORNL team, see Figure 76. It was found that the experimental measurements and the simulation findings are in a good agreement. This will allow us to investigate more active heating scenarios for more complex AM shapes without the need for conducting lengthy and expensive experiment. It was found that, in the case of a 304.8 mm (12") height block with insulation and cartridge heater 12.7 mm (0.5") away from the surface, the molding surface temperature was just 95 ºC after 5 hours of heating. This temperature is still far below the SMC molding temperature. The experiment findings concluded that using a cartage heater as an active heating method for AM components will not be a viable solution. In order to heat the mold surface to the required molding temperatures, large numbers of cartridge heaters with small spacing intervals need to be added (i.e. increasing the heaters' surface area) or to have larger heaters with more power.

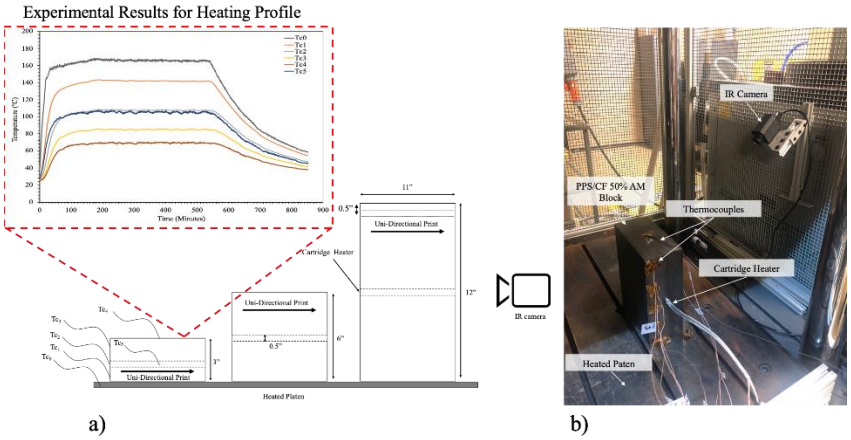

Figure 75. (a) Schematic for the cartridge active heating experimental setup, and (b) Experimental setup for active heating for AM PPS/CF 50% unidirectional block

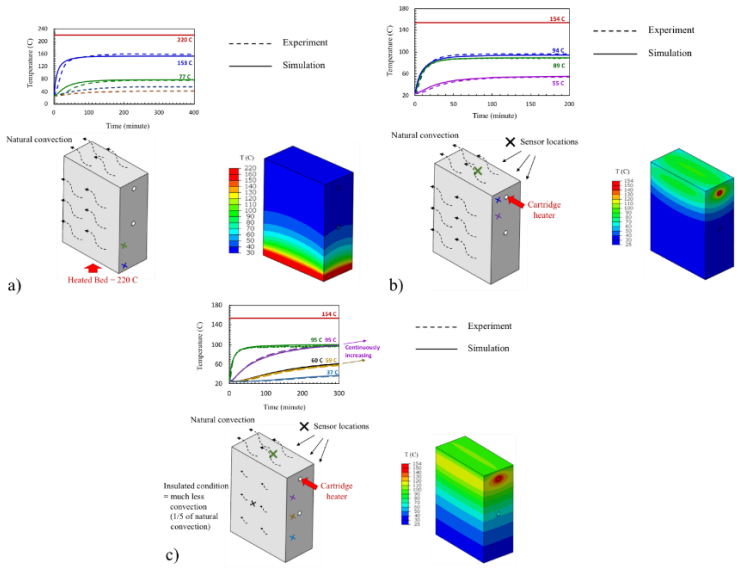

Figure 76. Experimental versus simulation for cartridge active heating method for AM blocks; (a) Heating by platen only (No insulation), (b) Heating by cartridge heater only (No insulation), and (c) Heating by cartridge heater and insulating the block

Active heating through resistive heating:

We believe that resistive heating methods are the most optimal solution for this application. We have divided our efforts into two approaches and techniques:

(a) Integrating resistive heating fabrics into the mold surface

Fibretech Composites is a company in Germany that we have partnered with to test and integrate their Fibertemp technology into our molds. Fibertemp technology is based on an electroconductive carbon fiber fabric that can be resistively heated by applying an electric potential. To test the technology, ORNL printed flat panels and 355.6 mm x 355.6 mm (14” x 14”) demo molds with contours on them and shipped them to Germany. Fibretech Composites received the molds and conducted preliminarily tests on integrating their active heating fabrics to the AM molds. The trials led to interesting and promising findings. Two approaches were investigated, one on a machined female mold, see Figure 77 (a), and another on a flat “As printed” panel, see Figure 77 (b). Both were printed out of PPS/CF 50% wt..

The team conducted the initial experiment on the female machined mold, where no insulation layer was added to the PPS/CF mold (i.e. it was thought that the conductivity was not high enough to manipulate the heating field function). A rectangular heating field and electrical connections were fed through the mold. It was noted that the PPS/CF had reasonable conductivity and the heating field without the insulation did not work.

The second experiment was performed on the flat “as printed” panel. A 300g/m² basalt veil was integrated as a 1st layer. This was to enable proper vacuum infusion in the presence of the gaps between

the printed rows (i.e. the heating field canvas would not fill the gaps between the as printed-beads). The basalt veil nicely smoothed the “as printed” surface and the adhesion to epoxy appeared to be good. A rectangular heating field was used, and the heating field was partially covered with a 2 x 300 g/m² basalt veil. This was intended to be machined to the final mold surface tolerances. The printed part was cycled 15 times between 80 °C and 140 °C. The printed part was also cycled under “thermal shock conditions”. The heating field was covered with 100 mm rockwool and brought to 140 °C. The tool was soaked isothermally for intervals of 20 minutes, then the insulation was removed for 10 minutes and then put back on. The heating fields were active throughout the entire cycling period. The AM part was heated effectively, and no damage or cracking was observed. The same experiment was applied to the mold and similar successful results were observed.

In order to integrate the heating fields to a large mold, several steps need to be considered (see Figure 78.)

1) Print the mold with an undersized offset (8 mm -12 mm for the basalt veil + heating fabrics + epoxy)

2) Resistive heating fabrics and elements need to be designed to fit the mold contour and shape

3) A basalt veil layer needs to be added to the “As printed” surface to enable proper vacuum infusion

4) Heating field integration to the mold surface

5) Infusion of a protective layer of tooling epoxy to the heating fields (oversize the mold final dimension by 1 mm – 2mm)

6) Machining the molding surface to the finale tolerances.

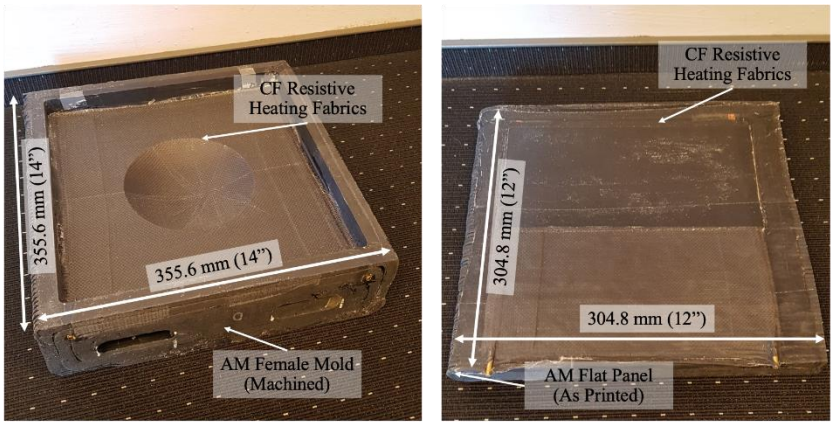

Figure 77. (a) PPS/CF 50% wt. machined female AM mold with integrated resistive heating fields, and (b) PPS/CF 50% wt. as AM panel with integrated resistive heating fields

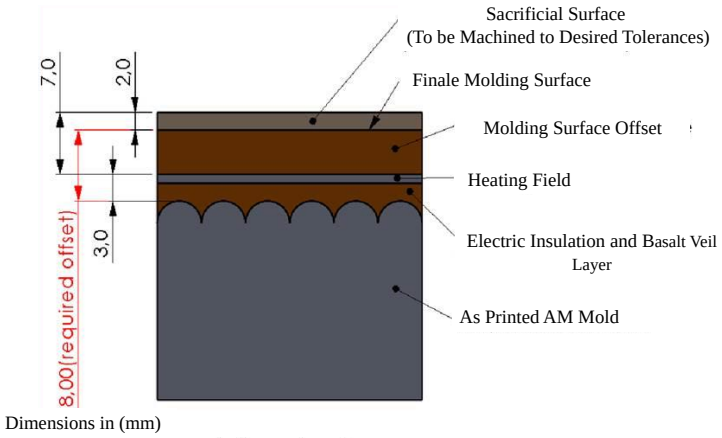

Figure 78. Schematic for integrated resistive heating fields method

b) **Integrating resistive heating wires to the mold surface**

In this method, we incorporated the wires manually (as a proof of concept) to the molding surface of the seat back mold. Figure 79 shows the seat back mold with integrated restive heating Nichrome wires. 72 wires were placed with a spacing of 6.35 mm between each wire. The mold was divided into two heating zones with 36 wires each. Each zone was divided into four wires bundled in series with each other and each bundle consisted of nine parallel wires. Each zone was then powered using a 1000W power supply. The Nichrome wires were then covered by a layer of aluminum-filled epoxy to protect the wires. This successfully fulfills the proposed Milestone 3.7.4.2 (i.e. "Demonstration of feasibility of shape representative tool using additive manufacturing").

We heated the mold in different configurations and setups (i.e. 20 ºC increment, insulating the molding surface, and soaking the mold for a period of time under a targeted power input) and the heating profile of the molding surface was monitored using infrared (IR) camera. In conclusion, we were successful to meet the proposed Milestone 3.7.4.3 (i.e. "Demonstration of feasibility of full-scale liftgate tool using additive manufacturing"). The effort and results for this milestone are briefly described as follows:

Incremental heating every hour

Table 11 shows the voltage, current, corresponding power and recorded mean temperature of the molding surface for the entire heating cycle. Figure 80 shows the IR thermal profile for the heating profile of the mold for every 1-hour increment at a given power input. We noticed that we managed to heat up the mold efficiently; however, it can be noticed from Figure 80 c) that the mean temperature at the molding area was 104.4 ºC. We believe that the mold needs to be insulated and isothermally heat "soaked" at this given temperature for a longer period of time (> 1 hour).

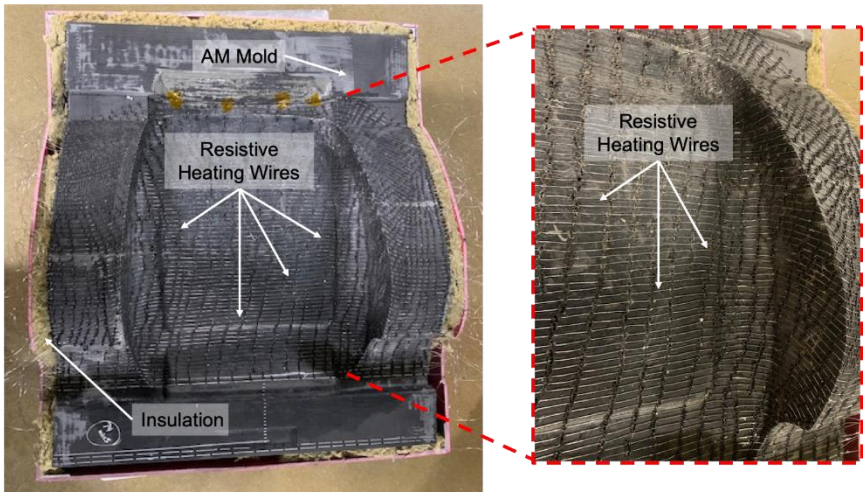

Figure 79: AM mold with integrated resistive heating Nichrome wires

Table 11. Voltage, current, corresponding power and recorded mean temperature for incremental heating method

Time Interval (Hours)	Input Voltage (V)	Input Current (Amp)	Corresponding Power (Watts)	Mean Temperature (ºC)
1	3.2	1	6.4	23.2
2	8.1	2.25	36.5	29.4
3	17.25	5.47	189	38.1
4	22	7	308	49
5	30.7	9.5	584	67.7
6	35.2	10.8	764	81.9
7	41.8	12.84	1072	104.4

Effect of insulation

In this experiment, we investigated the effect of insulation on the molding surface temperature (simulating heating the mold in a closed state). Insulation was placed over the molding surface, while the mold was kept at 145 ºC for 3 hours. We have removed the insulation and started recording the temperature of the molding surface in 5 minutes intervals, as seen in Table 12. It can be noticed in Figure 81 that the insulation assisted in increasing the mean temperature of the mold to 165.1 ºC and the temperature distribution across the molding surface got uniform. It should be noticed that even after 20 minutes of removing the insulation, the molding surface was at 130 ºC which is still above the SMC molding temperature.

Constant voltage, current, and corresponding power input for a total of three hours of isothermal heating "Soaking"

In this experiment, the power supply was set to a constant setting of 49.4 Volts, 15.1 Amps and a

corresponding power of 1492 Watts. The temperature was monitored and recorded for the entire 3-hours heating cycle. After 3-hours, the mold temperature was 132.7 ºC with a uniform temperature distribution across the surface, see Figure 82.

Table 12. Recorded mean temperature for the molding surface after removing the insulation

Time Interval After Insulation Removal (Minutes)	**Mean Temperature (ºC)**
Right after removal of the insulation	165.1
5	153.2
10	142.3
15	135.3
20	130
25	126
30	122.9

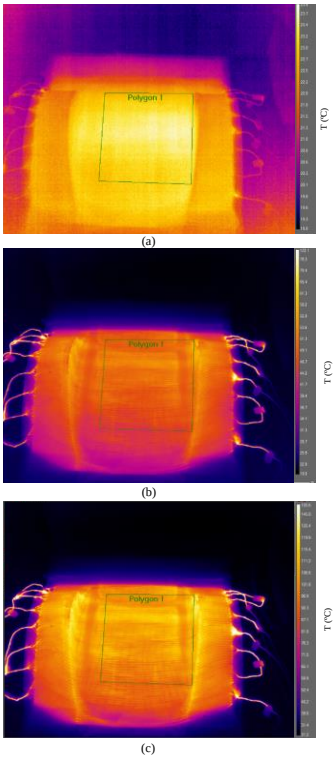

Figure 80. IR for the heating profile for the incremental heating experiment for every hour; (a) After 1 hour, (b) After 4 hours, and (c) After 7 hours of heating

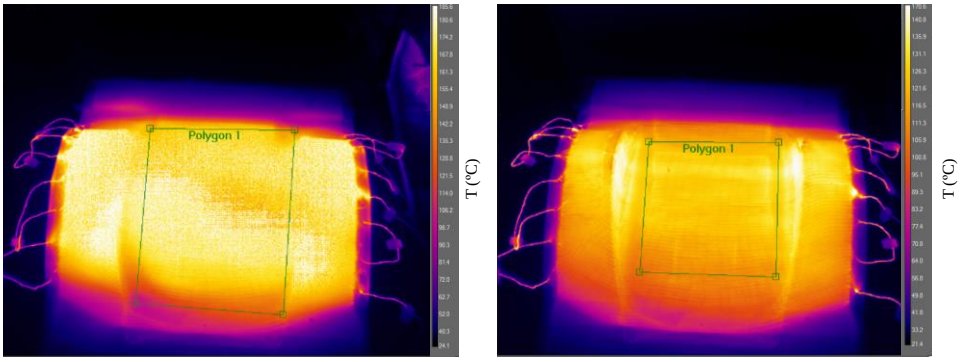

(a) (b)

Figure 81. IR profile for the molding surface showing the effect of insulation; (a) Immediately after removing the insulation, and (b) 30 minutes after removing the insulation

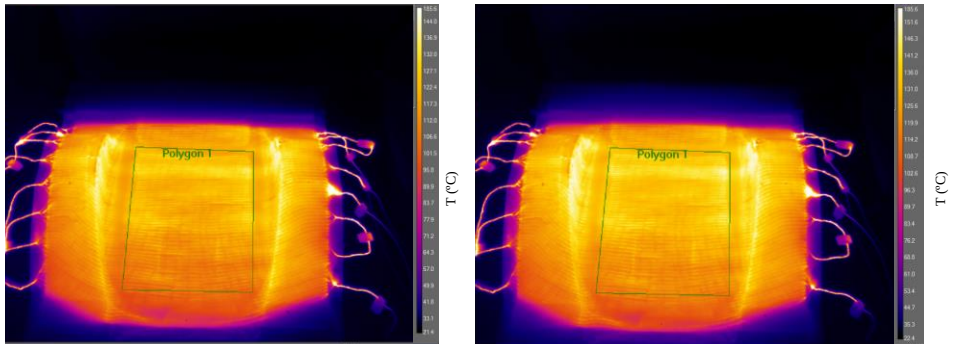

(a) (b)

Figure 82. IR profile for the molding surface at a constant setting of 49.4 Volts, 15.1 Amps and a corresponding power of 1492 Watts and soaking for 3 hours; (a) After 1 hour of heating, and (b) After 3 hours of heating

The experiment showed that resistive heating wires can be integrated to an AM mold and can effectively heat the printed mold to SMC molding temperatures. Some future work and improvements to the method can be considered and can be summarized as:

a) In this work, we were limited to two zones and individual control of the input current through each zone. We set a constant current value for all wires in the mold. An improvement in the heating profile uniformity can be achieved by dividing the molding area to an optimized number of multiple, smaller heating zones. These zones can be controlled separately by setting different current values through the wires that correspond to the resulted variance in temperatures in the mold surface. As an example, areas with higher temperatures will have a lower current, while lower temperature zones will be compensated by sending a high current through the wires. Applying this solution will allow for active control of the molding surface temperature uniformity.

b) We were limited by the power supplies (off shelf) we had available. More powerful and specialized power supplies can be designed. These power supplies can provide more power and hence attain higher heating temperatures.

c) The resistive heating wires were integrated manually into the molding surface. In the scope of another project, the ORNL team developed a technique that can integrate wires into the mold during the printing process itself. The developed hardware can be integrated into the BAAM extruder head in order to co-extrude wires during the printing process. The wire-embedding hardware consists of three primary sub-assemblies: a wire feeder, a wire cutter, and a nozzle. The wire co-extrusion process was developed under DOE-AMO AOP funding and was tested and successfully demonstrated. The technique can be used to incorporate resistive heating wires during the printing process, which can eliminate the manual labor and the process of epoxy coating the wires. Several molds (up to 736.6 mm (29") in length x 381 mm (15") in width) and flat panel examples were printed using the coextrusion technique. Figure 83 a) shows a schematic for the concept and Figure 83 b) shows examples for printed beads with the co-extruded wires. ORNL is still working on multiple development aspects for this process, such as slicing and automation of a selective placement of the wires in a complex structure, optimization of the wire location, number and placement, and investigation of different wire material and power options.

The technique discussed above allows for the integrated active heating of the tool. Experiments conducted in the scope of this study have shown that active heating is necessary to reach SMC molding temperatures. Passive heating is not applicable due to the generally low thermal conductivity of plastics. Fused deposition modeling with carbon fiber reinforced high-temperature thermoplastics is still significantly less cost-intensive than other applicable AM techniques, such as metal sintering. The size and scale of compression molding tools requires a printing area larger than that of most commercially available 3D printers. The BAAM is capable of printing such tools, but some parameters require further development, such as reducing porosity in printed parts.

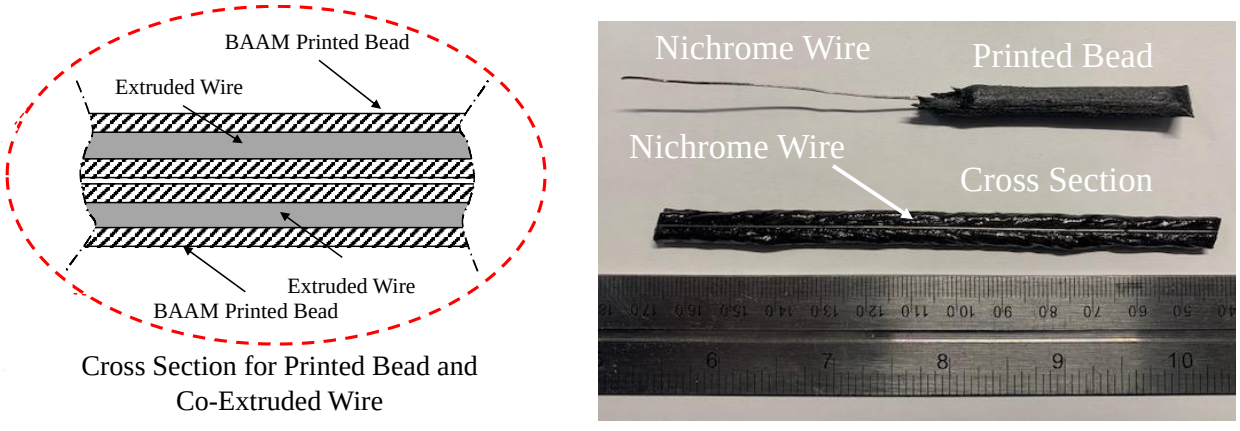

Figure 83. (a) Schematic showing the wire co-extrusion concept, and (b) Example for a printed BAAM bead with embedded co-extruded resistive heating wires

1.2.2.6 SMC Materials and Processing Studies

The various aspects of these studies were to: (A) Evaluate and selection of SMC resin systems for short cycle times. This task includes the down selection of fast reacting resin system to cycle times of 300s or less. (B) Evaluate understanding of the SMC material systems in representative shapes to capture the flow process encountered. Here we used an aluminum seat back rest tool; (C) Demonstrate a 0.7 m2 part for scale up SMC parts production. Here we used a tractor hood tool that was to the scale required; and (D) SMC class-A trials on product level IACMI tool to evaluate the class-A finish of the outer panel. These aspects, in the order listed above, are described in the following paragraphs.

A. Evaluation and selection of a resin system for short cycle times: This task includes the down selection of fast acting resin system, which is able to realize cycle times of 300s or less.

- In this task we selected the resin systems for (a) structural SMC inner and (b) class-A SMC outer, and (c) tape reinforcements. The glass fiber used is from Owens Corning, and the resin is from Ashland (INEOS). The specifics of the system are:

(a) Structural Inner: The material system is from IDI composites IDI M-211. The datasheet for the M-211 material is shown in Table 12. The M-211 is tuned for structural applications and not a class-A version. This M-211 would be somewhat of a "worst case" on the appearance and the fiber flow issues. However, it provides the highest strength and durability.

(b) Class-A outer: The lower glass percentage and better surface finish class-A materials is the optimal option. Table 13 represents the data sheet for the IDI S31 class-A SMC. This is the Ashland 770 series and the 1975 glass by Owens Corning. There were three versions with different densities. The "standard density" (1.9SG) was expected to have the best surface finish and the lowest SMC cost (by weight). It was also likely that the 1.5SG version delivers the best overall benefit for vehicle light-weighting while maintain the required surface finish. Hence both options were kept open. Also see Figure 84.

Table 13: M-211 SMC for structural inner – represents 48% glass content.

SERIES: M-200 SERIES
PRODUCT DESCRIPTION: MECHANICAL GRADE SHEET MOLDING COMPOUND

Properties	48% Glass Content	
	Imperial	SI
Flexural Strength Test Method: ASTM D790	41,000 psi	283 MPa
Flexural Modulus Test Method: ASTM D790	2.0 x 10^6 psi	14 GPa
Tensile Strength Test Method: ASTM D638	20,000 psi	138 MPa
Compression Strength Test Method: ASTM D695	35,000 psi	241 MPa
Impact Strength, Notched Izod Test Method: ASTM D256	28.0 ft.•lb./in.	140 kJ/m^2
Moisture Absorption Test Method: ASTM D570	0.14%	
Specific Gravity Test Method: ASTM D792	1.66	
Shrinkage Test Method: ASTM D955	0.1%	
Bulk Factor App. Test Method: ASTM D1895	1	

Table 14: Class-A outer with S31 series SMC – uses Ashland 700 series resin and Owens Corning 1975 glass.

SERIES: S31 CLASS A SMC
PRODUCT DESCRIPTION: TOUGH CLASS A SMC

Properties	S31-31T-29	S31-41T-36	S31-51T-40
Glass Content	29%	36%	40%
Flexural Strength Test Method: ASTM D790	231 MPa	193 MPa	170 MPa
Flexural Modulus Test Method: ASTM D790	11,031 MPa	8,400 MPa	8,000 MPa
Tensile Strength Test Method: ASTM D638	105 MPa	105 MPa	82 MPa
Tensile Modulus Test Method: ASTM D638	11,037 MPa	9,300 MPa	7,500 MPa
ALSA Value Test Method: Ashland Method	46.1	59	65
Orange Peel Test Method: Ashland Method	9.6	9.0	8.5
Distinction of Image Test Method: Ashland Method	100	89	80
Specific Gravity Test Method: ASTM D792	1.9	1.5	1.2

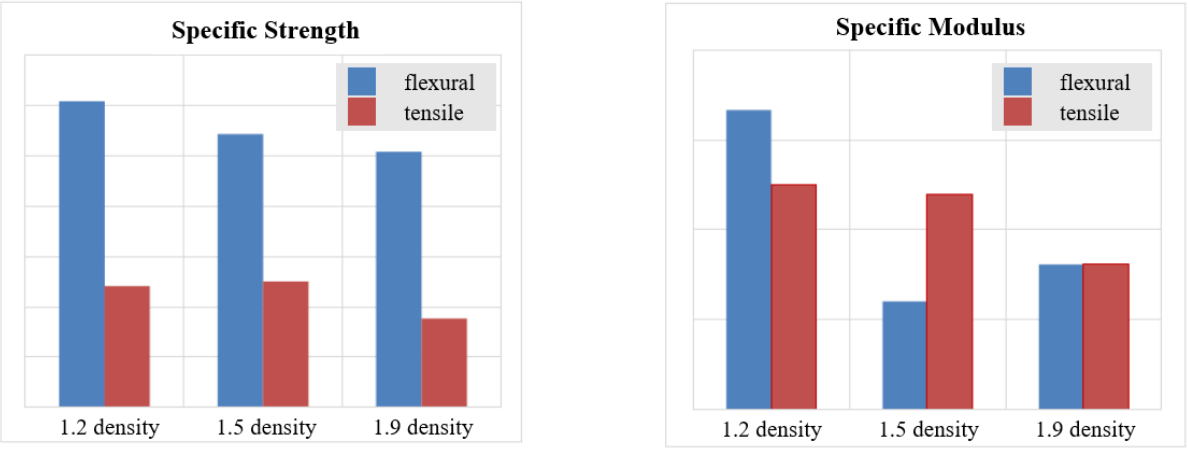

Figure 84. Density variations in SMC to make different compositions of Class A and Structural versions

B. Demonstration of cycle times of 300s or less with new resin system in lab scale. Evaluation of the resin system for cycle times, cure, consolidation and dimensional stability

Approximately twenty seat back rest parts were molded using an aluminum tool (see Figure 85) to demonstrate the 300 s cycle times with the M211 structural system shown in Table 12. These contain 48% glass content by weight. The parts were molded on a full-scale seat back rest tool of nominal dimensions 914 mm x 762 mm x 457 mm (36" x 30"'x 18"). The part dimensions are approximately 457 mm x 508 mm x 76 mm (30" x 20" x 3") at the sides, the part thickness is approximately 4 mm (0.15"). Figure 86 illustrates examples of the molded seats.

The cycle times for these were approximately 200 s. The SMC charge covered about 2/3rd of the tool (i.e. 66% mold coverage). For tape overmolding studies, the OC-Ashland resin tape was placed in the periphery of the seat, and two strip were laid to run from top to bottom along the center. This provided an avenue to observe the wash and tape movement. The parts molded with excellent bonding of the tape to the SMC. There was little to no movement of the tapes and they integrated with the SMC bulk.

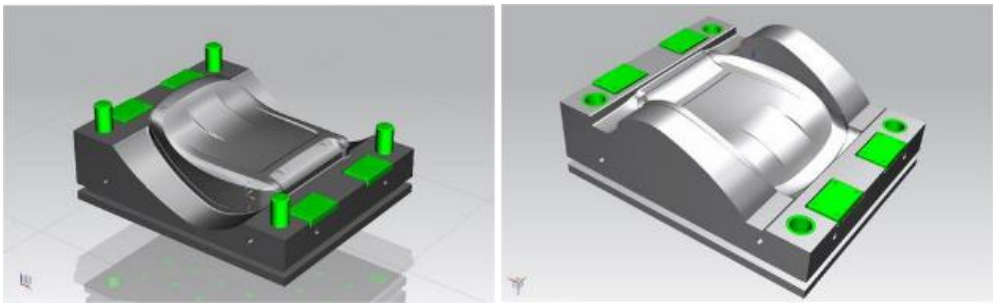

Figure 85. Top and bottom cavity of tool.

Figure 86. Illustration of parts molded under 300 s cycle time with M-211, one of the identified systems. (a) tape placement in the seat periphery and center; (b) SMC placement about 2/3rd mold coverage; (c) example of molded SMC seat, still in the tool; (d) molded SMC seats for repeatability, and (e) molded seats with peripheral and center overmolded tape (on back side)

The molded seat back was tested for representative properties and that data is provided below.

One of the molded seat back rests were sectioned into samples for mechanical characterization, as shown in Figure 87.

Process flow:

1. Building SMC charge
2. Compression molding
3. Seat back tool
4. Samples characterized for flexure and tensile strength; Flexure test ASTM D790, Tensile test ASTM3039

Mechanical testing:

Flexure test conducted on Test resources frame, tensile test conducted on MTS frame. Figure 88 summarizes the flexure results ‘across’ and ‘along’ the seat, while Figure 89 summarizes the tension results ‘across’ and ‘along’ the seat.

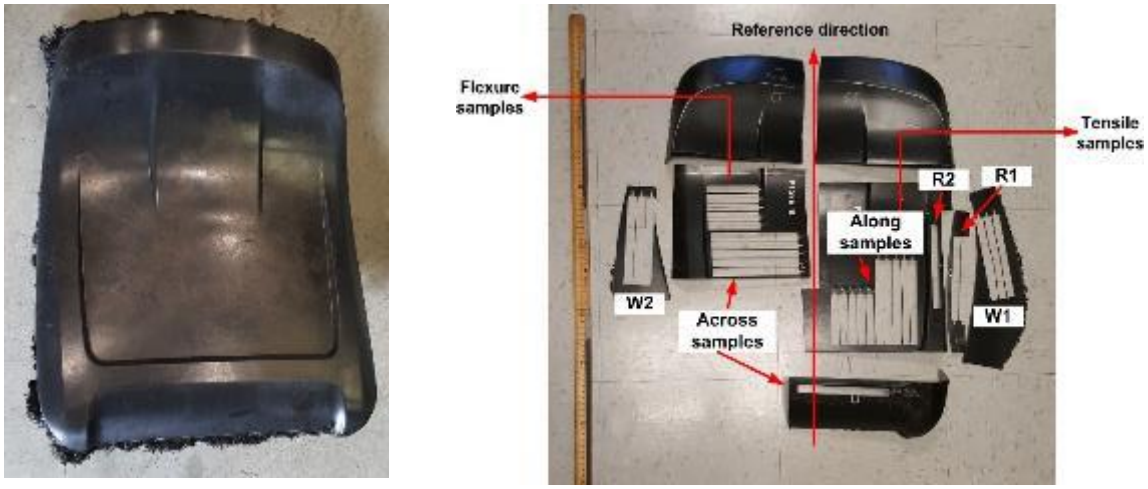

Figure 87. Flexure and tensile samples collected from various locations

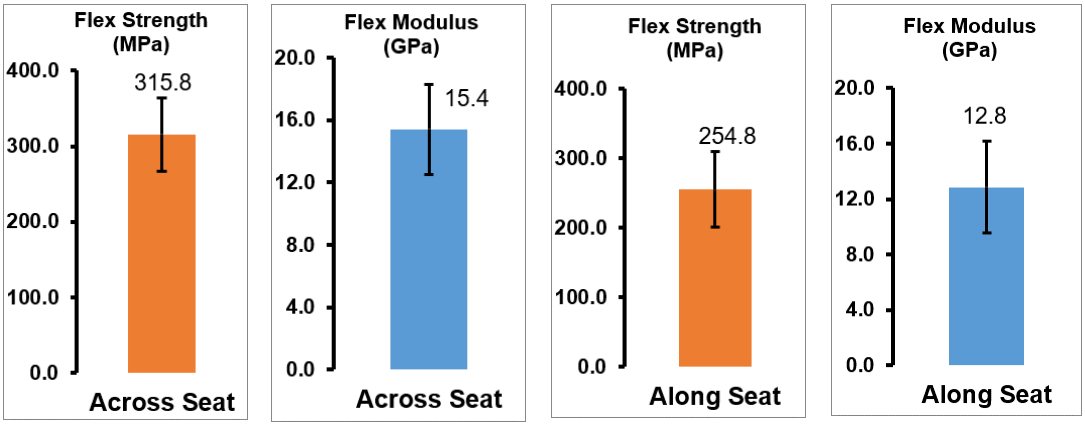

Figure 88. Summary of flexure results 'across' and 'along' the seat

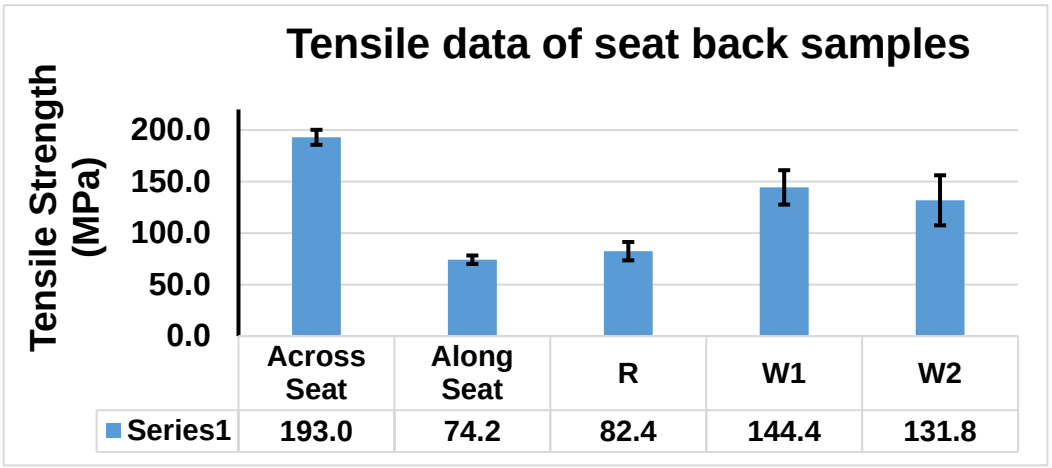

Figure 89. Summary of tensile results 'across' and 'along' the seat.

Charge placement and flow has marked influence on the properties. In the limited study here, the **f**lexure test shows that samples *across the seat* have higher strength and modulus than *along the seat* or reference direction.

The tensile samples also reveal similar distribution; across seat samples have higher strength than along seat samples. W1 and W2 (samples from the sides) have narrow distribution.

Observations

1. Across seat samples show higher strength properties than along seat samples
2. Placement of the charge affects the properties due to fiber orientation
3. SMC charge has conveyor belt and cross directions, future tests will evaluate the charge placement in cross ply so that the properties can be maximized in transverse and longitudinal directions.

C. Development and optimization/stabilization of a high volume composite production process

High volume class-A SMC trials on a part were conducted on August 30th 2017, employing a large area truck part mold. The process was optimized and stabilized for production of 2.5 minutes (150 seconds). The part of dimension 1.43 m^2 were run with class-A SMC material to provide high quality finish.

Representative parts have been painted and some left unpainted. These are going through class-A evaluations at (a) Ashland Resins using the ALSA protocol; (b) at UT with the wave scan approach, and (c) other sources per VW recommendations.

A representative class-A evaluation of the as-molded SMC class-A parts was conducted as shown in Figure 90. This uses the ALSA (Ashland Laser Surface Analyzer) method. In brief a line of laser is projected on the surface of the sample. The reflected line is obtained and digitized into array of data representing the reflected line. A polynomial regression analysis is applied to determine the best fit line. The amount of deviation between the reflected line and best fit line is used to calculate the ALSA number. The smaller the number, the higher is the quality of the surface. The calculations are also applied to calculate the Distinctness of Image (DIO) and Orange Peel values.

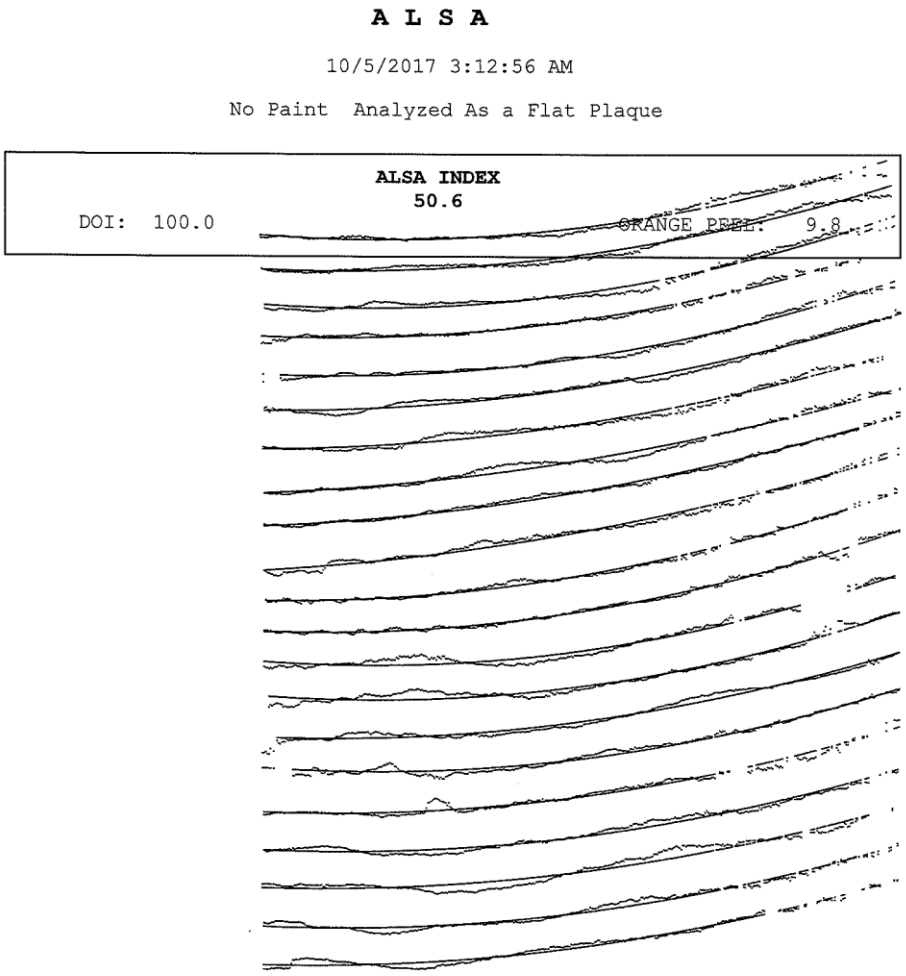

Figure 90. Class-A confirmation with ALSA test protocol of the as-molded class-A SMC panels of the 1.43 m^2 part.

The demonstrator part chosen was a representative tractor hood of 1.43 m^2 scale. The September 2017 milestone called for a 0.7 m^2 class-A finish SMC part/feature. IACMI did not have a large class-A tool to cover the 0.7 m^2 requirement for this milestone. Hence, we adopted an economical approach by engaging a SMC parts producer – Mastermold, WI. Mastermold is a proven molder with 150 to 4000 ton press capacity in various plate sizes and shapes.

Mastermold has a good collection of class-A tools – but most of these are customer tools- and subject to customer IP. Hence, there are some restrictions in terms of access to the tools. Despite these – we were able to get two types of parts molded against the upcoming milestone. The class-A tool is a customer tool for a tractor front hood. The tool has chrome finish and used to produce class A IDI class-A material S31-31T-29, as per the technical data sheet (TDS). This material is in off-white ivory color

family. The charge size relative to the tool size is shown in Figure 91. Figure 92 illustrates the SMC charged placed on the tool and Figure 93 and Figure 94 shows examples of molded parts.

Table 15: Molding parameters

Material	IDI Class A SMC S31-31T-29 (1.9 grams/cc)
Color	Off-white
Press tonnage available	2000 ton
Press tonnage applied	550-600 ton
Tool surface are	1.88 m (68”) x 0.76 m (27.5”)
Temperature	Top tool: 300 F, Bottom: 280F
Cycle time	60 seconds @550 tons + 2.5 minutes@250 tons = 3.5 minutes
Charge weight	19.5 to 20.7 lbs
Mold coverage	42%
Ejection	Ejector system on tool

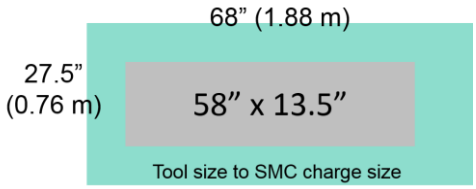

Figure 91. Charge size relative to the tool size

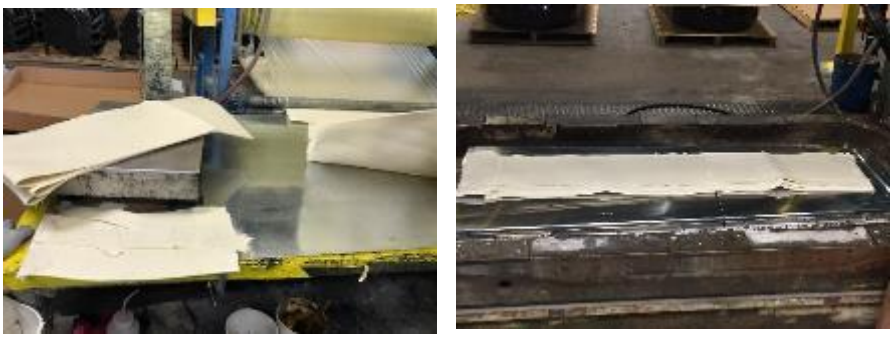

Figure 92. Illustrates the class A SMC charge placed on the chrome-finished class-A tool.

Figure 93. (Left) Front side of finished part; (Right) Right side of finished part (backside)
The part is 1.43 m^2 in surface area

The molded part had excellent surface finish and is going through post-painting (Figure 94) class-A measurements were done on both the as-molded and post-painted parts as would be encountered in actual production. The demonstrator part chosen was a representative tractor hood of 1.43 m^2 scale. In some smaller parts, a structural stiffener was bonded to the outer to represent the actions on the real tailgate (inner bonded to the outer), see Figure 95. This was performed to evoke potential bond-line read-throughs, which might disrupt the class-A surface. The bonding process did not evoke read-throughs.

Figure 94. Painted and finished class-A SMC tractor hood part for demonstration

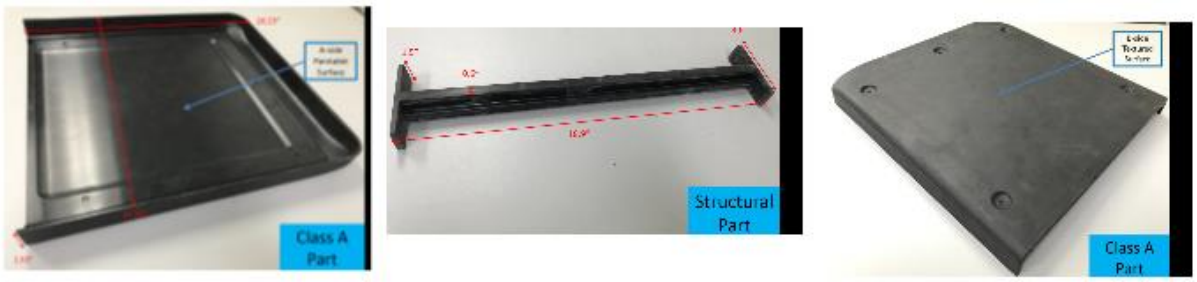

Figure 95: Bonding trials of inner stiffener to outer SMC class-A. Eventually the lift gate is bonded in the form of outer to inner.

D. Class-A Production Level SMC Tool and Trials

IACMI has commissioned a production level steel tool for SMC class-A with a 864 mm x 1054 mm (34” x 41.5”) footprint, which can produce a 457 mm x 356 mm (18” x 14”) plaque, see Figure 96, Figure 97, and Figure 98. The tailgate outer requirement calls for a class-A SMC finish. Design of experiments included SMC S31-31T29 and related systems for helping the production of the final component. The tool features are:

- Produces a 457 mm x 356 mm plaque with a deep rib insert
- Tool base 864 mm x 1054 mm
- Unique vacuum assist for class-A production

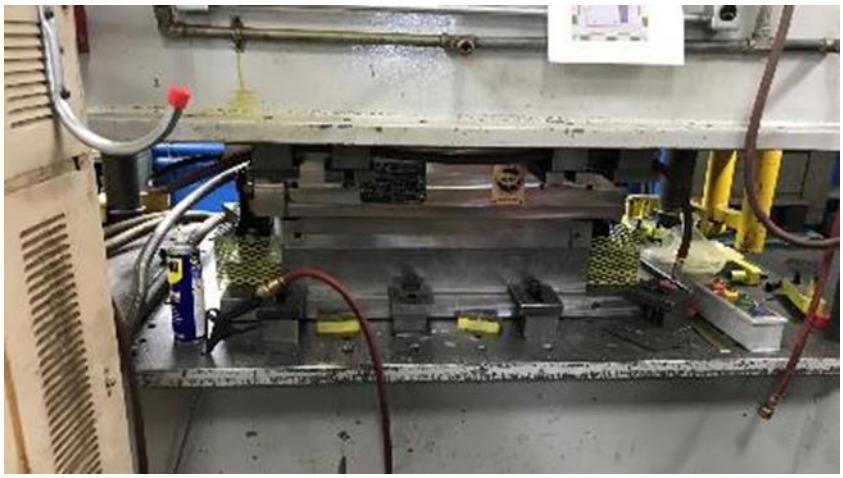

Figure 96: Class-A SMC Production Level tool 864 mm x 1054 mm footprint

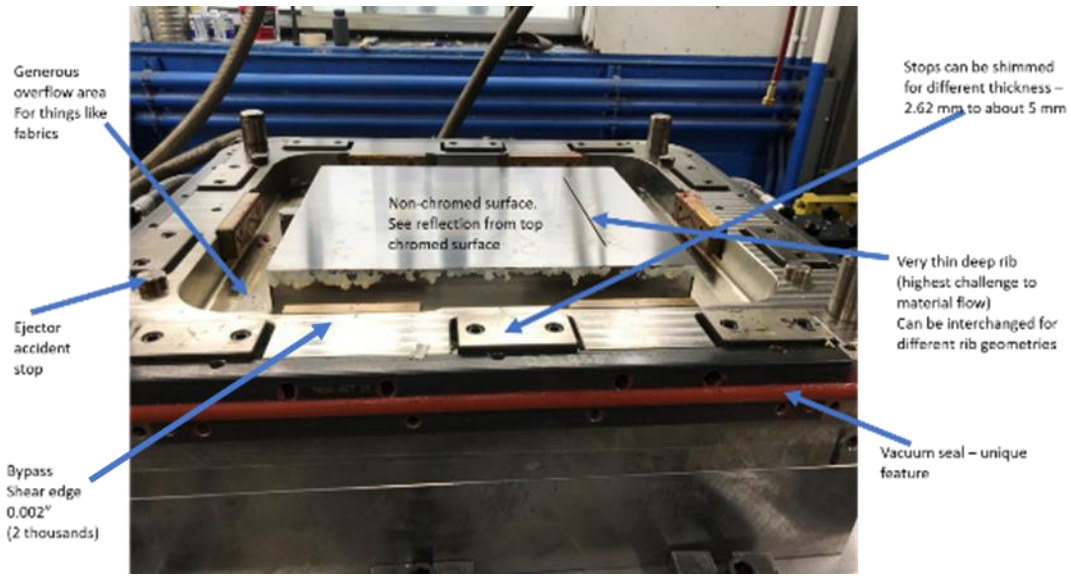

Figure 97. Details of the features of the production level class-A finish SMC tool

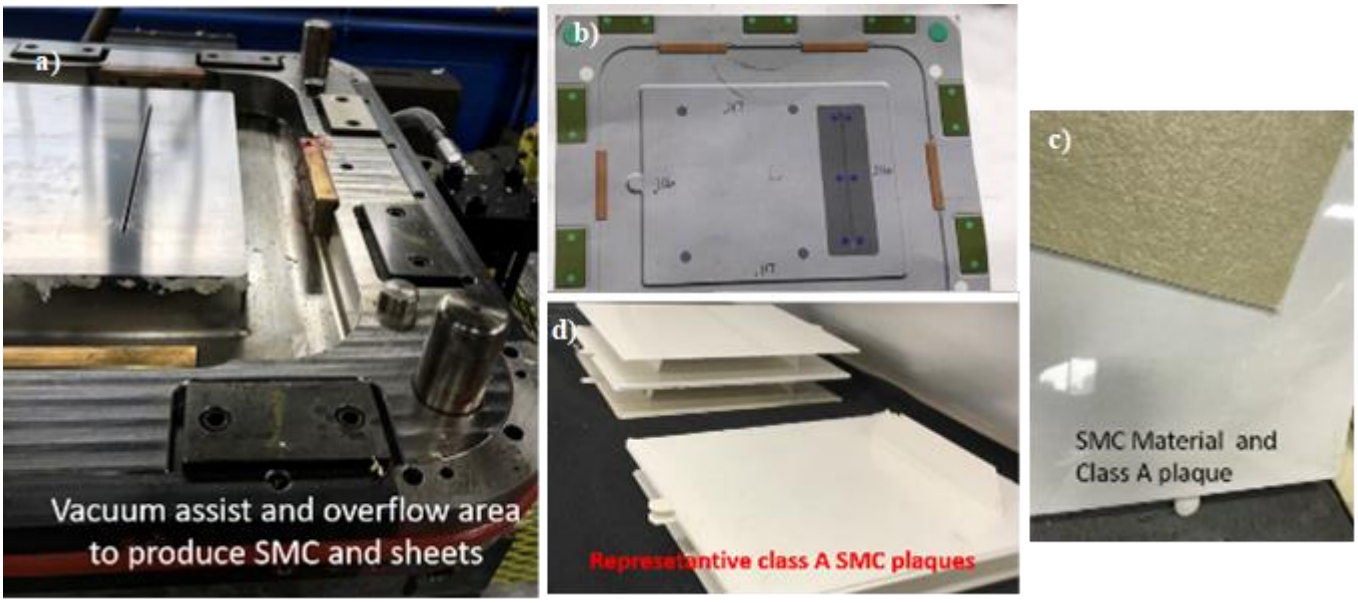

Figure 98: Details of the tool with vacuum features; (b) Map of the tool; (c) Raw materials and (d) Finished glass/vinyl ester SMC Class A finish plates

All molded plaques were tested for ALSA and met class-A requirements in terms of short and long wavelength(s).

Summary:

The preceding four aspects (a) SMC materials selection for structural and class-A; (b) the shape trials on the seat back rest; (c) The large scale molding with the tractor hood with SMC class-A formulations; and (d) class-A Production level tool were illustrated in this report. All trials were successfully completed.

1.3 IMPACTS

This program has shown the opportunities given by replacing metal parts with SMC.
The team could prove the following project goals successfully:

- Property targets fulfilled, part properties comparable to a metal lift gate
- Weight saving target fulfilled, 35% weight reduction achieved compared to the series production steel version
- Through the substantial weight saving, a reduction in use-phase emission was proven.
- Part cost target fulfilled: production costs less than aluminum version of the lift gate
- Saving tooling costs in comparison to conventional metal parts production demonstrated
- Applicable for more than 100.000 parts per year demonstrated
- Class-A surface quality proven
- The project results are summarized in Figure 99.

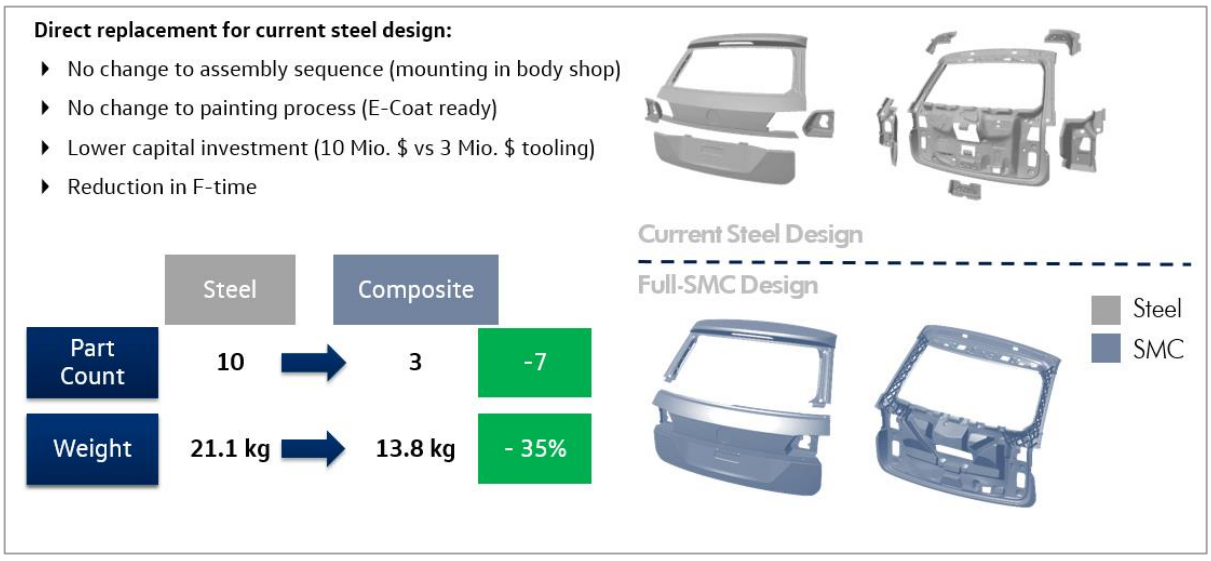

Figure 99: Summary of project results.

The manufacturing process for the Volkswagen Atlas SMC liftgate, as developed in this project, achieved all project goals and has proven to be ready for automotive mass production. The technology demonstrators manufactured can be used for further testing, and as active demonstrators of the SMC system.

1.4 CONCLUSIONS

- Through the close collaboration of companies along the supply chain of SMC parts manufacturing, research institutes and an automotive OEM, the full potential of sheet molding compounds was utilized.
- A fully functional prototype liftgate was designed, simulated, and manufactured to demonstrate the technology.
- The automotive industry has been historically set up for steel part manufacturing. Endeavors like the one outlined in this report are necessary to showcase and accelerate composite applications with all its advantages.
- Project partners extended their know-how and experience in the field.
- Project partners made valuable connections along the supply chain.
- The next steps for deployment in manufacturing environment are now the full component testing and feasibility studies for implementation in possible car projects in the Volkswagen Group.

1.5 PAPER AND CONFERENCE CONTRIBUTIONS

Mainka H, Laduch T, Drees T (2019) Development of a Class-A Lightweight SMC Liftgate for the Volkswagen Atlas. Society of Polymer Engineers Automotive Composite Conference and Exposition, Novi, MI.

Bogdanor M, Mainka H, Laduch T, Sharp N, Pipes R, Rademacher M (2017) Reduction of CO2 Emissions through Lightweight Body Panels Design and Optimization of a SMC Liftgate for the Volkswagen Atlas. Proceedings of the 32nd ASC Technical Conference, West Lafayette, IN.

Kardos M, Körner E, Penumadu D, Modler N (2020) The influence of fiber volume fraction and fiber length on the evolution of pore content and the paintability of sheet molding compounds. Composite Part B: Engineering, Volume 185, 107760.

1.6 REFERENCES

[1] *Ecoinvent 3.4*. [Online]. Available: https://www.ecoinvent.org/database/older-versions/ecoinvent-34/ecoinvent-34.html

[2] *European Platform on Life Cycle Assessment* [Online]. Available: http://eplca.jrc.ec.europa.eu/ELCD3/

[3] *DATASMART LCI Package*. [Online]. Available: https://ltsexperts.com/services/software/datasmart-life-cycle-inventory/

[4] R. Hischier *et al.*, "Implementation of Life Cycle Impact Assessment Methods, Final Report Ecoinvent v2. 2 No. 3," *Swiss Centre for Life Cycle Inventories, Dubendorf, Switzerland*, 2010.

[5] V. D. Ingenienure, "Cumulative energy demand-Terms, Definitions, Methods of Calculation," *VDI-Richtlinie*, vol. 4600, p. 5, 1997.

[6] J. Bare, "TRACI 2.0: the tool for the reduction and assessment of chemical and other environmental impacts 2.0," *Clean Technologies and Environmental Policy*, vol. 13, no. 5, pp. 687-696, 2011/10/01 2011, doi: 10.1007/s10098-010-0338-9.

[7] J. C. Bare, "TRACI: The tool for the reduction and assessment of chemical and other environmental impacts," *Journal of industrial ecology*, vol. 6, no. 3-4, pp. 49-78, 2002.

[8] M. Oktaviandri and A. S. B. Safiee, "Modelling Electrical Energy Consumption in Automotive Paint Shop," in *IOP Conference Series: Materials Science and Engineering*, 2018, vol. 319, no. 1: IOP Publishing, p. 012060.

[9] W. S. Association, "Methodology report: life cycle inventory study for steel products," *Brussels, Belgium*, 2011. [Online]. Available: https://www.worldsteel.org/en/dam/jcr:6a222ba2-e35a-4126-83ab-5ae5a79e6e46/LCA+Methodology+Report.pdf.

[10] S. Das, "Life cycle assessment of carbon fiber-reinforced polymer composites," *The International Journal of Life Cycle Assessment*, vol. 16, no. 3, pp. 268-282, 2011.

[11] F. Del Pero, M. Delogu, and M. Pierini, "Life Cycle Assessment in the automotive sector: a comparative case study of Internal Combustion Engine (ICE) and electric car," *Procedia Structural Integrity*, vol. 12, pp. 521-537, 2018.

[12] M. Messagie, F.-S. Boureima, T. Coosemans, C. Macharis, and J. Mierlo, "A range-based vehicle life cycle assessment incorporating variability in the environmental assessment of different vehicle technologies and fuels," *Energies*, vol. 7, no. 3, pp. 1467-1482, 2014.

[13] S. M. Schexnayder *et al.*, "Environmental evaluation of new generation vehicles and vehicle components," *Engineering Science and Technology Division, Oak Ridge National Lab., US Dept. of Energy, Oak Ridge, Tennessee*, 2001. [Online]. Available: https://info.ornl.gov/sites/publications/Files/Pub57172.pdf.

[14] L. Bushi, T. Skszek, and T. Reaburn, "New ultralight automotive door life cycle assessment," *The International Journal of Life Cycle Assessment*, vol. 24, no. 2, pp. 310-323, 2019.

[15] S. Das, "Life Cycle Assessment -Energy and CO2 Emissions of Aluminum-Intensive Vehicles," ed, 2013.

[16] EuCIA. *Composites Recycling Made Easy*. [Online]. Available: https://eucia.eu/userfiles/files/20130207_eucia_brochure_recycling.pdf

[17] E. EuCIA, ECRC. "Glass fibre reinforced thermosets: recyclable and compliant with the EU legislation " Materials Today. http://csmres.co.uk/cs.public.upd/article-downloads/EuCIA-position-paper-52816.pdf (accessed.

[18] P. Asokan, M. Osmani, and A. D. Price, "Assessing the recycling potential of glass fibre reinforced plastic waste in concrete and cement composites," *Journal of Cleaner Production*, vol. 17, no. 9, pp. 821-829, 2009.

[19] M. Ribeiro *et al.*, "Recycling approach towards sustainability advance of composite materials' industry," *Recycling*, vol. 1, no. 1, pp. 178-193, 2016.

[20] A. Yazdanbakhsh and L. C. Bank, "A critical review of research on reuse of mechanically recycled FRP production and end-of-life waste for construction," *Polymers*, vol. 6, no. 6, pp. 1810-1826, 2014.
[21] S. Job, "Recycling glass fibre reinforced composites–history and progress," *Reinforced Plastics*, vol. 57, no. 5, pp. 19-23, 2013.
[22] S. J. Pickering, "Recycling technologies for thermoset composite materials—current status," *Composites Part A: applied science and manufacturing*, vol. 37, no. 8, pp. 1206-1215, 2006.
[23] B. P. Weidema, "System expansions to handle co-products of renewable materials," in *Presentation summaries of the 7th LCA case studies symposium SETAC-Europe*, 1999, pp. 45-48.
[24] J. L. Rivera and T. Reyes-Carrillo, "A framework for environmental and energy analysis of the automobile painting process," *Procedia CIRP*, vol. 15, pp. 171-175, 2014.
[25] K. Toda, A. Salazar, and K. Saito, *Automotive Painting Technology: A Monozukuri-Hitozukuri Perspective*. Springer, 2012.
[26] A. Mayyas, A. Qattawi, M. Omar, and D. Shan, "Design for sustainability in automotive

2 LEAD PARTNER BACKGROUND

About Volkswagen

Founded in 1955, Volkswagen of America, Inc. is an operating unit of Volkswagen Group of America and a subsidiary of Volkswagen AG, with headquarters in Herndon, Virginia. Volkswagen's operations in the United States include research and development, parts and vehicle processing, parts distribution centers, sales, marketing and service offices, financial service centers, and its state-of-the-art manufacturing facility in Chattanooga, Tennessee. The Volkswagen Group is one of the world's largest producers of passenger cars and Europe's largest automaker. Volkswagen sells the Arteon, Atlas, Atlas Cross Sport, Golf, Golf GTI, Jetta, Jetta GLI, Passat, and Tiguan vehicles through more than 600 independent U.S. dealers. Visit Volkswagen online at www.vw.com or media.vw.com to learn more.